NONLINEAR ANALYSIS OF THE HUMAN ELECTRORETINOGRAM

Thesis by

Arthur Joseph Koblasz

In Partial Fulfillment of the Requirements

for the Degree of

Doctor of Philosophy

California Institute of Technology

Pasadena, California

1977

(Submitted August 20, 1976)

ACKNOWLEDGMENT

I am very grateful to my advisor Professor D. H. Fender for his support and guidance throughout my graduate years. I also appreciate the many helpful suggestions and the encouragement I have received from Professors Ken I. Naka and Tom E. Ogden.

Much of the theoretical insight I have gained during my thesis work has been acquired by conversations with Dr. Syozo Yasui. I have also enjoyed many challenging conversations with Dr. Aileen Morris and Dr. Stanley Klein. I must also thank Dr. Morris for her help in editing this thesis.

I have spent many enjoyable hours working in the lab with Ross Larkin, Rinus Dekker and Shirley Lucas. Many of my initial experiments were unsuccessful and their enthusiasm spurred me to continue trying.

Finally, I must express my most sincere appreciation to Professor G. D. McCann, the faculty and staff of our department, and the university for providing me with outstanding training and research facilities.

ABSTRACT

The human electroretinogram (ERG) has been studied for about a century and has been in use as a clinical tool for perhaps half that time. Like most other biopotentials, the ERG is probably the result of nonlinear operations, but there have been surprisingly few attempts to study these nonlinear characteristics. We have characterized the human ERG system using Wiener kernels, which reflect separately the linear and nonlinear operations.

One of the difficulties with conventional analyses of the ERG for small amplitude flash stimuli is the variability of the response, both between subjects and for the same subject. This is often the result of poorly controlled experimental conditions rather than pitfalls in the analysis. For example, differences in retinal illumination can change both the stimulus and the system. Also, different placement of electrodes can cause different impedence and noise effects. We reduced both these artifacts by providing a maxwellian view of the stimulus and by using an eyecup electrode of our own design. The inherent nature of the flash stimulus can produce other artifacts which the quasi-random stimulus avoids. For example, flash stimuli are more

likely to evoke nonvisual responses than the random intensity stimulus. Also large amplitude flashes test the retina with non-physiological levels.

We first demonstrated the reliability of the first- and second-order Wiener kernels for characterizing the human ERG system by measuring standard deviations of the kernels for a variety of experimental conditions. We also used the kernels to predict responses to flash stimuli. For the cases considered, the first- and second-order kernels characterized the human ERG system more completely and accurately than measured flash responses.

We next examined the changes in the kernels for different mean levels of quasi-random stimuli. The first- and second-order kernels change suddenly for a step increase or decrease in stimulus mean. The size and latency of the kernel components increase as the stimulus mean decreases and a second b-wave appears as a distinct component of the first-order kernel for low stimulus means.

This second b-wave was shown to be attenuated for a red (663 nm) stimulus and reduced for a Retinitis Pigmentosa patient. Furthermore, when the stimulus bandwidth is increased, other components of the first-order kernel increase in size but the second b-wave remains the same. Hence, the second b-wave of the first-order kernel probably reflects the functioning of rod systems, much like the scotopic b-wave of the flash response.

Next we compiled all experimental evidence to construct models of the ERG system which produce the observed adaptation effects. Separate photopic and scotopic models were derived which offer a simple interpretation of the first- and second-order Wiener kernels. The photopic system is described as a cascade of a nonlinear system without memory followed by a linear filter with a long time constant. This seems appropriate since the first-order kernel for photopic stimulus levels does not change shape with different depths of modulation and since the second- and third-order kernels main diagonals resemble the shape of the first-order kernel. The characteristics of both elements of the model were estimated using experimental observations.

A scotopic model is also described which accounts for some of the observed changes in dynamics for scotopic stimulus levels. An additional linear integrator with a short time constant is added in series to the photopic model, positioned in front of the nonlinear element. Small changes in the time constant of this linear stage produce large changes in the total dynamics of the model. If the linear operations of this stage become more complex, then some of the structure of the second-order kernel away from the main diagonal can be accounted for.

Finally, we measured the ERG responses to one and to two simultaneous quasi-random stimuli of different wavelengths. The first-order kernels change significantly for different wavelength

stimuli. However, the differences can be accounted for by changes in the relative adaptation states of photopic and scotopic components.

The two-input experiments produce cross-kernels which can indicate cross-talk between receptor systems. However, if all receptor systems receive some proportion of both stimuli, then the cross-kernel can be dominated by self second-order kernels. This is the case for two inputs of red (663 nm) plus blue (423 nm) stimuli.

Other evidence for interactions between receptor systems is available from observing the changes in the first-order kernel for a single input when a second input of different wavelength is added to the stimulus. For example, the background red stimulus changes the response to the blue stimulus, and the background blue stimulus changes the response to a red stimulus. However, simple adaptation differences can again account for the observed changes.

The original goal of this project was to prove the feasibility of analyzing human retinal function using quasi-random stimuli. The small amplitudes characteristic of the quasi-random stimulus and the large noise levels customary for the human ERG made our analysis difficult. Furthermore, subjects would only tolerate a few minutes of steady fixation. Results are not presented for about half the subjects tested because of excessive noise levels. However, the Wiener kernels can provide more information about retinal function than alternative characterizations. Changes in the lower order Wiener kernels can be empirically linked to retinal diseases even when higher order kernels are ignored. We hope that our procedure and interpretations will provide a means for eventually improving the resolution of the clinical ERG.

TABLE OF CONTENTS

CHAPTER I

EARLY HISTORY OF ELECTRORETINOGRAPHY

Ben Franklin's well known studies of lightning and electricity (about 1765) triggered extensive research interest in electrophysiology toward the end of the 18th century (cited in Van Doren, 1938). A few years later, Galvani connected the nerve of a partially dissected frog's leg to a lightning rod and observed muscle contractions during lightning flashes (cited in Boring, 1942). He deduced from this first experiment in electrophysiology that living tissue produces electricity to make muscles function.

Du Bois-Reymond (1849) examined the current flow between different points of living tissue including the eye. He used a recently invented galvanometer to measure the current flow between the cornea and the optic nerve of enucleated eyes of frogs, fish and turtles.

Du Bois-Reymond's observations of "resting potentials" aroused Holmgren (1865) to conduct a set of experiments in Sweden to test for an electrical response to visual stimuli. His experimental techniques were similar to those introduced by Du Bois-Reymond, using an

enucleated frog's eye. He observed small electrical changes following step increases in retinal illumination.

Several years later, Dewar and Mc Kendrick (1873) performed nearly the same experiments in Scotland. They were also strongly influenced by Du Bois-Reymond's experiments but seemed unaware of Holmgren's work. They noted (1876) a surprising difference in polarity between vertebrate and invertebrate eyes. They also reported (1877) that visual responses could be observed between a wick electrode over the cornea and a reference electrode inserted into a wound on the back of a frog. Later Dewar (1877) performed the first ERG experiments on human subjects. He placed a ring of clay filled with saline over the cornea and attached a reference electrode to the subject's hand. An electrode was immersed in the saline solution which contacted the eye. The apparatus was reported to be very uncomfortable for the subjects; consequently, frequent eye movements and blinks occurred. The resulting large noise signals made Dewar's analysis very difficult. In fact, none of the early experimenters could overcome these difficulties; therefore, several decades passed before good data were available from human subjects.

Dewar and Holmgren both recognized the potential for nonvisual artifacts using intact or enucleated eyes. Kühne and Steiner (1881) succeeded in measuring responses from a dissected retina. These experiments confirmed that at least part of the observed electrical changes originate in the retina.

Unfortunately, the galvanometers available at this time could not resolve any details of the retinal response. In 1893, Burch

invented the capillary electrometer. Experimenters could then obtain a photographic copy of the electroretinogram waveform by passing a recording chart in front of a beam of light which was refracted by the electrometer.

Using this instrument and a rather fancy optical system, Gotch (1903) recorded the electrical responses to step changes in illumination of enucleated vertebrate eyes. He observed first a negative then a positive deflection following a step increase in illumination. He also described differences between the "on and off effects" for step increases and decreases in illumination. However, the responses which Gotch recorded were still somewhat distorted because of inadequacies of his equipment. For example, he could not resolve the second positive going deflection of the on-response (i.e., the c-wave) which was later reported by Ishihara (1906)

Einthoven and Jolly (1908) combined improvements in equipment and experimental techniques to resolve all components of the on and off responses for an enucleated frog eye. They described three components of the on-response — first a negative deflection or "a-wave," followed by a positive deflection or "b-wave," followed by a second positive deflection or "c-wave." The a, b and c designations which they made have become the accepted terms for classifying the normal electroretinogram waveform (Fig. 1-1).

Einthoven and Jolly noticed ripples superimposed on the b-wave, but did not speculate on their significance. Chaffee, Bovie and Hampson (1923) correctly speculated that these ripples reflected different retinal processes.

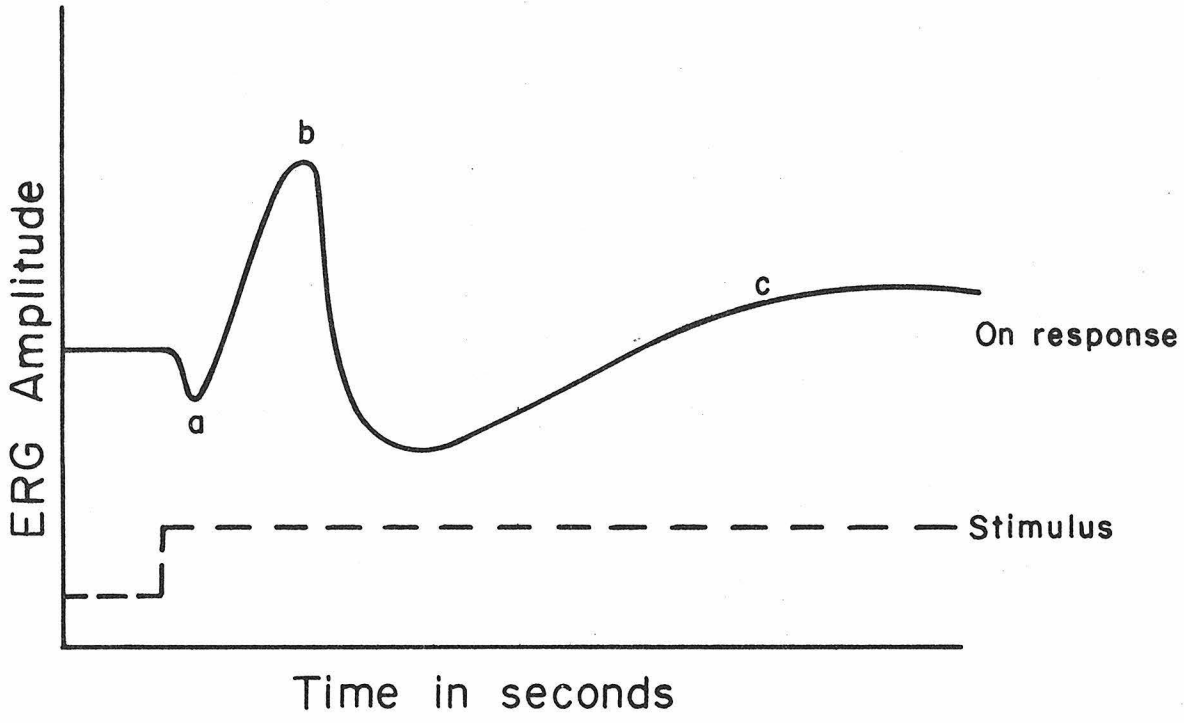

Fig. 1-1. Classification of the human ERG "on response" (Einthoven and Jolly, 1908).

Once the characteristic responses were identified, researchers began to focus on the functional significance of the different components. The most thorough analysis yet performed was reported by Granit (1963). He administered ether or other chemical agents to eyecup preparations of nocturnal and diurnal vertebrates. Three distinct components of the ERG response disappeared at different rates following the poisoning, which he called P1, P11 and P111 respectively. With ether first the P1 component disappeared, followed by P11, leaving only P111. The forms of these components are shown in Fig. 1-2. If the ether administration was discontinued, then both P1 and P11 returned, but if the administration was continued long enough, then all three components disappeared irreversibly. Other procedures produced different effects, e. g., asphyxia blocked P11 without affecting P1 or P111.

Granit proposed that the electroretinogram results from a weighted summation of distinct components, each component reflecting the activity of a single class of cells. The interactions between these components reflect interactions between retinal cells, which is the subject of primary interest to retina researchers.

Granit might have speculated about the origin of each component using the observed latency differences, i. e., earlier stages could produce a shorter latency component than later stages. However, there are obvious loopholes in this common argument, e. g., slight depolarization of a long latency process could trigger a short latency process, producing earlier peak activity in the later stage.

Granit speculated about the origin of the components based on the selective suppression he observed. P11 was blocked by a wide range of chemicals and was not affected by antidromic volleys in the optic

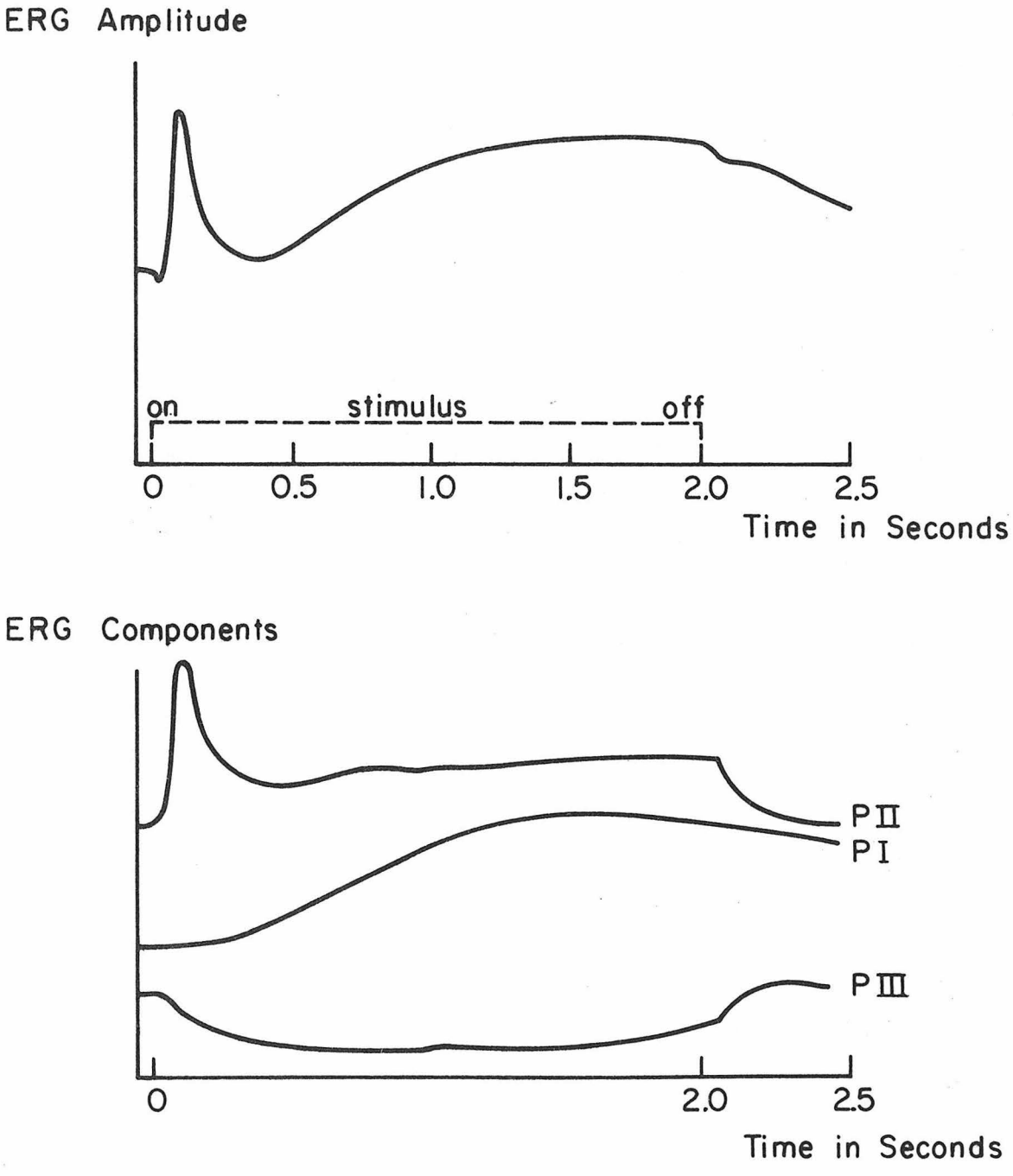

Fig. 1-2. Component analysis of the human ERG (Granit, 1963).

nerve (Granit and Helme, 1939). Furthermore, P111 was resistant to most manipulations. Granit incorrectly concluded that P11 arose from the bipolar layer, and correctly speculated that P111 originated in the receptor layer. He also concluded that the ganglion layer produces no measurable contribution. He could not ascertain the origin of the P1 component.

This generation of experimenters began to take more interest in human subjects. Hartline (1925) tried various schemes for accurately measuring the electroretinogram from human subjects. For some of his experiments he used a goggle filled with saline containing a mercury calomel electrode. He reported better results with other electrode designs; therefore, the goggle technique was not adopted by later researchers. We developed and used extensively a similar electrode device unaware of Hartline's pioneering work.

Sachs (1929) also performed successful experiments on human subjects using a wick electrode placed in light contact with the limbus. He cataloged the effects of changing many stimulus variables, e.g., intensity, wavelength and adaptation state of the eye. He also attempted experiments which claimed to change the size and position of the stimulus on the retina. Fry and Bartley (1935) later demonstrated that the amplitude and latency of the response depends only on the total flux entering the eye. Recent opinions attribute the majority of the electroretinogram response to stray light; therefore, Sachs had some difficulty in interpreting his results for presumed spatially different stimuli.

In recent years, experimenters have continued to focus on the origin of different components of the electroretinogram and the effects of changing stimulus parameters. Many have probed deeper into the neural maze of the retina examining the function of regions or single cells. The ultimate goal is to find out how the retina works or how it changes during a disease state. Table 1-1 lists the best current speculations about the origin of the electroretinogram.

The ERG is clinically useful for diagnosing diseases which affect large portions of the retina, e.g., retinitis pigmentosa. The entopic scattering of light makes focal testing very difficult. Brindley and Westheimer (1965) attempted focal studies of the human ERG using a small flickering spot stimulus with an adapting background. However, this technique has not been used extensively for clinical applications.

We have employed nonlinear systems analysis techniques to improve the resolution of the ERG. Each of the following chapters focuses on some aspect of retinal function or disfunction.

Table 1-1

Origin of the Components of the Human ERG

Component of the ERG	Principal Origin
Early receptor potential	Receptor outer segments
a-wave	Receptors
b-wave	Bipolar cell layer
1. Low-intensity d-c portion	?
2. High-intensity portion	Mueller cells
3. Oscillatory potentials	?
c-wave	Pigment epithelium
d-wave (off-response)	Interaction between a-wave and d-c portion of b-wave; possible additional source

(Krill, 1972)

CHAPTER II

QUASI-RANDOM VERSUS SINGLE-PULSE STIMULI

II-1. Introduction

The human electroretinogram (ERG) has been studied for about a century and has been in use as a clinical tool for perhaps half that time. Like most other biopotentials, the ERG is probably the result of nonlinear operations, but there have been surprisingly few attempts to study these nonlinear characteristics. We have characterized the human ERG system using Wiener kernels, which reflect separately these linear and nonlinear operations. The average flash response for comparable experimental conditions was also computed and compared with the predicted response using the kernels.

Previously, the best attempt at nonlinear analysis of the human ERG appears in the work of Troelstra and Schweitzer (1968, 1966, 1963). These authors point out that the scotopic response to single flashes is not a linear function of the flash energy except at very low energy levels. Generally, the response is smaller than expected by linear prediction, and the difference between the expected and measured response grows with the intensity of the flash. Their experiments involving double flash stimuli indicate a so-called nonlinear memory which is independent of the flash intensity. This relates to the observed nonlinear

interaction of the response to one flash with the response to a second flash, i.e., the first flash momentarily changes the characteristics of the retinal system. The duration of the change is a measure of the memory of the system; they determined that the decay time of this change for the human retina is about 100 msec. Troelstra and Schweitzer also proposed a nonlinear model to describe the relation between the light input and the human b-wave response.

An alternate method of stimulating the retina and analyzing the data has been used by Fricker and Sanders (1974, 1975) derived from techniques previously applied to radar and communication data processing. Their stimulus is a train of identical flashes with random spacing. The pulses are used to trigger the stimulus and also to generate a reference waveform in which each pulse at time t_n is replaced by the function

$$F(t) = A(1 + \text{Cos}\, 2\pi[t-t_n]\ /T)$$

where t takes values between $(t_n - T/2)$ and $(t_n + T/2)$. A characteristic response is obtained by cross-correlating the ERG potential recorded at the eye with the reference waveform. This procedure has certain advantages in combating noise and smoothing the response; the waveform that results is related to the first-order term of the Wiener functional expansion discussed below.

We have measured and analyzed the human ERG using a conventional nonlinear method. This approach uses a so-called gaussian white-noise input to a system. In our case the white-noise

variable is light intensity. Hence, white does not refer to the color of the light stimulus, but rather to the flatness of the power spectrum of the quasi-random intensity modulation.

II-2. Theory

A systems engineer can characterize a linear system entirely by its unit-impulse response. In many cases this simple analysis reveals the signal processing that goes on inside the linear system, e. g., integration, differentiation, delays, etc. Furthermore, once the unit impulse response of the linear system is known, the response to any input can be predicted. This is done by subdividing an arbitrary input into a sequence of pulses of different amplitude and superposing arithmetically the series of scaled unit-impulse responses elicited by the sequence of input pulses. Mathematically, this is equivalent to convoluting the impulse response with the input waveform.

The characteristics of a nonlinear system are generally changed during the time that the system is processing a signal. That is, the response to one pulse in the above sequence might be different from the response to other pulses. Many processes in biology fall into this category. For example, the active spring constant of a muscle is a function of the tension of the muscle. Thus, if a burst of motor-nerve activity is applied to a muscle we would record a change in isometric tension, but if a second identical burst of nerve impulses is applied while the muscle is still in tension, the new change in tension will not be the same as the first, because the properties of the muscle have changed. Hence, we cannot predict the double-pulse response for a nonlinear system simply by adding single pulse responses — the system does not obey the law of superposition.

Wiener (1958) proposed the following functional expansion to characterize stationary, nonlinear systems:

$$y(t) = G_0(h_0) + G_1(h_1, x(t)) + G_2(h_2, x(t)) + \ldots \qquad (2.1)$$

where

$$G_0 = h_0$$

$$G_1(h_1, x) = \int_0^{+\infty} h_1(\tau)\, x(t-\tau)\, d\tau$$

$$G_2(h_2, x) = \iint_0^{+\infty} h_2(\tau_1, \tau_2)\, x(t-\tau_1)\, x(t-\tau_2)\, d\tau_1 d\tau_2 - P \iint_0^{+\infty} h_2(\tau, \tau)\, d\tau \qquad (2.2)$$

The response $y(t)$ is defined in terms of a zero mean, gaussian, (band-limited) white-noise stimulus $x(t)$ with power density P and an infinite number of kernels $h_n(\tau_1, \tau_2, \ldots \tau_n)$.

The kernel h_0 is the expected average value of the response to the quasi-random stimulus. h_0 and $h_1(\tau)$ together provide the best linear prediction of the response in terms of least mean square error. Similarly, h_0, $h_1(\tau)$ and $h_2(\tau_1, \tau_2)$ provide the best quadratic prediction of the response. In general, higher order kernels increase the order of the characterization.

If all non-zero kernels are known, then we can predict the response to stimuli which are not gaussian or white (Yasui and Fender, 1975), such as pulses. If the only significant kernels are h_1 and h_2, then we can interpret these Wiener kernels in terms of expected impulse responses (Marmarelis, 1971).

That is, suppose an impulse of amplitude m occurs at time T_1, i.e., $m\delta(t-T_1)$ where $\delta(t-T_1)$ is a dirac delta function, then from Eqs. 2.1 and 2.2, the predicted response $y_1(t)$ would be

$$y_1(t) = C + mh_1(t-T_1) + m^2h_2(t-T_1, t-T_1) \tag{2.3}$$

where the constant $C = h_0 - P\int_0^{+\infty} h_2(\tau, \tau)\,d\tau$. (2.4)

The contribution of the first-order kernel is scaled by the factor m while the contribution of the second-order kernel is scaled by m^2.

Notice, if the system were linear, the second and higher order kernels would be zero; then changes in the magnitude of the impulse stimulus would only produce changes in the amplitude of the predicted response, i.e., $y_1(t) = C + mh_1(t-T_1)$. However, for a nonlinear system, because of the different scale factors for the first- and second-order kernels, the shape of the impulse-response can be a function of the magnitude of the input impulse.

If we next let the input be an impulse at time T_2 , then

$$y_2(t) = C + mh_1(t-T_2) + m^2h_2(t-T_2, t-T_2) \quad . \tag{2.5}$$

Finally, if the input is a combination of the pulse at T_1 and the pulse at T_2 , then the double-pulse predicted response $y_3(t)$, is

$$y_3(t) = y_1(t) + y_2(t) + 2m^2h_2(t-T_1, t-T_2) \quad . \tag{2.6}$$

The term $h_2(t-T_1, t-T_2)$ is a measure of the error in assuming the superposition of the single-pulse responses $y_1(t)$ and $y_2(t)$ referred to above. This error is usually dependent on the spacing between the two pulses (T_2-T_1) .

Hence, we could determine the second-order kernel for this special case by simply measuring the single-pulse responses for different magnitude pulses and the double-pulse responses for different spacing between pulses. The second-order kernel could be tabulated as in Table 2-1 or drawn as a contour map as in Fig. 2-1a. The axes of the contour map can be changed as in Fig. 2-1b or configured as the relief map shown in Fig. 2-1c.

This method for computing the second-order kernel would require extensive experimenting for a single second-order kernel. Fortunately, Lee and Schetzen (1961) derived a simpler, more general method for computing Wiener kernels involving cross-correlations between the gaussian white-noise input $x(t)$ and the output $y(t)$, i.e.,

$$h_n(\tau_1, \tau_2, \ldots, \tau_n) = \frac{1}{n!} p^{-n} E\left\{\left[y(t) - \sum_{k=0}^{n-1} G_k(h_k, x(t))\right]\left[x(t-\tau_1)\ldots x(t-\tau_n)\right]\right\} \tag{2.7}$$

Using this method, we can compute h_1 and h_2 from the results of one short experiment. These kernels then characterize our system for all stimuli contained in the original quasi-random input.

In this chapter, we will use the kernels computed by the Lee and Schetzen technique to predict the response to a single flash stimulus. We will compare this prediction with the measured flash response for different subjects. This will partially test the validity of truncating the Wiener expansion after the second-order term and also the reliability of the kernels used.

TIME BETWEEN PULSES IN MSEC \ TIME AFTER 1ST PULSE IN MSEC	0	15	30	45	60	75	90	105	120	135	150	165	180
0	21	87	0	-79	-69	-72	-46	-18	-8	-1	0	-5	-15
15		27	58	-91	-1	-7	-9	-1	4	15	19	22	17
30			16	-33	-18	64	45	26	18	31	33	34	41
45				9	-17	31	45	36	35	34	37	26	7
60					-14	-19	-9	10	23	26	33	17	0
75						-26	-36	-10	4	22	11	0	-11
90							-19	-20	-9	14	24	9	-4
105								-9	-7	-7	20	14	14
120									-21	-32	-31	-19	-18
135										-14	-28	-28	-21
150											13	9	11
165												15	19
180													-30

Table 2-1

Second-order kernel derived from two-pulse experiments. For the case described, the measured response is the superposition of single-pulse responses plus values shown in the table along a horizontal line specified by the spacing between the pulses.

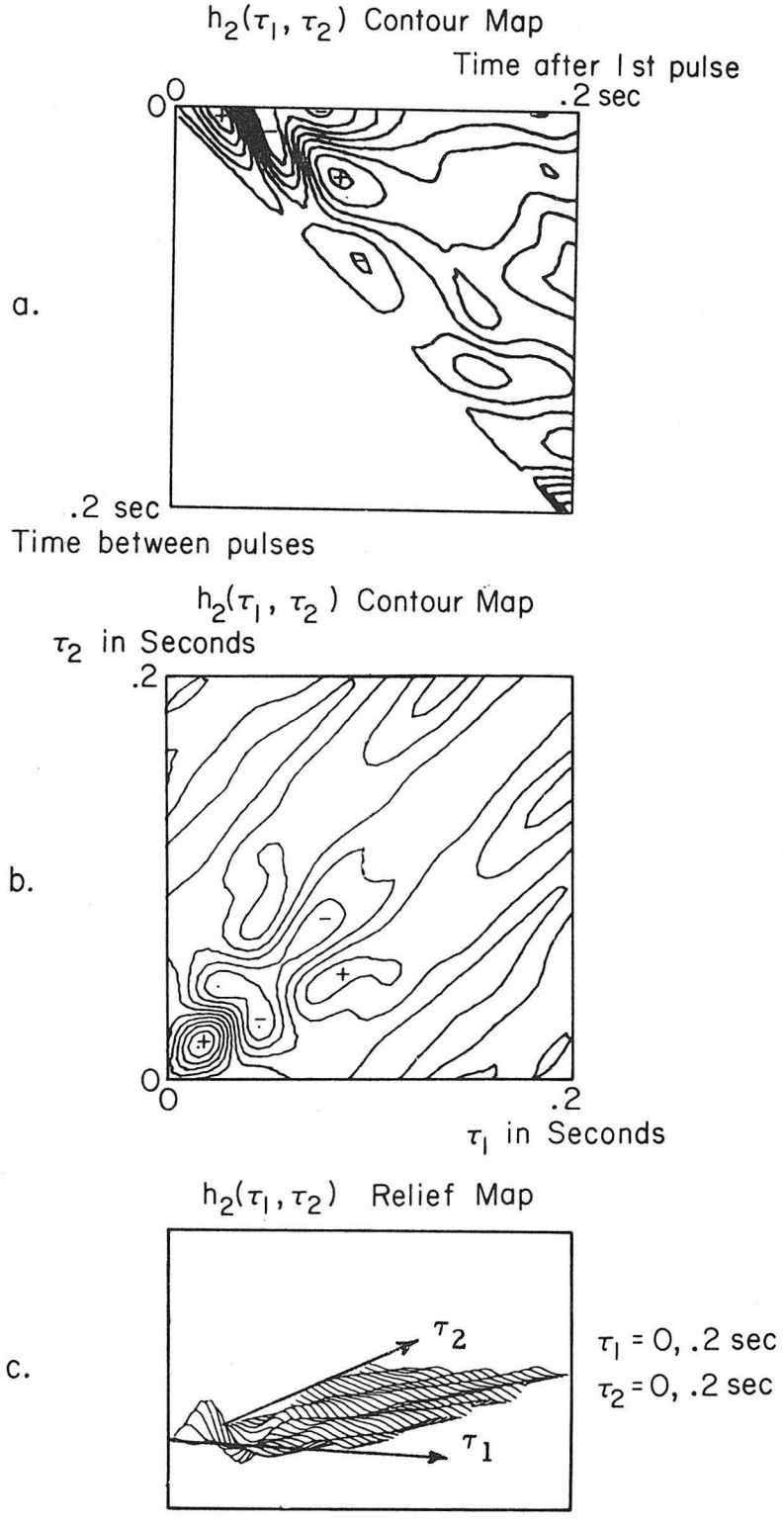

Fig. 2-1. Contour and relief maps of second-order kernel. Fig. 1a resulted when points of equal value in Table 1 were connected. Figs. 1b and 1c were produced by changing the orientation of the axes, noting symmetry.

II-3. Experimental Method

II-3-1. Quasi-random intensity stimulus

There are several ways to generate a gaussian bandlimited white-noise voltage signal. We used a design which applies the random-noise signal generated by a back-biased zener diode to a logic circuit arranged to produce a random period binary signal (Appendix A-1). When this is appropriately high- and low-pass filtered, it produces the desired continuous random signal (Mayo, et al., 1973 and Pawula and Tsai, 1969).

The Wiener theory also requires the defined input to have a mean of zero. Since in our case the input is light intensity, which is a non-negative quantity, the zero-mean random gaussian signal must be superimposed on a uniform background illumination. This, in turn, requires that the excursion of the zero-mean gaussian random process must be truncated at $\pm B$ where B is no greater than the value of the background illumination.

The choice of the bandwidth of the quasi-random stimulus is critical. A bandwidth too narrow or too wide can cause significant error in computing the Wiener kernels. The aim is to test the system with only the frequencies to which it responds (Marmarelis and Naka, 1973a). The appropriate bandwidth can be estimated by stimulating with a wide bandwidth signal and observing the bandwidth of the response. The bandwidth of the input is then reduced until the power spectrum of the response just begins to decrease. Using this approach, the bandwidth of the stimulus has been set for these experiments at

. 2 to 30 Hz (3 db down) with a high-pass slope of 40 db per decade and a low-pass slope of 160 db per decade. Other experimental conditions may require different optimum bandwidths.

Fig. 2-2 shows a design for an electro-optical bench which provides up to two independent quasi-random inputs of 3000 cd m^{-2} maximum illuminance, seen in 45^{o} maxwellian view. Each pen motor rotates a louver filter. The transmission through this filter is proportional to the cosine of the angle between the plane of the filter and the incident light. We use maximum louver excursions of only 6 degrees, and within this range the attenuation can be assumed proportional to the angle with an error less than . 2%; therefore, current modulations of the pen motor produce the desired random modulations of the light intensity.

Fig. 2-3 shows measured statistical properties of the quasi-random intensity stimulus which we use. The power of the stimulus is indeed flat from . 2 to 30 Hz. Also, the probability density plots are gaussian, except for a ± 3 standard deviations limit of amplitudes with a χ^2 of . 028 with 8 degrees of freedom. This implies a match to a gaussian distribution with a probability, p = . 99.

II-3. 2. Pulse stimuli

Provisions were also made available for stimulating the retina with short pulses of light. The linear motion transducer shown in Fig. 2-2 moves a knife-edge into one light channel of the optical system. The knife-edge moves across a small image of the source acting like a shutter which does not generate moving shadows.

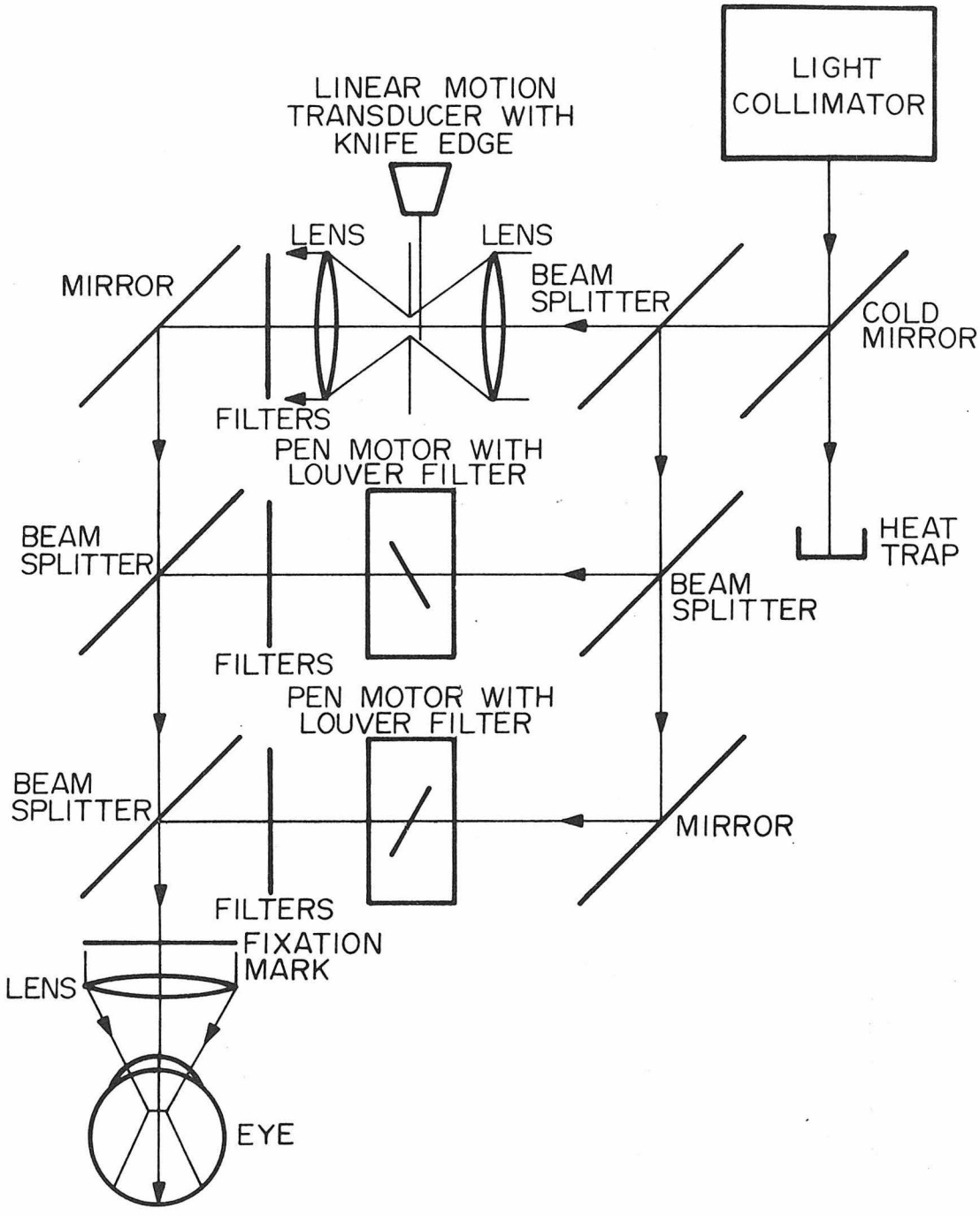

Fig. 2-2. Optical system.

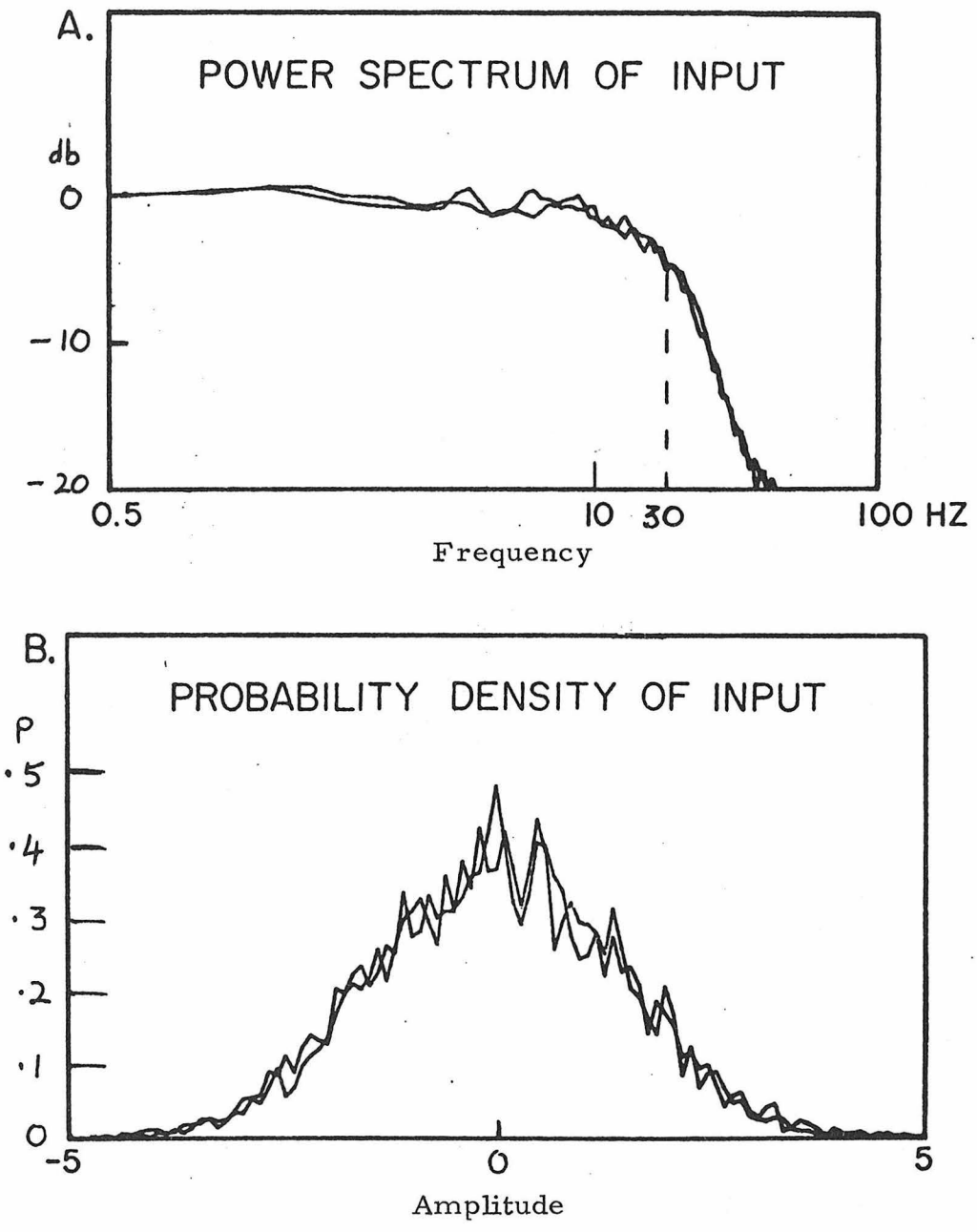

Fig. 2-3. Statistical properties of quasi-random stimulus.

The pulse stimuli were superimposed on a constant background set at one log unit less than the mean (background) of the white-noise stimulus. This seems to produce comparable photopic adaptation states and increases the amplitude of the pulse response. The pulse duration was set at 5 msec, and the amplitude was set equal to one-half the maximum peak-to-peak excursion of the white-noise stimulus.

II-3-3. Electrodes

Armington (1974) has surveyed the many varieties of electrodes used in ERG recording. For research purposes, the ERG is frequently measured using a contact lens electrode (Riggs, 1958), whereas for clinical purposes various derivatives of the Burian-Allen electrode are popular. Both of these electrodes have certain shortcomings.

The use of a contact-lens electrode produces large signals, but it requires a contact lens individually fitted for each subject. Also, unless the subject is an experienced contact lens wearer, the lens causes a large number of blinks. Each blink interrupts the light stimulus which generates an artifact in the analysis. The electrode picks up large muscle potentials from the blink, but the measurement is not badly contaminated by the Electro-oculogram (EOG) since the contact lens moves with the eyeball.

The Burian-Allen electrode causes frequent blinks in most subjects, but the speculum prevents the eyelids from closing during a blink. Hence, the stimulus is not interrupted. However, the electrode

records large artifactual potentials from the blink, and the record is also contaminated with the EOG signal since the lens cannot move with the eye.

We have developed an ERG electrode with some features similar to a design proposed by Hartline (1925); our eyecup apparatus shown in Fig. 2-4 improves the comfort of the subject and increases the reliability of recording. Superficially, this electrode appears to have disadvantages discussed above — a blink interrupts the light stimulus, and the electrode records potentials both from the blink and from the EOG. However, the noise arising from the EOG is mainly of lower frequency than the ERG and can be reduced by filtering. The damaging artifact is therefore caused by the blinks. In practice, if the pH and temperature of the artificial tear fluid filling the eyecup is matched to that of natural tears, the blink reflex is very nearly suppressed. Subjects typically go several minutes between blinks.

From the signal processing point of view, the ultimate test of an electrode is its signal-to-noise ratio. We have measured the response characteristics of a Lovac ERG contact lens, a Riggs-type scleral contact lens containing a peened 3 mm diameter Ag/AgCl disk electrode, and our eyecup electrode. For the purpose of estimating the relative signal-to-noise ratios, we considered the signal to be the average response to 60 flashes of 8500 troland (td) amplitude superimposed on an adapting background of 85 td. The noise was estimated by measuring the response to the steady background level of illumination only. The r. m. s. signal/noise ratio for each electrode

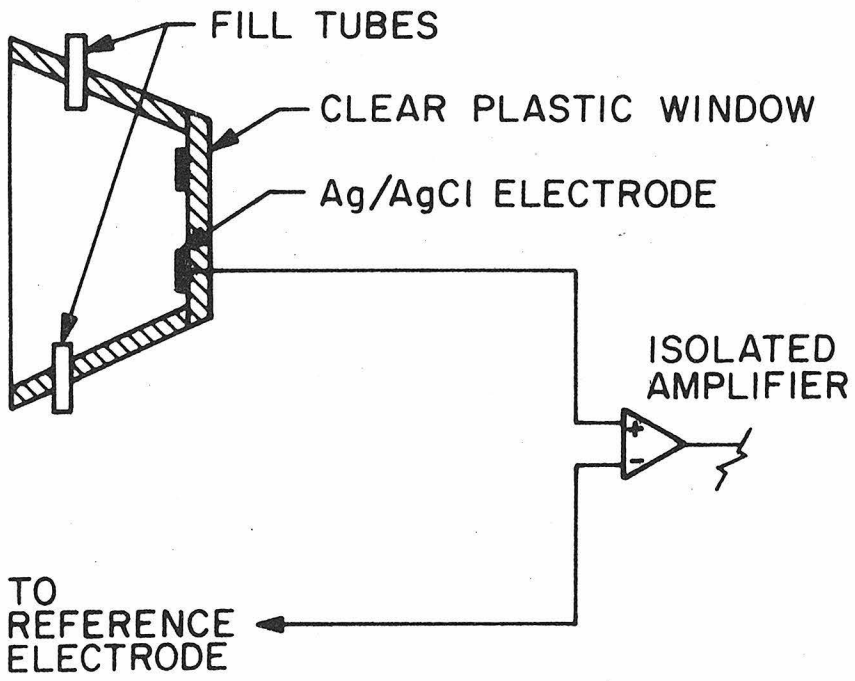

Fig. 2-4. ERG eyecup electrode.

was as follows: Lovac, 0.39; Riggs, 0.58; and eyecup, 0.66. The eyecup electrode gives the best signal/noise ratio as well as being more comfortable for the subject. It also requires no custom fitting for adult subjects.

II-3-4. Data recording and analysis

During an experiment, stimuli and responses were recorded on a four-channel analog tape recorder. At the same time, the signals were sampled at 5 msec intervals (i.e., 100 Hz nyquist folding frequency) by a 12 bit analog-to-digital converter and multiplexed on a digital tape. The digital signals were analyzed using a PDP 11/45 computer system. For quasi-random experiments, a masking program was available to set the response equal to zero shortly before and after the occurrence of a blink, then other programs performed filtering functions on both the stimulus and the response data sets. After this data preparation, the first- and second-order Wiener kernels were calculated as shown in Eq. 2.3. For flash experiments, the same filtering programs were used for preparing the response data set, then another program performed the simple average calculation.

II-3-5. Experimental protocol

Four healthy male subjects were used in these experiments. After adapting to 300 cd m^{-2} maximum ambient illumination for about 15 minutes, each subject's right eye was further adapted for 3 minutes with white light of mean retinal illuminance 850 td. Immediately following this controlled adaptation period, each subject was then exposed to 2 minutes of flashes of white light spaced one

second apart. The flashes were 8500 td superimposed on the steady 850 td background, seen in the same maxwellian view. Immediately following this, the stimulus was changed to 3 minutes of quasi-random intensity modulation with 8500 td mean illumination and ±3 standard deviations depth of modulation, again seen in 45° maxwellian view.

II-4. Results

II-4-1. Wiener kernels

The data obtained for each subject during the 3 minute period of random intensity stimulation was segmented to give four nearly blink-free sections, each of duration 30 seconds. Each segment was individually analyzed to produce a set of first- and second-order Wiener kernels.

Fig. 2-5 shows the mean value of the ensemble of first-order kernels for each subject. The curves above and below each mean are the mean plus and minus one standard deviation of the mean.

The mean values of the corresponding second-order kernels for each subject are shown in Fig. 2-6 along with a two-dimensional plot of the standard deviation of this mean for subject AK.

While the standard deviation of the mean reflects the reproducibility of a kernel, it tells us little about the accuracy of the function — if it adequately characterizes the system. One test for accuracy is to predict the response for the same random input used to generate the kernels. The mean-square-error between this model response and the real response quantifies the accuracy of the kernels. This procedure works well for a preparation that is relatively noise-free, but unfortunately the human ERG is a noisy measurement; therefore, the mean-square-error calculated as above arises mainly from the noise in the measured response rather than from inadequacies of the kernel characterization.

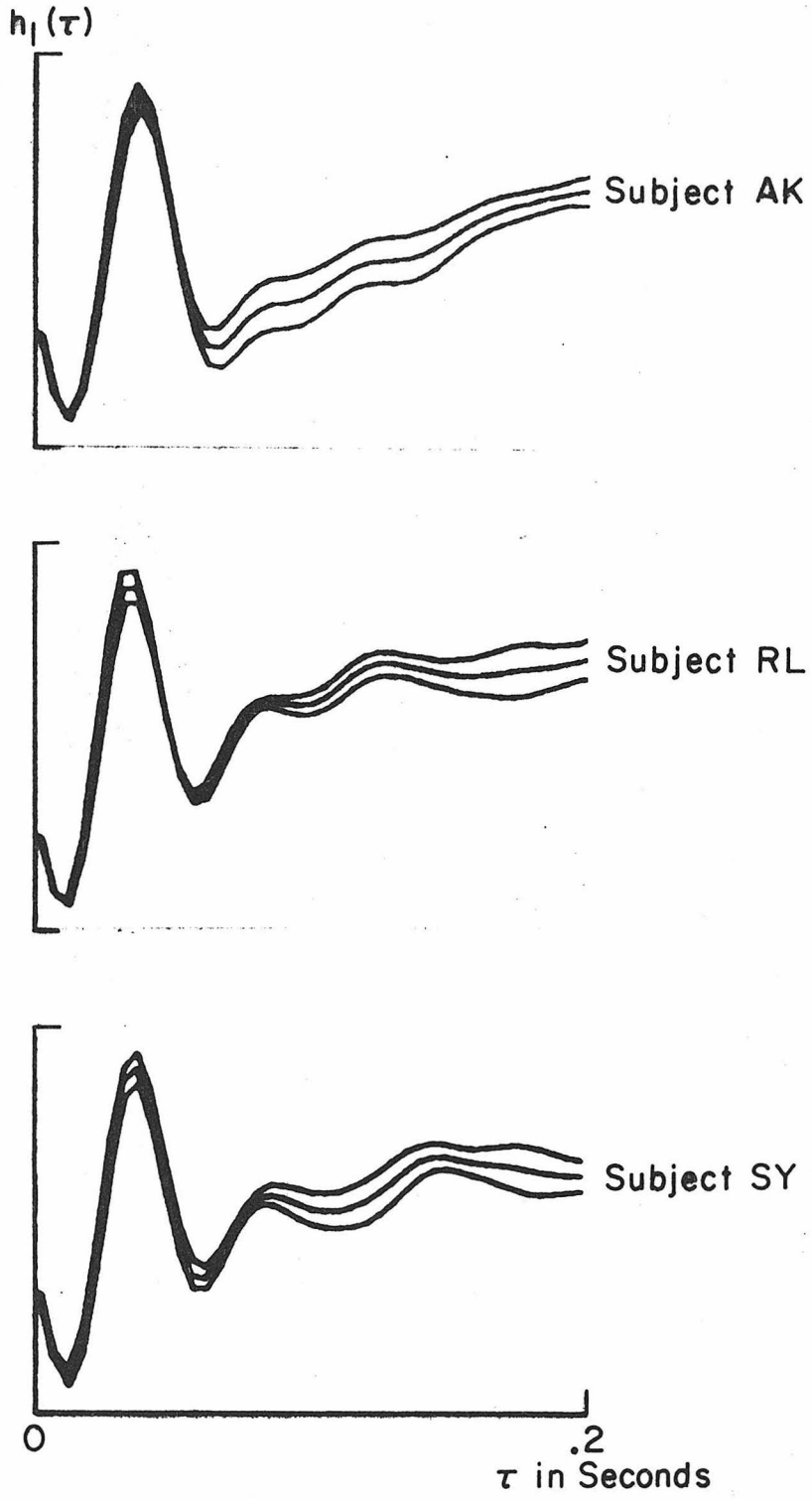

Fig. 2-5. Mean h_1 and mean ± sdm for three subjects with scales adjusted to give best match between subjects. Following figures show relative amplitudes.

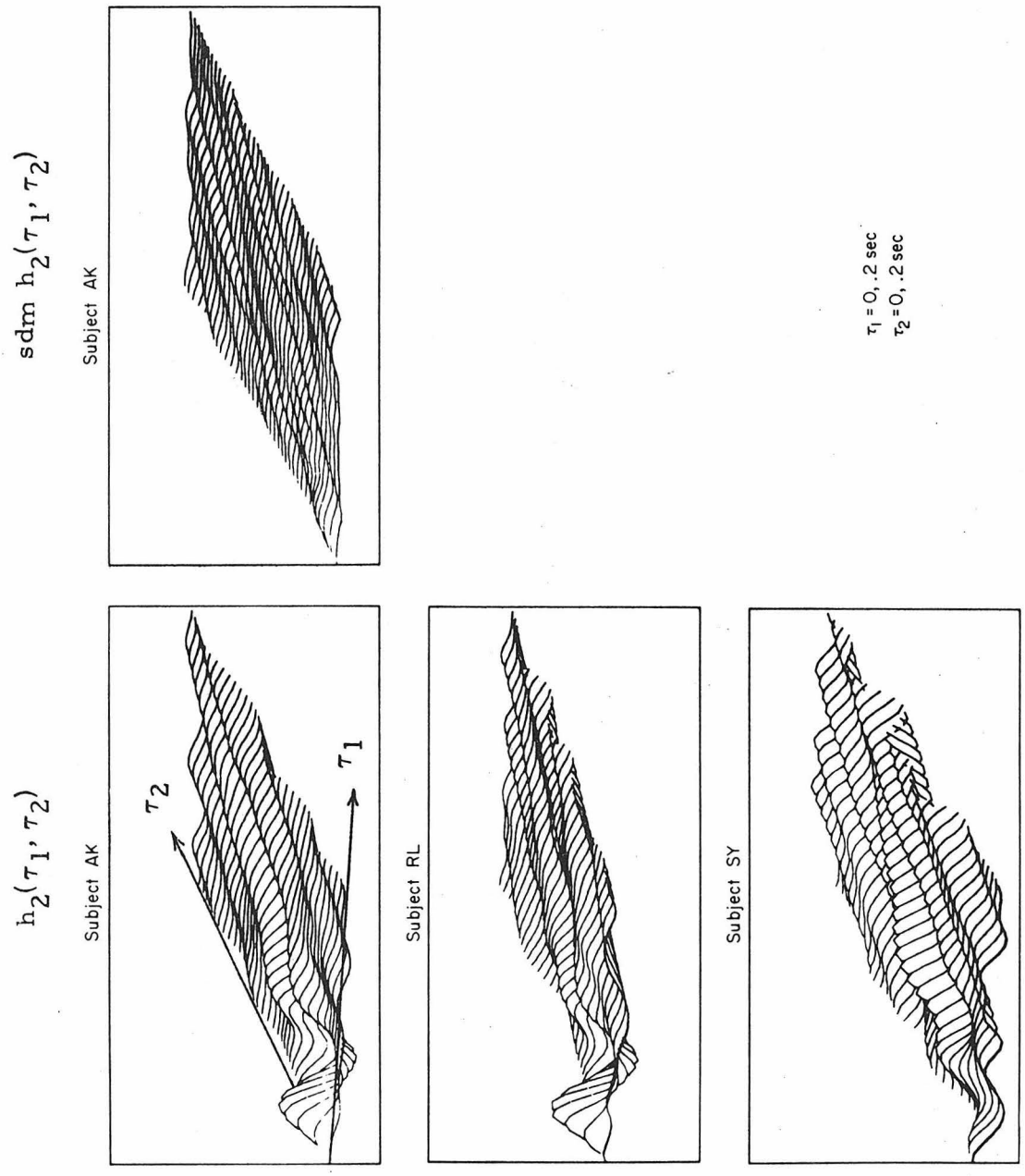

Fig. 2-6. Mean h_2 for each subject and sdm for subject AK.

Frequently, we can find sections of the random intensity response which are relatively noise-free. Fig. 2-7 shows such a section and the predictions of the response using first alone and first plus second-order kernels.

As an alternative test for the accuracy of the kernels, we used the kernels to predict the flash response recorded from the same subject.

II-4-2. Predicted versus measured flash responses

A single flash response is contaminated with the same amplitude noise as the response to the random intensity stimulus. However, averaging the responses to 30 flashes reduces the noise effects to tolerable levels. We could have just as well repeated the same random intensity stimulus 30 times and averaged these responses with similar improvements. However, we prefer to appeal to flash experimenters in this chapter.

The flash ERG was recorded as described previously, and the response obtained by simple averaging of the response to 30 repetitions of the flash. Each flash was a pulse of magnitude +42.5 td. sec. Several response curves were then averaged together to produce a mean curve and its standard deviation as shown for each subject in Fig. 2-8.

The first 75 msec of the measured and predicted responses for each subject are displayed in Fig. 2-9. The first-order kernel alone predicts the measured flash response fairly accurately; the main diagonal or principal vector of the second-order kernel improves the pre-

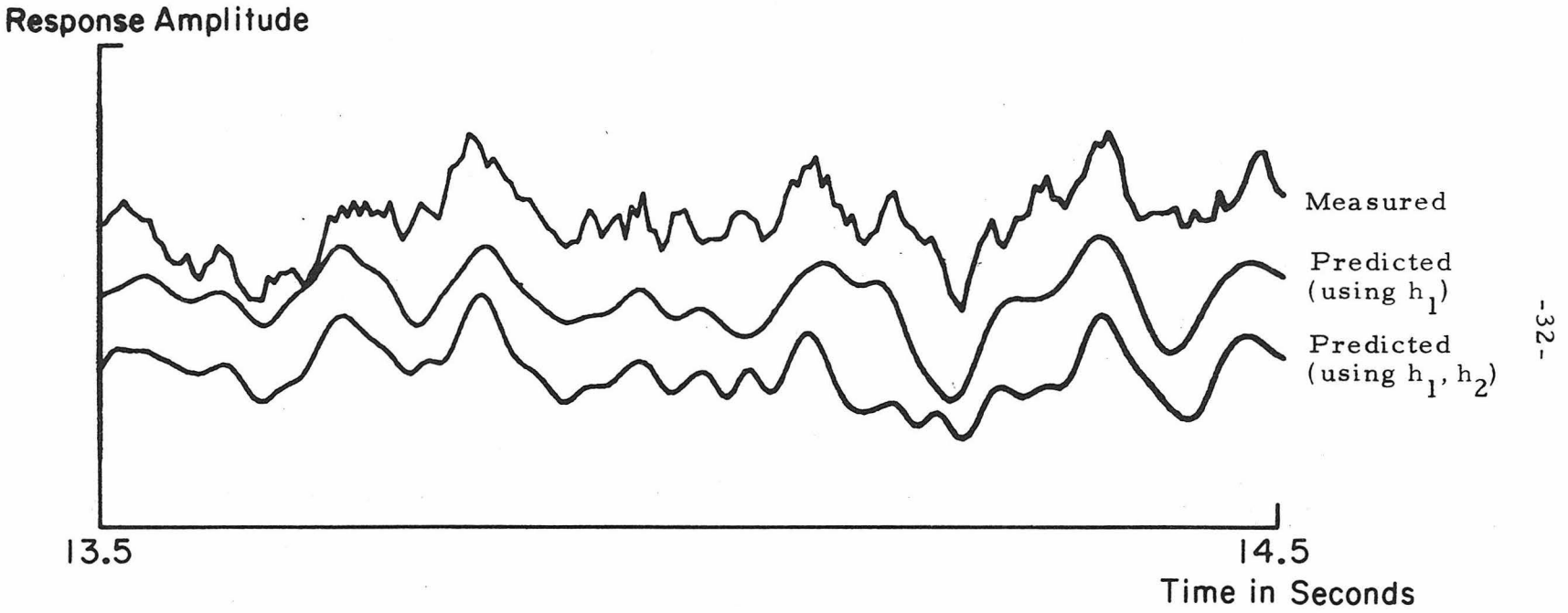

Fig. 2-7. Measured versus predicted response to quasi-random stimulus.

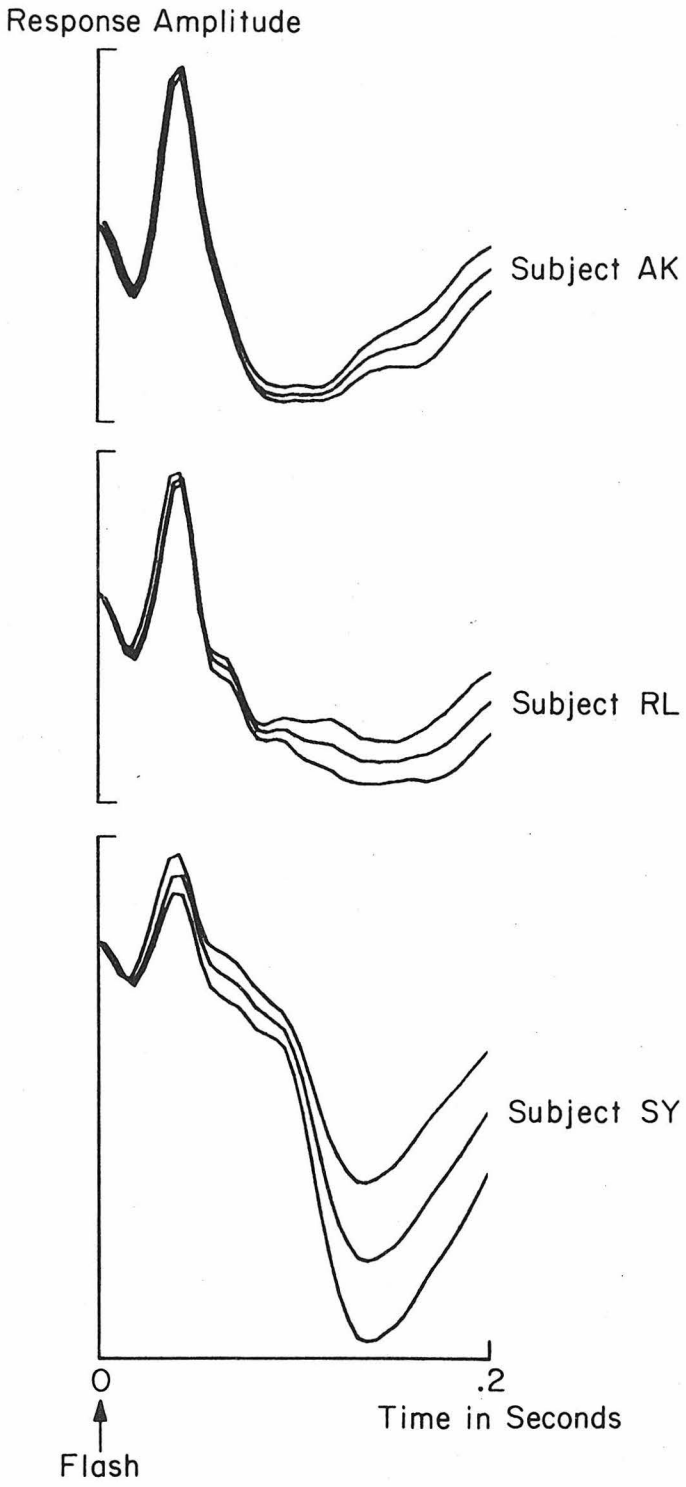

Fig. 2-8. Mean measured flash response and mean ± sdm for three subjects. The first 75 msec of the response for subject SY is slightly reduced in amplitude possibly because of retinal pigmentation differences. After 75 msec the response for subject SY is distorted by the effects of blinking.

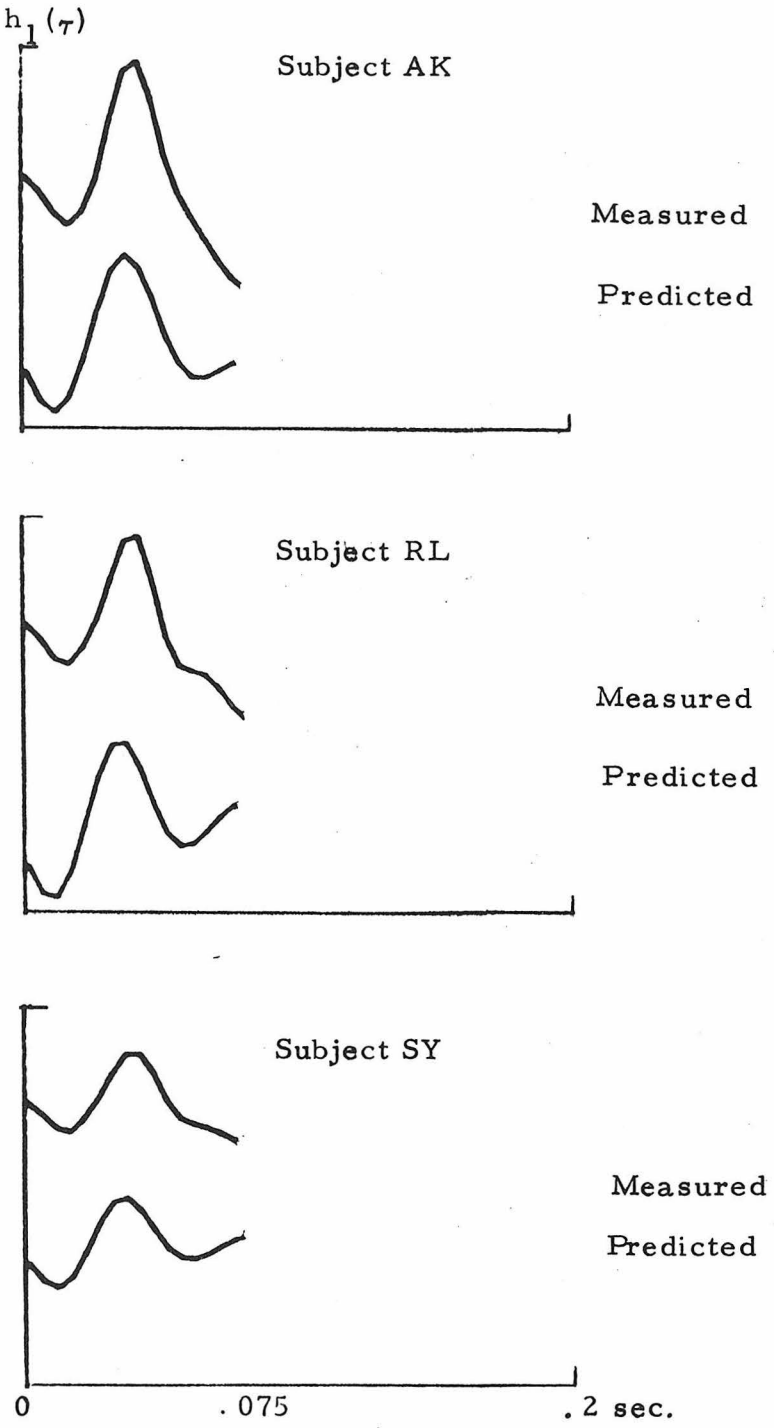

Fig. 2-9. Mean measured versus predicted responses to flash stimulus for three subjects. The first 75 msec of the measured and predicted curves match with a best scaled percent mean square error of 23 %.

diction only slightly. Discrepancies are probably caused by slight differences in the adaptation states between the random and flash experiments or by nonretinal evoked responses to the flash stimuli.

II-5. Discussion

One of the difficulties with analyzing the ERG response to flash stimuli of small amplitudes is the variability of the response, both between subjects and for the same subject.

This is often the result of poorly controlled experimental conditions rather than pitfalls in the analysis. For example, differences in retinal illumination can change both the stimulus and the system. Also, different placement of electrodes can cause different impedence and noise effects. We reduced both these artifacts without using a medriatic by providing a maxwellian view of the stimulus and by using the eyecup electrodes previously described.

These are possible errors which would have affected our kernel computations also. The inherent nature of the flash stimulus can produce other artifacts which the quasi-random procedure avoids. For example, flash stimuli are more likely to evoke nonvisual responses than the random intensity stimulus. Also large amplitude flashes test the retina with nonphysiological levels.

Figs. 2-5 and 2-6 demonstrate that the first- and second-order kernels are very reproducible. In order to achieve comparable standard deviations for the flash experiments, we found it necessary to reduce the background level to 1/10 the mean of the quasi-random stimulus (which produced small adaptation changes). In general, the kernels provide a more repeatable indication of retinal function than a flash ERG at the same stimulus level.

Furthermore, the kernels accurately predict the first 75 msec of the measured flash responses as shown in Fig. 2-9. (After 75 msec, the measured flash responses become badly distorted by noise effects.) This is evidence for the accuracy of the kernel characterization and the validity of ignoring the principal vector of higher order kernels.

The flash response was predicted using the first-order kernel and only the principal vector of the second-order kernel. Thus, the flash stimulus does not probe for any of the information concerning retinal function that is contained in all the regions of the second-order kernel below the principal vector.

Our methods improve subject comfort and produce a more reliable and efficient characterization than other known procedures. However, the analysis requires extensive computer processing. In order to make the methods more accessible to others, we have designed an inexpensive special purpose computer which will compute on-line estimates of the first- and second-order Wiener kernels (Appendix A-III).

II-6. Conclusion

We have measured the photopic human ERG with an electrode of our own design offering improvements in subject comfort and average signal/noise. First- and second-order Wiener kernels were computed for 30 second segments of a white-noise stimulus, and average flash responses were computed for sets of 30 flashes.

The first- plus second-order kernels accurately predict the first 75 msec of the measured response to flash stimuli. Our methods offer significant improvements in accuracy of the ERG characterization for the stimulus amplitudes considered.

CHAPTER III

ADAPTATION EFFECTS

III-1. Introduction

The human visual system performs remarkably well over a range of six or more decades of light illumination. Various empirical models describe the adaptation processes which adjust the sensitivity of the retina for different light conditions (Rushton, 1962). Two different mechanisms are usually considered – bleaching of receptor pigment and neural interactions.

For example, the parametric feedback model of Fuortes and Hodgkin (1964) assumes receptor signals pool together forming an input I, to one neuron junction. They assume the neural analog of a thin, leaky cable then conducts the signal a distance s with a uniform leakance α. The output V_1 of the cable is related to I_1 by the equation

$$V_1 = I_1 e^{-s\alpha} \tag{3.1}$$

next they assume that the output V_1 feeds back instantaneously to control the leakance α, i.e.,

$$\alpha = \alpha_0 + \alpha_1 V_1 \tag{3.2}$$

Thus,

$$\ell n I_1 = \ell n V_1 + s(\alpha_0 + \alpha_1 V_1) \quad . \tag{3.3}$$

Letting

$$V = s\alpha_1 V_1 \quad \text{and} \quad I = s\alpha_1 I_1 e^{-s\alpha_0} \quad , \tag{3.4}$$

we obtain

$$\ell n I = \ell n V + V \tag{3.5}$$

or

$$I = V e^{V} \tag{3.6}$$

During a bleaching adaptation process, a signal β_1 from bleached receptors can enter the model through the feedback; in this case, Eq. 3.2 becomes

$$\alpha = \alpha_0 + \alpha_1(V_1 + \beta_1) \tag{3.7}$$

and Eq. 3.6 becomes

$$I = V e^{V+\beta} \tag{3.8}$$

This final equation matches many of the experimental observations of changes in incremental threshold during bleaching adaptation.

In this chapter we will characterize the ERG response to quasi-random intensity stimuli of different mean levels of illumination. The characterization will be in the form of Wiener kernels rather than incremental threshold measurements. In the next chapter, we will use these results to construct a model for the human ERG system.

III-2. Method of Procedure

III-2-1. Equipment

The optical stimulator and eyecup electrode used for this work have been described previously. All items are unchanged for the work reported in this chapter except that the maxwellian optics and the eyecup electrode have been built together as one unit (Fig. 3-1). This unit is coupled to the primary optics through a coherent fiber-optic bundle. A second eyecup electrode measures the ERG of the unstimulated eye, and this signal is used as the reference. The eyecups are canted slightly forward so that the subject can adapt an attitude similar to that required when looking through a conventional binocular microscope. The eyecups are filled with artificial tear fluid before the subject assumes his viewing position.

A constant background is necessary for the zero-mean quasi-random stimulus. This mean can be changed in steps by inserting neutral density filters into the optical path. The amplitude of the stimulus always extends between zero and twice the mean with a gaussian distribution clipped at ± 3 standard deviations. The power spectrum is flat between .2 and 30 Hz, with a high-pass rolloff of 40 dB/decade and a low-pass rolloff of 160 dB/decade.

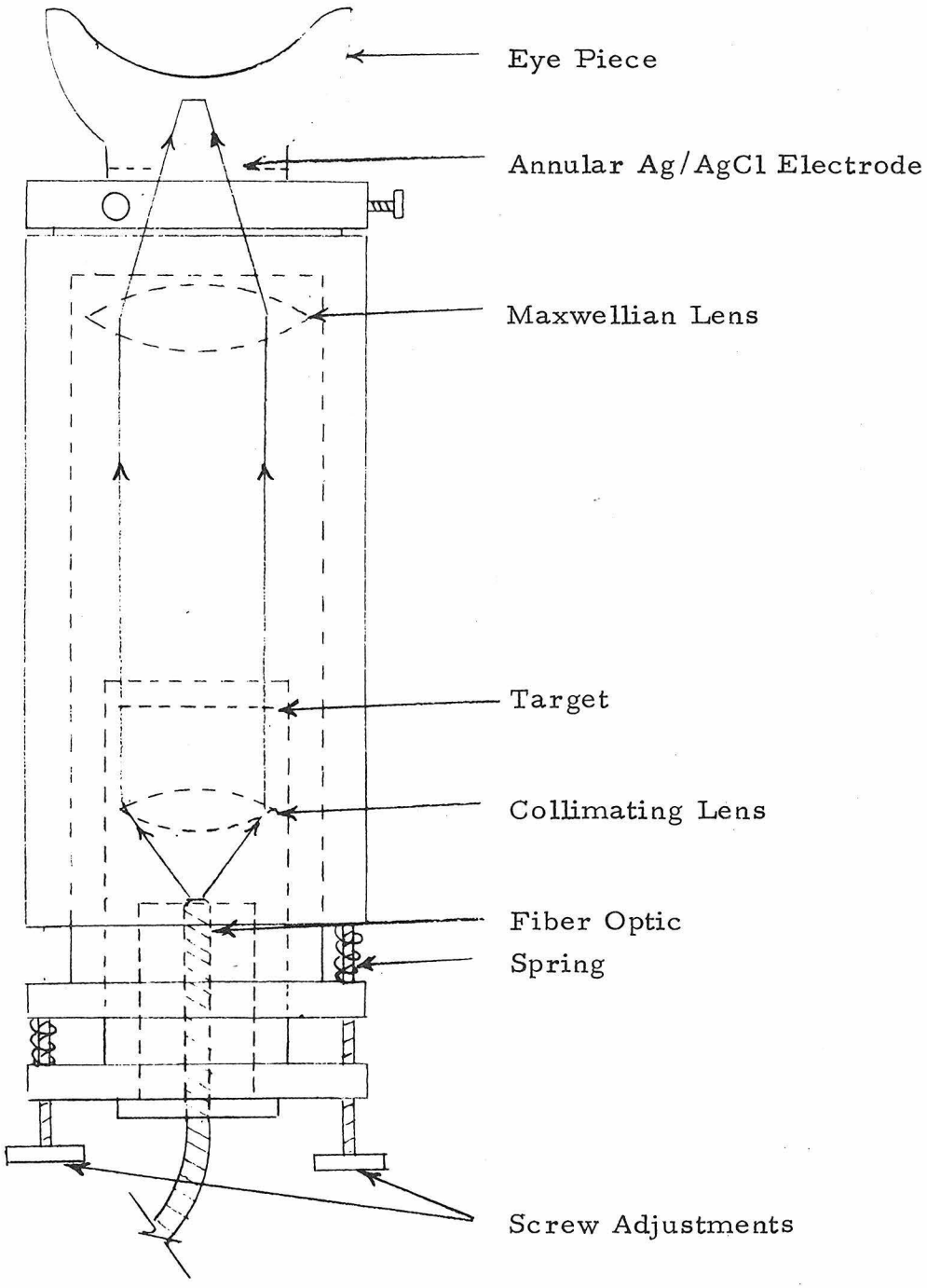

Fig. 3-1. ERG cup electrode with condensed maxwellian optical system.

III-2-2. Experimental protocol

1. Light adaptation

Three of the subjects selected were adult males with no known retinal impairment. The fourth subject was a 28 year old female with suspected retinitis pigmentosa of different progression in each eye. The ERG responses were measured from the right eye of each normal subject and from both eyes of the RP patient.

The subjects were initially exposed to ambient room illumination of less than 3 cd/m^2 for about 15 minutes. After this preliminary adaptation period, each subject looked into the maxwellian optics system which projected a 45^o maxwellian view of the quasi-random stimulus. The mean of the random stimulus was held at 85 td. for the first three minutes, then immediately changed to 850 td. for a second three minute period, and finally changed to 8500 td. for the last three minutes.

2. Dark adaptation

The three normal subjects repeated the preliminary procedures, then viewed the previous 8500 td. stimulus for five minutes. After this controlled adaptation period, the stimulus mean decreased to 85 td. and remained at this level for eight minutes while recording the ERG response continuously.

III-3. Results

Fig. 3-2 shows for one subject the mean first-order kernel ± 1 standard deviation of the mean for an ensemble of four 30 second segments of data at each intensity level. The mean second-order kernel for each level is also shown for this subject.

These results are similar for all three healthy subjects. Fig. 3-3 shows the mean first-order kernels at each level for all three subjects.

The results for the RP patient are strikingly different. Fig. 3-4 indicates substantial ERG losses in the left eye and only small losses in the right eye. The progression of the disease was previously diagnosed more advanced in the left eye, although unilateral effects are unusual for this disease. Scotopic components of the ERG were expected to be reduced for the left eye (T. Ogden, personal communication).

For the dark adaptation experiment, the data were divided into 30 second segments immediately after the 2 log decrease in mean illumination. The first-order kernels presented in Fig. 3-5 are for the first four 30 second sections for all three subjects. The corresponding second-order kernels for one subject are shown in Fig. 3-6. There is no large change with time of either the first- or second-order kernels, although the differences in dynamics between the high- and low-adaptation states are significant.

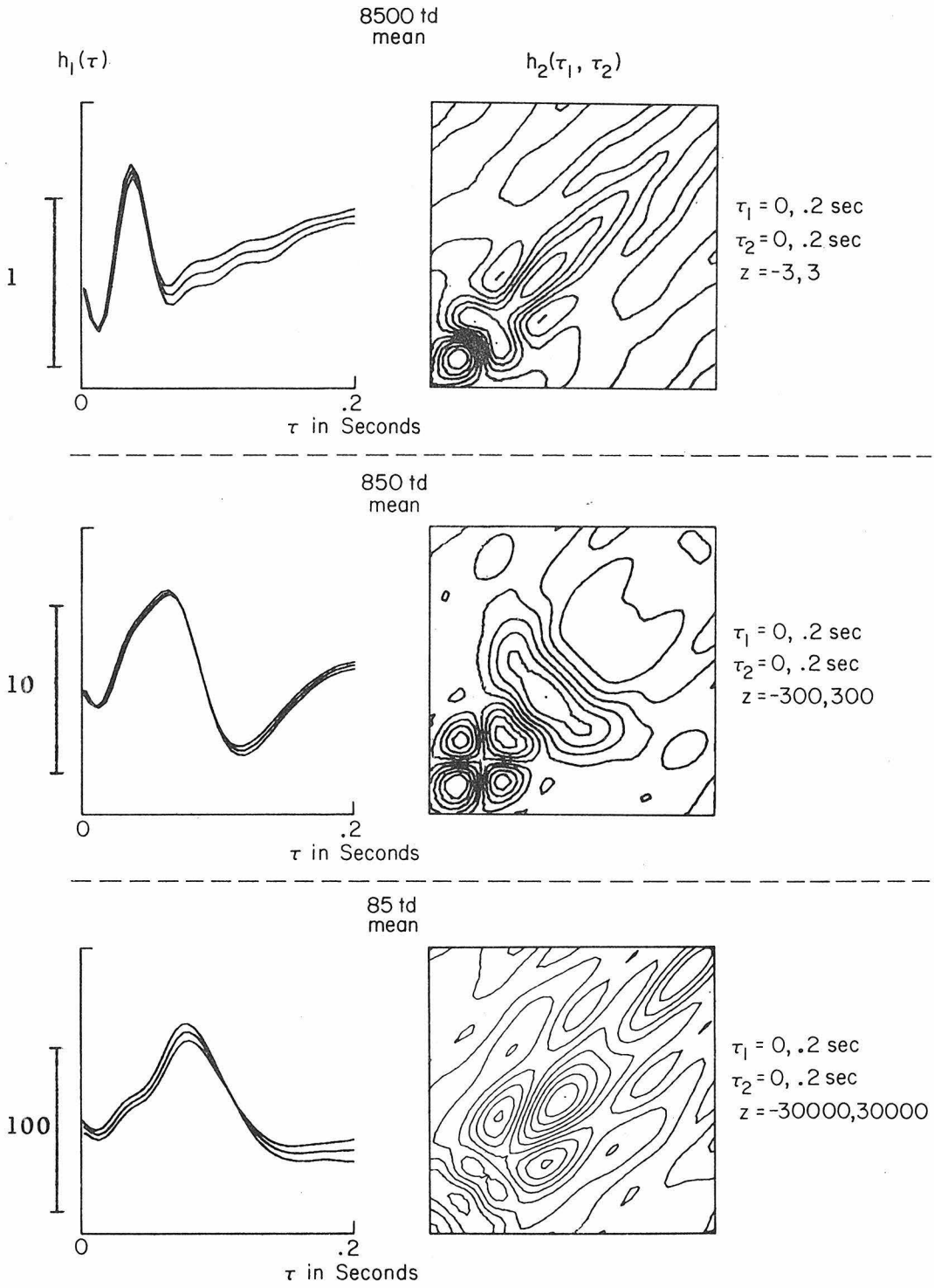

Fig. 3-2. Mean and mean ± sdm of $h_1(\tau)$ along with mean of $h_2(\tau_1, \tau_2)$ for different mean levels of quasi-random stimuli (subject AK). The numbers alongside the vertical axes of the first-order kernel plots indicate the relative size of the first-order kernels.

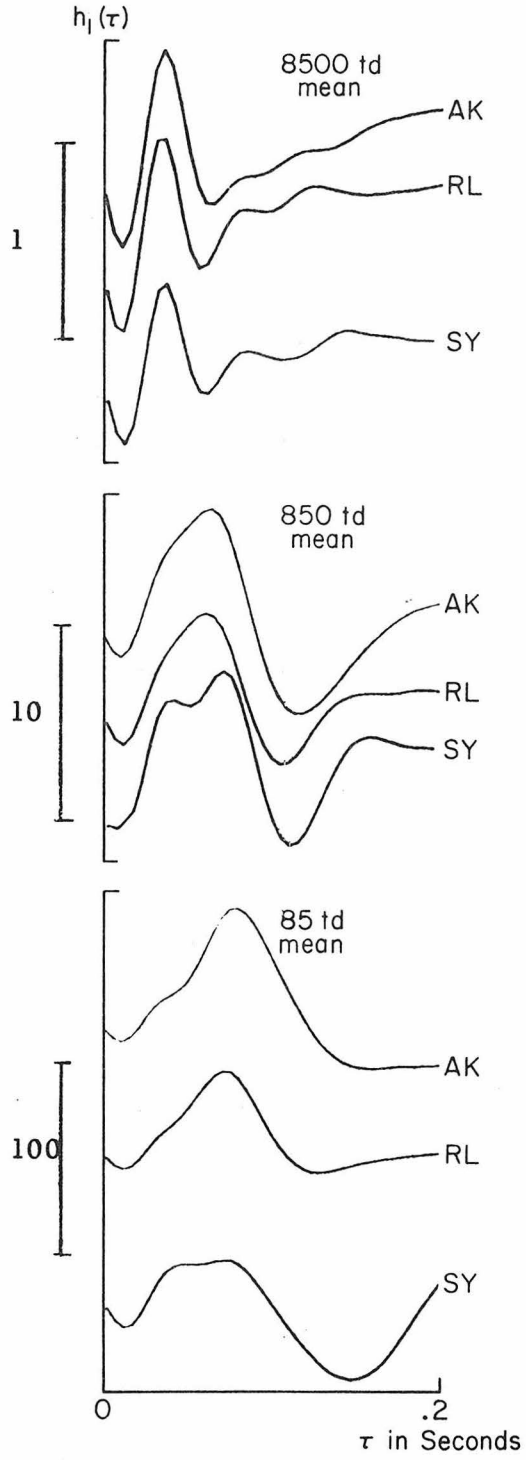

Fig. 3-3. Mean $h_1(\tau)$ for different mean levels of quasi-random stimuli for three subjects. Small differences in relative amplitudes of components are apparent for subject SY, but the large changes in overall kernel size are the same for all three subjects.

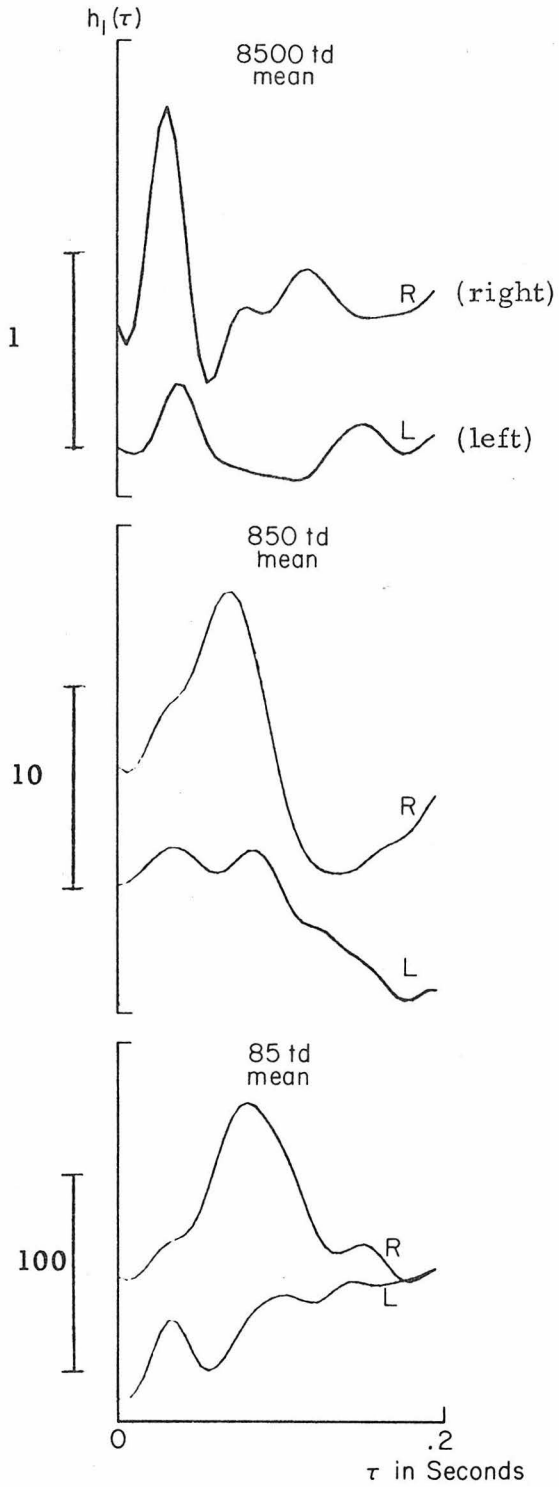

Fig. 3-4. Mean $h_1(\tau)$ for right (R) and left (L) eyes of RP patient exposed to different mean levels of quasi-random stimuli. The patient had difficulty maintaining the maxwellian view of the stimulus and also blinked frequently; therefore, the kernels are somewhat distorted by noise effects. However, the overall size of the kernels and the relative size of the presumed scotopic b-wave appear reduced in the left eye.

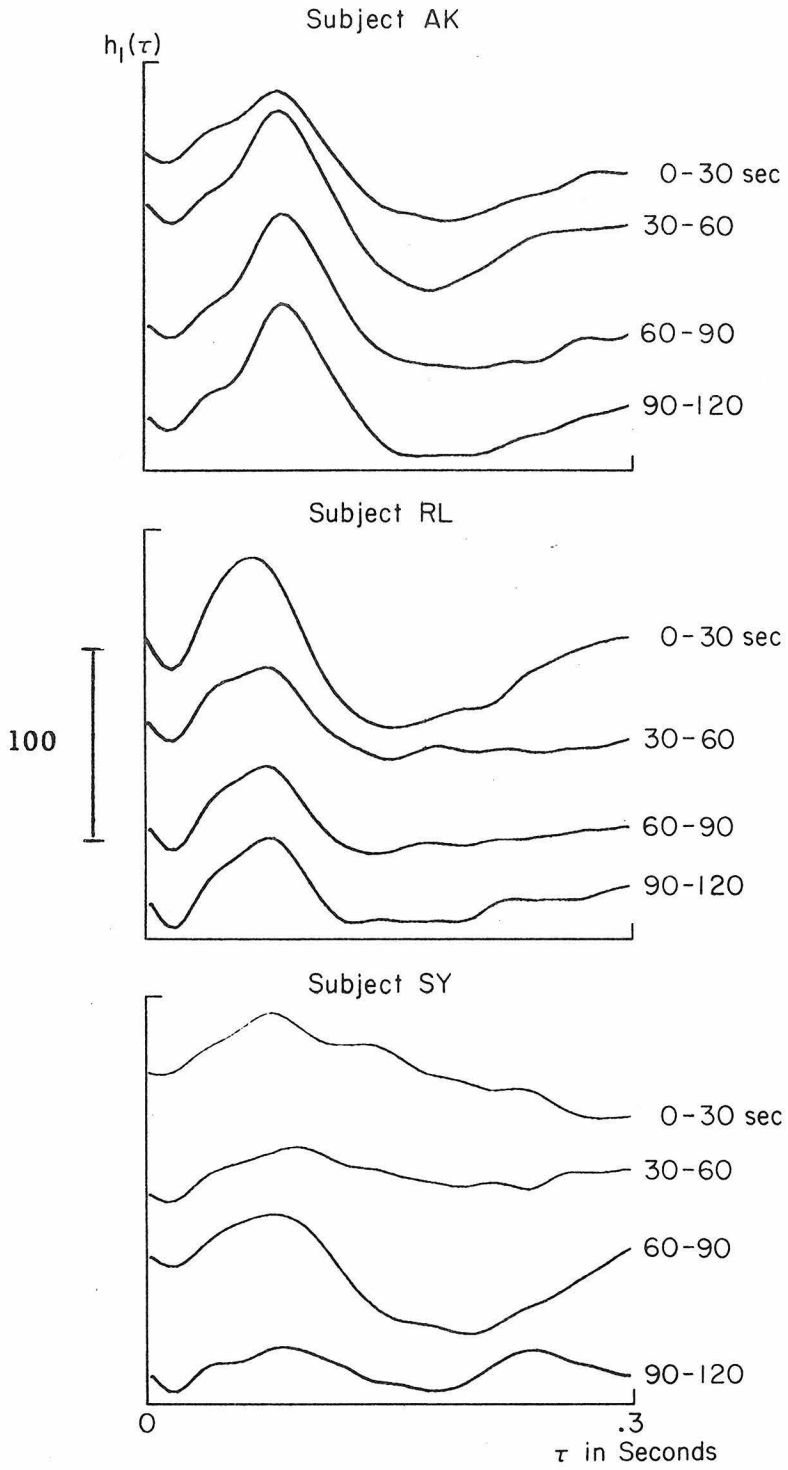

Fig. 3-6. $h_1(\tau)$ for successive 30 second intervals after 2 log step decrease in quasi-random mean, shown for three different subjects.

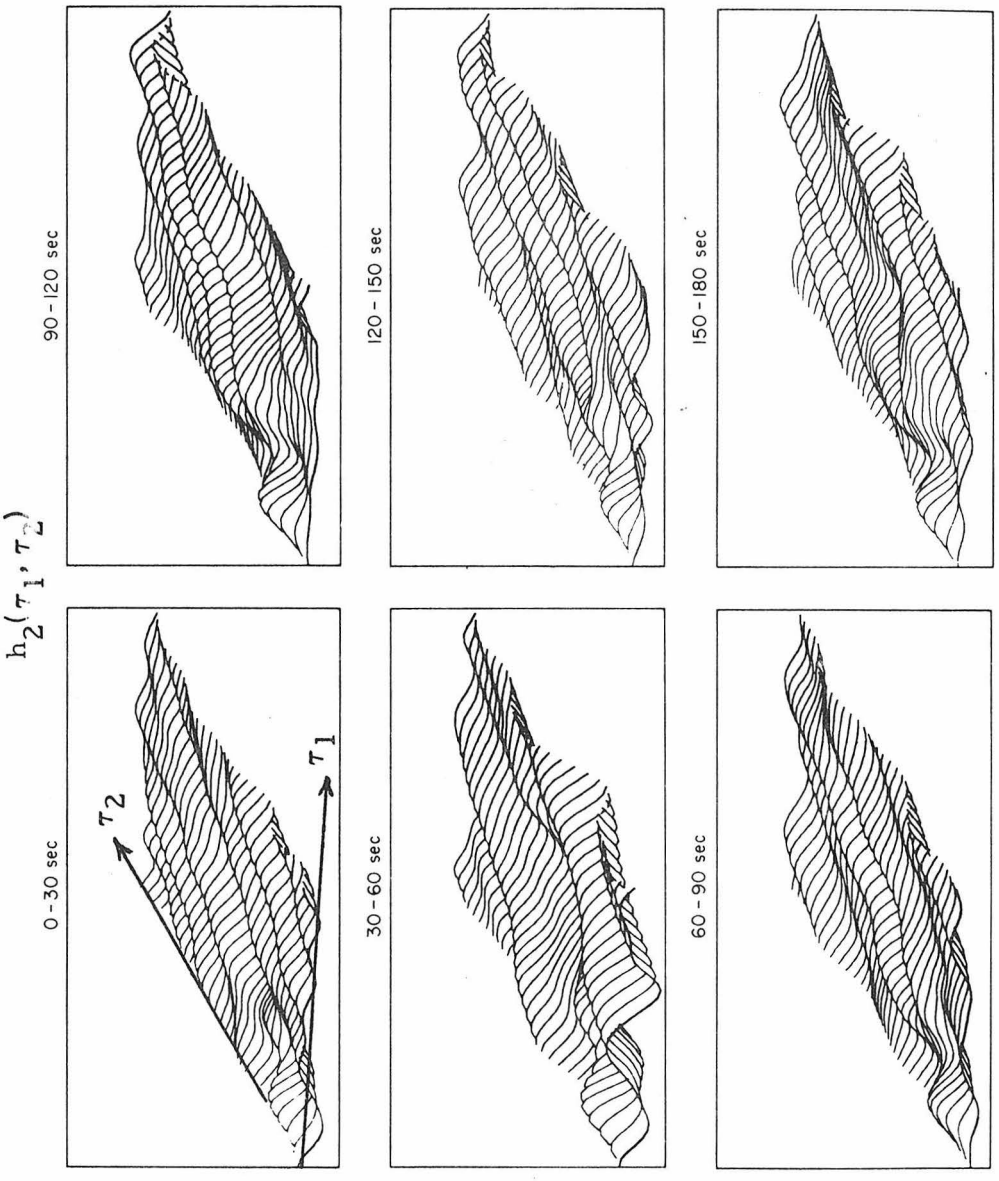

Fig. 3-7. $h_2(\tau_1, \tau_2)$ for successive 30 second intervals after 2 log step decrease in quasi-random mean (subject AK).

III-4. Discussion

We obviously want to know what the kernels mean in terms of retinal function. We have previously demonstrated that the first-order kernel plus principal vector of the second-order kernel provide a good prediction of the single-flash response. The remainder of the second-order kernel can quantify the nonlinear interaction between double-flash responses.

The first-order kernels decrease in amplitude with increasing stimulus mean reflecting a decrease in retinal sensitivity. The first-order kernels also reflect differentiable photopic and scotopic components, analogous to single-flash responses. As the mean of the stimulus decreases, a second distinct (presumed scotopic) b-wave appears with increasing latency, and the amplitudes of the photopic a- and b-waves decrease (Chaffee and Hampson, 1923). The latencies of the photopic a- and b-waves do not change much with stimulus mean, for the range of stimulus amplitudes tested, which supports the functional model described in Chapter IV for the photopic system.

The results for the RP patient provide more evidence for a distinct scotopic b-wave. Retinitis pigmentosa produces functional and morphological changes in receptor and pigment epithelial layers. Tight junctions are destroyed which changes the impedence properties of the retina. The first-stage symptoms involve night blindness which suggest larger scotopic than photopic losses. The first-order kernels computed for her left eye indeed show a reduced scotopic b-wave.

The same trend is apparent for the second-order kernels, i.e., larger amplitudes and latencies result from stimuli of smaller mean levels. However, it is difficult to identify distinct photopic and scotopic components.

The dark adaptation experiment was performed to estimate the time constant of the change in dynamics observed between the high- and low-adaptation states. The time constant expected for the regeneration of rhodopsin is about 7.5 minutes (Rushton, 1962), but steady-state bleaching differences between these two levels should amount to only a few percent. Nevertheless, small changes at the first stage of the retinal system can cause large changes in overall observed dynamics (as discussed in Chapter IV).

Figs. 3-6 and 3-7 demonstrate qualitatively that the changes observed in dynamics occur too quickly to be resolved by the kernels. This rapid change must involve mechanisms other than pigment bleaching. The mechanism suggested in Chapter IV is the variation of a first stage linear filter for different stimulus levels.

III-5. Conclusion

The first- and second-order Wiener kernels change significantly for a step increase or decrease in stimulus mean. The component amplitudes and latencies of the kernels increase as the stimulus mean decreases, and a presumed scotopic b-wave appears as a distinct component of the first-order kernel for low stimulus means.

The changes in dynamics for different adaptation states results from some mechanism other than pigment bleaching. Further experiments and a functional interpretation of the first- and second-order kernels are described in the next chapter.

CHAPTER IV

MODEL FOR ADAPTATION EFFECTS

IV-1. Introduction

In the previous chapter we characterized the human ERG for different light adaptation states using the Wiener functional expansion. The first- and second-order kernels change significantly after a step increase or decrease in mean of the quasi-random stimulus. We will now compile experimental results in order to contrive a small-signal model for the human ERG which reproduces these adaptation effects and offers a functional interpretation of the kernels.

IV-2. Photopic Versus Scotopic Components

In Chapter III we suggested that the first-order kernel contains a second distinct b-wave at scotopic stimulus levels. This component decreases in amplitude and latency as the stimulus mean increases. We also tested an RP patient with suspected scotopic losses and observed first-order kernels with the second b-wave attenuated.

Similar changes in system dynamics are observed when the background level is changed for flash plus background stimuli. Fig. 4-1 displays average flash responses for 8500 td. flashes and 5 msec duration superimposed on different background levels.

In Chapter V we will describe differences in first-order kernels dependent on the wavelength of the quasi-random stimulus. A red (663 nm) stimulus does not produce the second b-wave, whereas a blue (423 nm) or green (494 nm) stimulus does.

As a further test for the validity and meaning of the first-order kernel, we repeated the quasi-random experiment of Chapter III for a stimulus mean equal to 850 td. and different stimulus bandwidths. Fig. 4-2a shows the first-order kernel for the increased stimulus bandwidth of $[.2, 45\ \text{Hz}]$. Curve b of the same figure is the first-order kernel for the normal stimulus bandwidth of $[.2, 30\ \text{Hz}]$. We expect the increased bandwidth to provide additional stimulus energy to cone systems without changing the stimulus to rod systems (Fricker, 1969) and to increase the frequency resolution of the kernel computations.

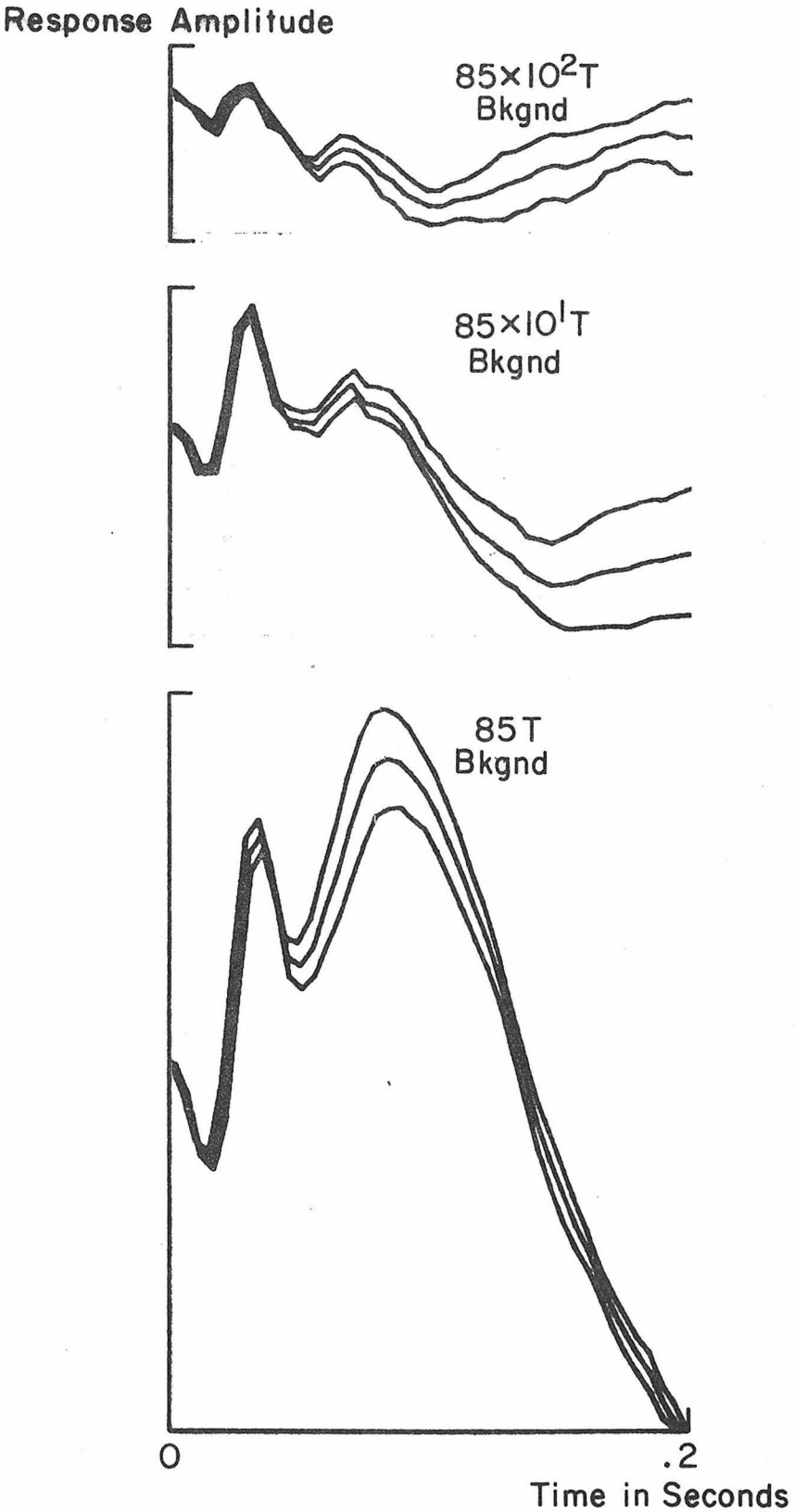

Fig. 4-1. Mean flash response and mean ± sdm for different background levels. Flash amplitude = 85×10^2 T.

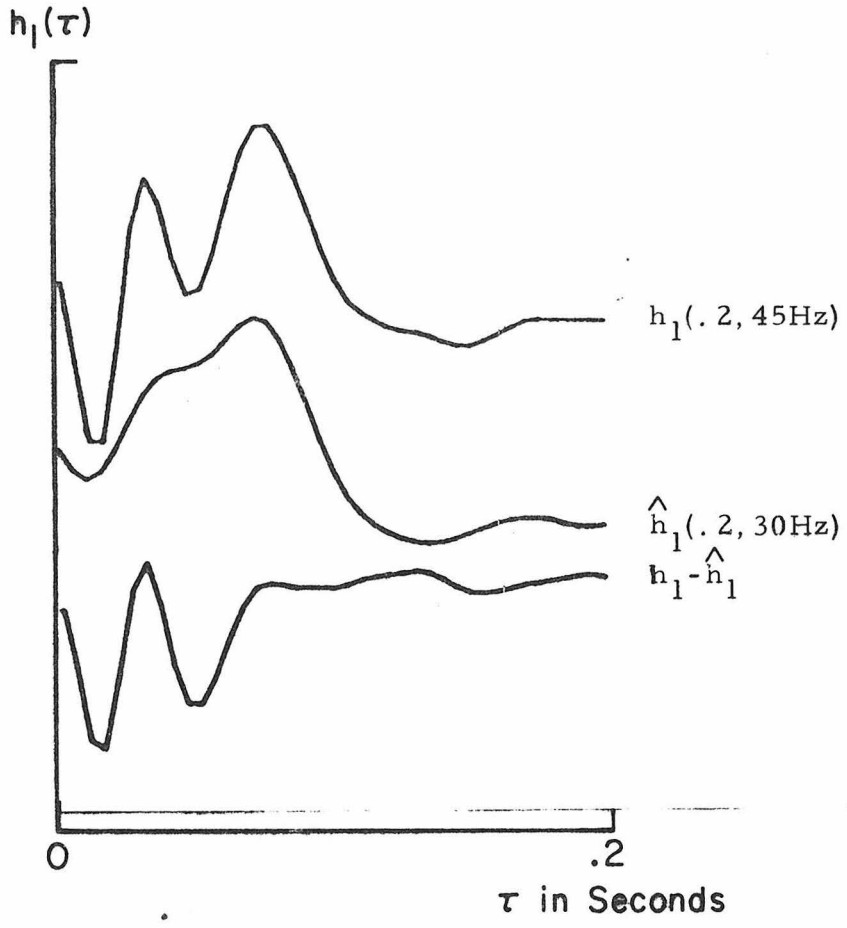

Fig. 4-2. Dependence of $h_1(\tau)$ on stimulus bandwidth for the same stimulus mean (8500 td.). $(h_1 - \hat{h}_1)$ shows increased frequency resolution plus enhancement of photopic components.

Fig. 4-2 shows a significant difference between h_1 and $\hat{h}_1$. The increased bandwidth does not introduce new components to the first-order kernel, but it does seem to increase the size of the claimed photopic components. This also indicates wider bandwidths are more appropriate for studies at photopic levels (Chapter V).

IV-3. Rapid Changes of First-Order Kernel

The first- and second-order kernels change significantly with changes in stimulus mean. As the stimulus mean increases, both photopic and scotopic components decrease in size and scotopic components decrease in latency. This indicates a decrease in retinal sensitivity.

The kernels seem to change suddenly after a step change in stimulus mean, but how suddenly? In Chapter III, we determined that the change must be completed in less than 30 seconds after a .2 log decrease in mean. The following experiment attempts to resolve whether the response reflects only the instantaneous level of the stimulus.

Flashes of amplitude 8500 td. and 5 msec duration were superimposed with spatial equality onto a quasi-random stimulus of mean 850 td., 100% relative depth of modulation, and [.2, 30 Hz] bandwidth. Fig. 4-3a shows the average response for a previous experiment, when the same flashes were superimposed on a constant background of 850 td. Fig. 4-3b shows the average flash response for flashes superimposed on the quasi-random background triggered to occur when the quasi-random signal reached its mean level, with a maximum flash rate of one per second. Fig. 4-3c shows the average flash response when the trigger level was set at the zero level of the quasi-random signal.

Curve a is very similar to curve b. In these two cases, the instantaneous background levels are the same. However, curve c

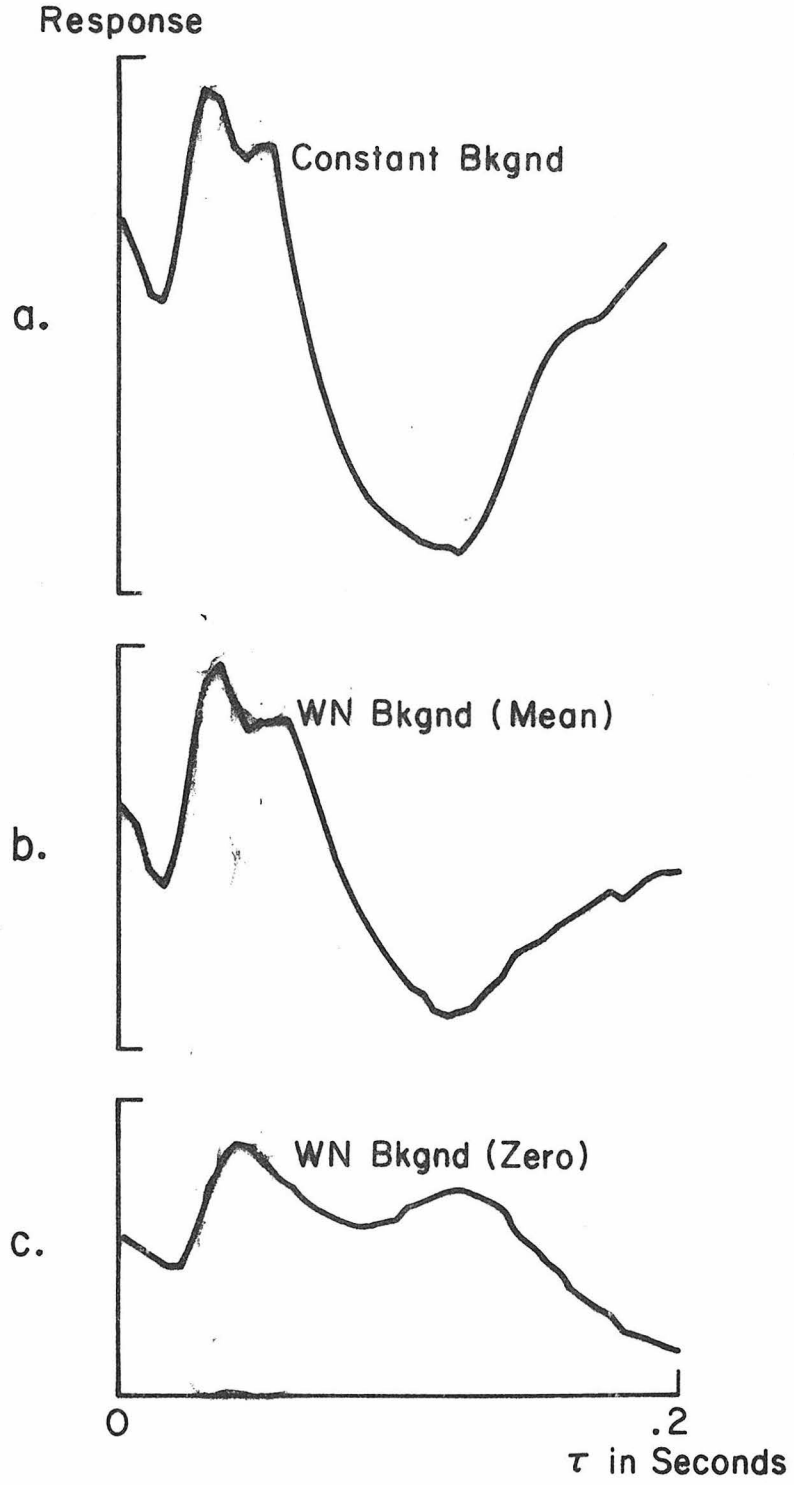

Fig. 4-3. Mean flash responses for constant and for random backgrounds. A specific level of the random background triggers the flashes.

reflects a lower adaptation state. Hence, the flash response changes with the background level with a short time constant. We could accurately estimate this time constant using sine-wave backgrounds, but it is sufficient for our model to claim a time constant much less than 1/.2 Hz = 5 sec, where .2 Hz is the lowest significant frequency contained in the quasi-random stimulus.

IV-4. A Photopic Model

In Chapter II, we described experiments which tested the ERG system at stimulus levels which produced a relatively small scotopic response. These and other experiments demonstrated that the dynamics of the photopic system do not change with changes in stimulus parameters for the stimulus amplitudes tested — only the amplitude of the photopic response changes.

We can further test this feature of the photopic system by comparing first-order kernels for quasi-random stimuli of different relative depths of modulation. Fig. 4-4 displays first-order kernels for a quasi-random mean equal to 8500 td. with 100%, 50% and 25% relative depths of modulation.

The first-order Wiener kernel increases in size as the depth of modulation decreases, but does not change shape. This is evidence for the significance of higher odd order Wiener kernels (G. D. McCann, personal communication) since the first-order Wiener kernel can be defined in terms of odd order Volterra kernels with contributions of higher order Volterra kernels scaled by factors dependent on the stimulus power (Yasui, 1975). Furthermore, the amplitude is a nonlinear function of the stimulus depth of modulation. These characteristics can be reproduced by the model in Fig. 4-5a which depicts a nonlinear system without memory followed in series by a linear system with memory.

Decreasing the relative depth of modulation should decrease the significance of ignored higher order Wiener kernels. However, decreasing the modulation also reduces the signal/noise of the

measured response, making the computed first-order kernels less reliable. For the results presented the first-order kernel predicts the response equally well for all three modulation cases, i.e., 98% mse between the measured and predicted response.

We could estimate the nonlinear relationship between x and y simply by providing pulses of different amplitude at x and measuring the amplitude of the response z. That is, a pulse at x produces a pulse at y of different amplitude and the response z is proportional to the amplitude of y. Unfortunately, pulse responses cannot be measured accurately at the stimulus levels of interest.

We can also estimate the nonlinear operator using quasi-random stimuli of different depths of modulation. Fig. 4-5b presents a plot of the expected relationship between x and y from the kernel data of Fig. 4-4.

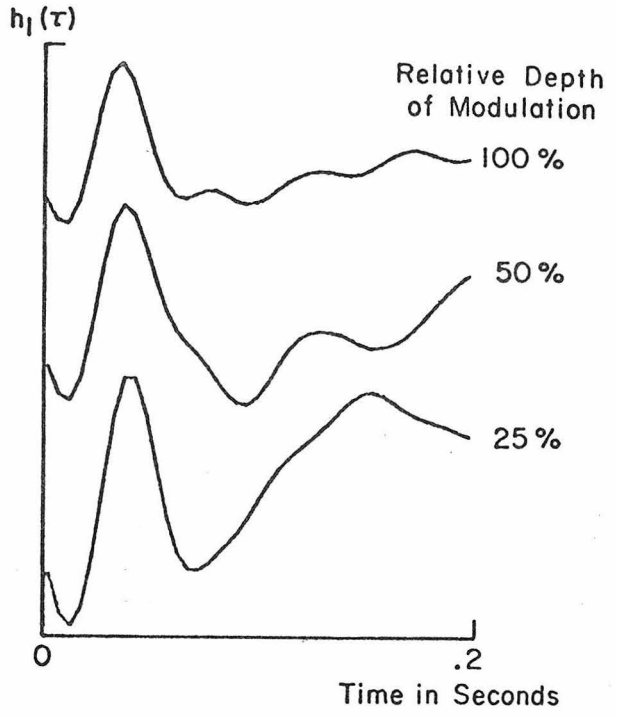

Fig. 4-4. Different $h_1(\tau)$ for quasi-random inputs with different percent relative depth of modulation, but same mean level.

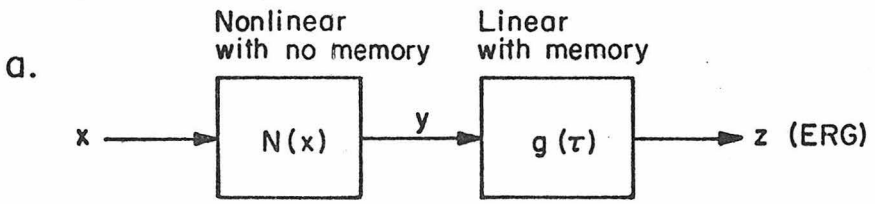

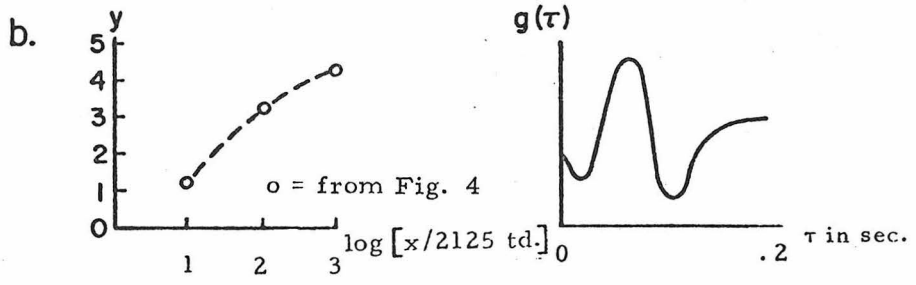

Fig. 4-5. (a) Photopic model.
(b) Characteristics of the elements of the photopic model.

IV-5. A Scotopic Model

We have emphasized that the scotopic components of the kernels change in both size and latency with changes in stimulus parameters. The model of Fig. 4-5 does not account for these observed changes in dynamics. What is more, this model produces a second-order kernel that is zero everywhere except along the main diagonal (Marmarelis, 1975).

We could account for the scotopic observations by reversing the order of the stages in the photopic model, but this arrangement is not as functionally appealing. The model of Fig. 4-6 accounts for scotopic effects and simply adds an additional stage to the photopic model. The new stage is simply a linear integrator with a variable stop. Changing the position S of this stop is analogous to changing the critical period of the receptors. The first- and second-order kernel dynamics change significantly for only small changes in the stop position. The photopic model results when S is set equal to zero. Fig. 4-7 displays measured first- and second-order kernels for a typical human subject alongside kernels which characterize the scotopic model for different S.

The second- and third-order Wiener kernels provide additional evidence for the ordering of stages as in the scotopic model. First, large positive and negative values of the second-order kernels are located along the main diagonal as displayed in previous chapters,

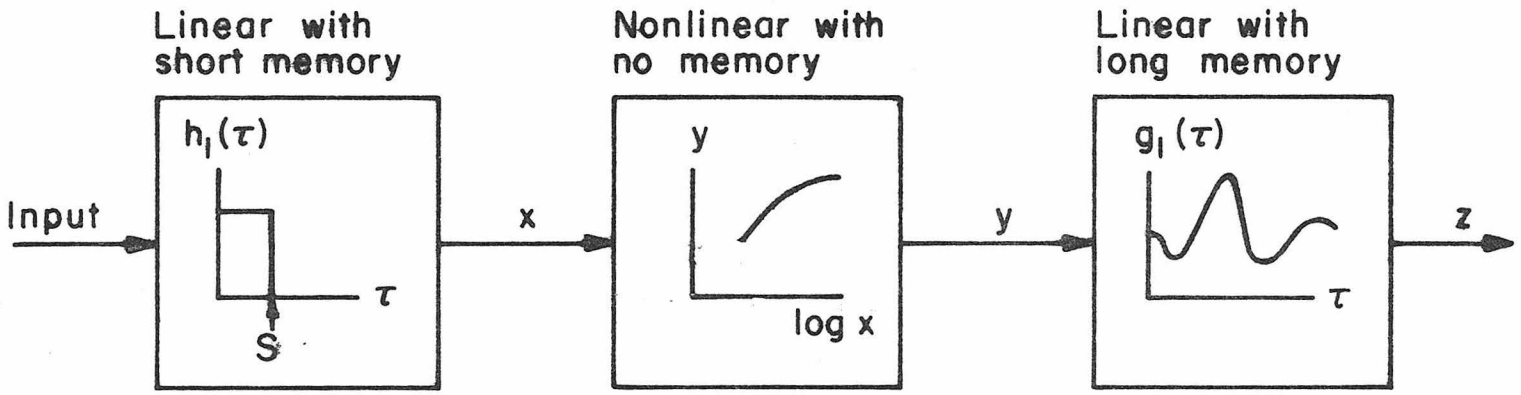

Fig. 4-6. Scotopic model.

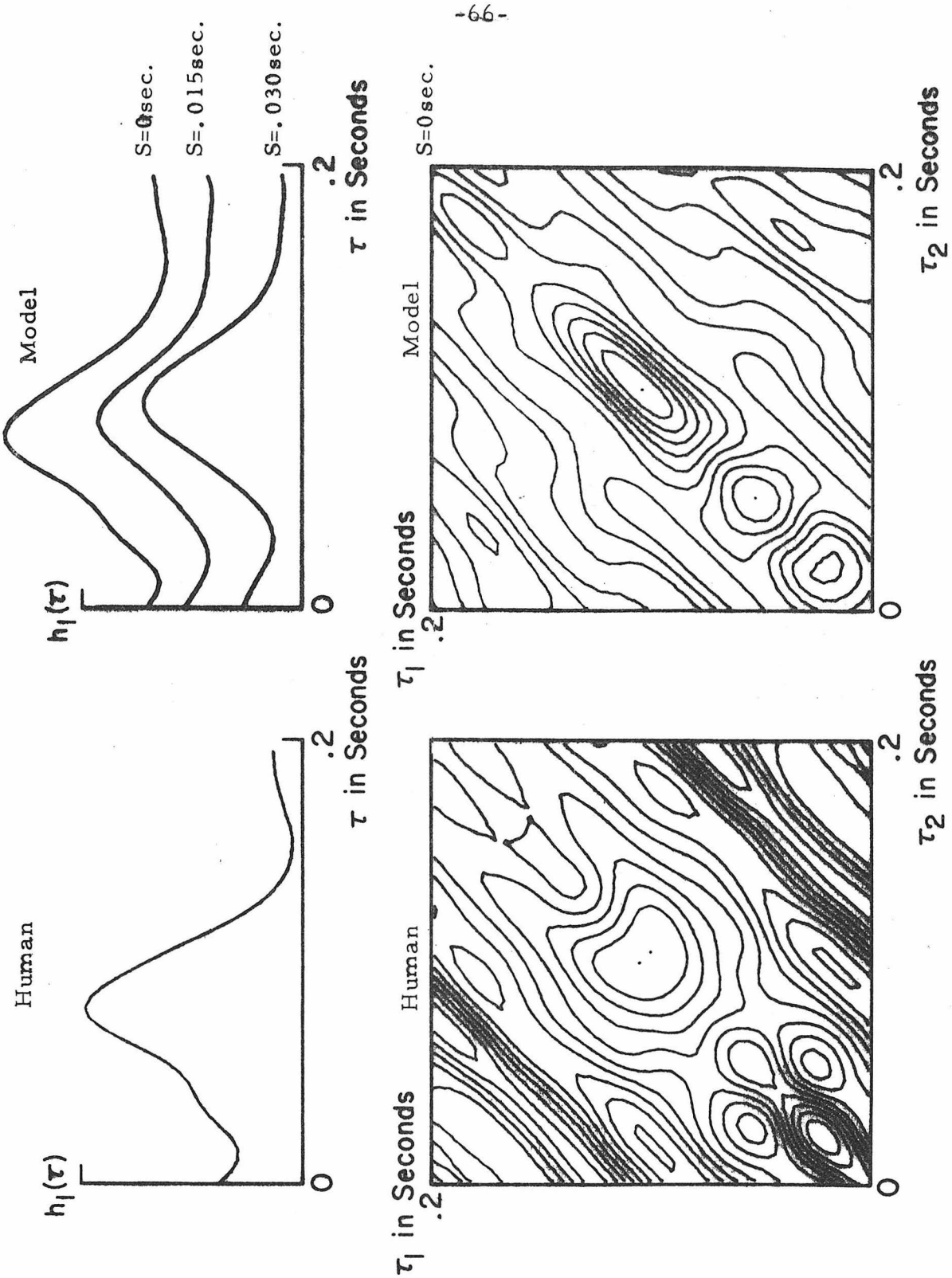

Fig. 4-7. First- and second-order kernels for human versus scotopic model. Model kernels shown for different settings S of integrator stop.

e. g., Chapter II, Fig. 2-6. Second, the main diagonals of both second- and third-order kernels have the same shape as the corresponding first-order kernel, except that the second-order main diagonal is of opposite polarity. This is demonstrated in Fig. 4-8 for one subject. If the nonlinear operation is a log transformation, then the Taylor series expansion of the log function indicates the observed polarity differences of the main diagonals.

Unfortunately, there is no unique functional interpretation of the Wiener kernel, and there are regions of the second-order kernel not described by the proposed models. If the linear operations of the integrator stage become more complex, then some of the structure of the second-order kernel away from the main diagonal can be accounted for (S. Klein and S. Yasui, personal communication). However, it is impossible to construct any simple model which uniquely describes the ERG system.

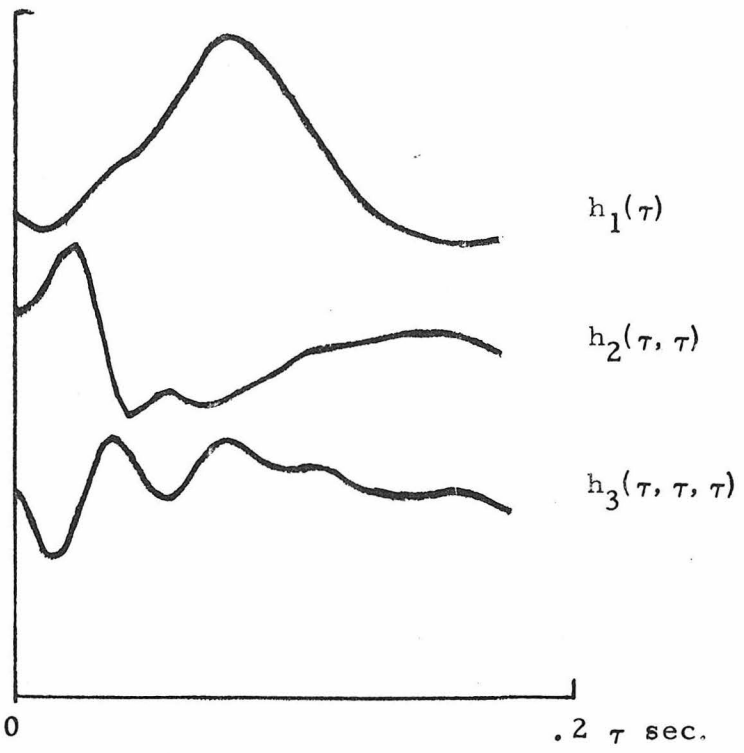

Fig. 4-8. First-order kernel (scotopic), second-order kernel main diagonal (photopic) and third-order kernel main diagonal (photopic) for subject AK.

CHAPTER V

COLOR PROCESSING

V -1. Introduction

We have previously reported the results of using Wiener kernels to characterize the human ERG for single quasi-random inputs. The kernels reflect the linear nature of the ERG system, e. g., the response to a single flash. They also reflect nonlinear operations, e. g., the nonlinear interaction between two or more flash responses.

A similar characterization procedure is possible for two simultaneous random inputs (P. Marmarelis, 1972). The nonlinear interaction between the two systems producing the responses is apparent from kernels computed by multiple cross-correlations between the response and both quasi-random stimuli. This is a simple scheme for analyzing the cross-talk between separate color systems of the retina.

We have measured the human ERG responses to one and to two simultaneous quasi-random light stimuli of different wavelengths. Different single color inputs produce kernels with different temporal characteristics. The two-input results could indicate cross-talk

between receptor systems, but this is not apparent because of the dominant effects of each receptor system receiving inputs from both stimuli.

V -2. Theory

Wiener (1958) defined the response y to a gaussian white-noise input u in terms of the following functional expansion:

$$y(t) = c + \int_0^\infty h_1(\tau)\, u(t-\tau)\, d\tau + \iint_0^\infty h_2(\tau_1, \tau_2)\, u(t-\tau_1)\, u(t-\tau_2)\ d\tau_1\, d\tau_2 + \ldots \quad (5.1)$$

where c is a constant and h_n are kernels which completely characterize the system. This expansion is valid for finite-memory, time-invariant systems, which describes most biological systems during steady-state operations.

P. Marmarelis (1972) extended the above expansion for two independent white-noise inputs u and v

$$\begin{aligned} y_{uv}(t) = c &+ \int_0^\infty h_1(\tau)\, u(t-\tau)\, d\tau + \int_0^\infty h_1(\tau)\, v(t-\tau)\, d\tau \\ &+ \iint_0^\infty h_2(\tau_1, \tau_2)\, u(t-\tau_1)\, u(t-\tau_2)\, d\tau_1\, d\tau_2 \\ &+ \iint_0^\infty h_2(\tau_1, \tau_2)\, v(t-\tau_1)\, v(t-\tau_2)\, d\tau_1\, d\tau_2 \\ &+ 2\iint_0^\infty h_2(\tau_1, \tau_2)\, u(t-\tau_1)\, v(t-\tau_2)\, d\tau_1\, d\tau_2 \\ &+ \ldots \end{aligned} \quad (5.2)$$

If we consider the summation of responses to single inputs,

$$\begin{aligned} y_u + y_v = k &+ \int_0^\infty h_{1_u}(\tau)\, u(t-\tau)\, d\tau + \int_0^\infty h_{1_v} v(t-\tau)\, d\tau \\ &+ \iint_0^\infty h_{2_u}(\tau_1, \tau_2)\, u(t-\tau_1)\, u(t-\tau_2)\, d\tau_1\, d\tau_2 \end{aligned}$$

$$+\iint_0^\infty h_{2_v}(\tau_1, \tau_2)\, v(t-\tau_1)\, v(t-\tau_2)\, d\tau_1\, d\tau_2$$

$$+ \ . \ . \ . \qquad (5.3)$$

then we are led to conclude

$$y_{uv} = y_u + y_v + 2\iint_0^\infty h_{2_{uv}}(\tau_1, \tau_2)\, u(t-\tau_1)\, v(t-\tau_2)\, d\tau_1\, d\tau_2 + \ . \ . \ . \qquad (5.4)$$

The last term or cross-kernel shown in Eq. 5.4 can be interpreted as the effect of interactions between parallel systems, as depicted by Fig. V-1a.

If the cross-talk involves a simple addition of inputs as shown in Fig. 5-1b, then we can define the response in terms of kernels for systems A and B,

$$\begin{aligned} y_{uv}(t) = c &+ \int_0^\infty h_{1_A}(\tau)\left[u(t-\tau_1) + v(t-\tau_1)\right] d\tau_1 \\ &+ \int_0^\infty h_{1_B}(\tau)\, v(t-\tau)\, d\tau_1 \\ &+ \int_0^\infty h_{2_A}(\tau_1, \tau_2)\left[u(t-\tau_1)\, u(t-\tau_2) + v(t-\tau_1)\, v(t-\tau_2)\right. \\ &\qquad \left. + 2\, u(t-\tau_1)\, v(t-\tau_2)\right] d\tau_1\, d\tau_2 \\ &+ \int_0^\infty h_{2_B}(\tau_1, \tau_2)\, v(t-\tau_1)\, v(t-\tau_2)\, d\tau_1\, d\tau_2 \end{aligned} \qquad (5.5)$$

The cross-correlations of interest are

$$\frac{1}{p} E\left\{y_{uv}(t)\, u(t-\tau)\right\} = h_{1_A}(\tau)$$

$$\frac{1}{p} E\left\{y_{uv}(t)\, v(t-\tau)\right\} = h_{1_A}(\tau) + h_{1_B}(\tau)$$

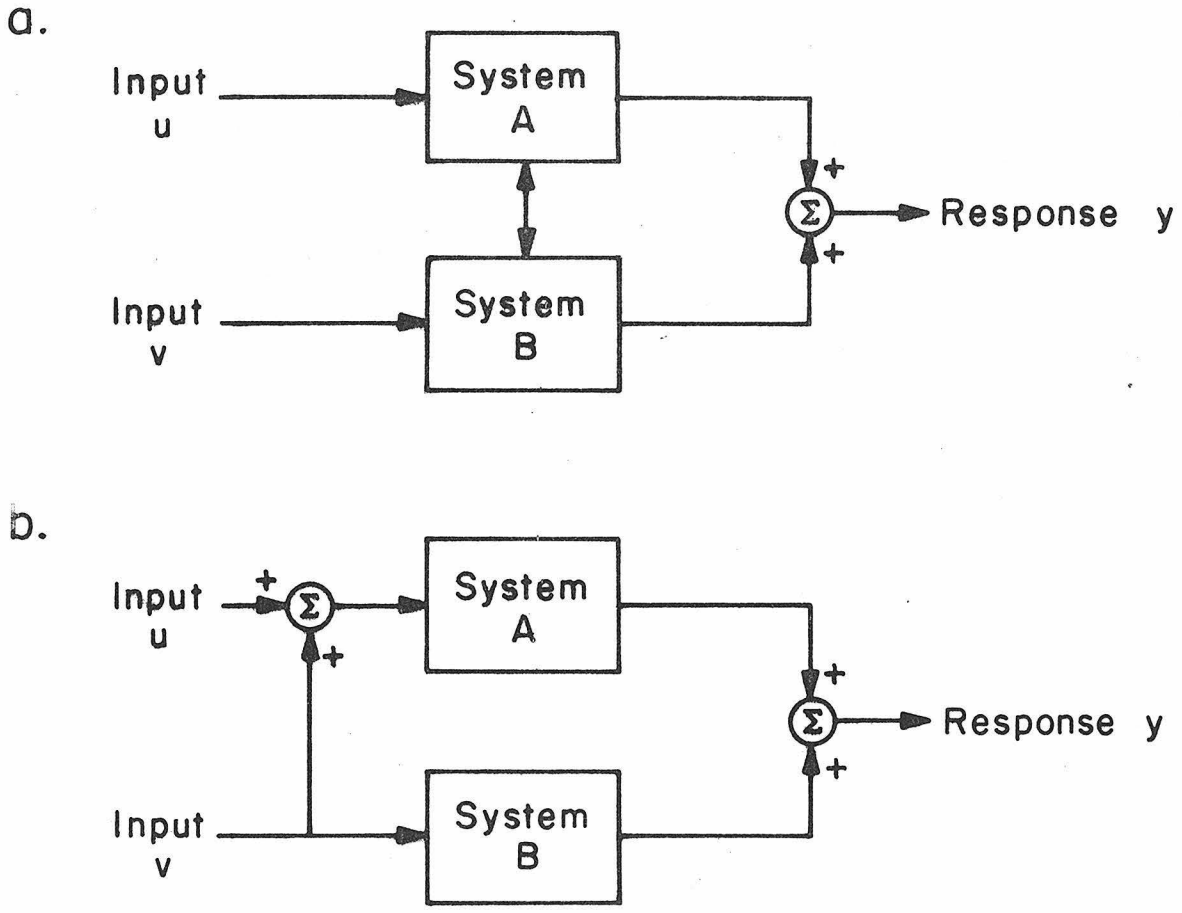

Fig. 5-1. (a) General nonlinear interaction between two systems.

(b) Specific type of nonlinear interaction involving cross-inputs.

$$\frac{1}{p^2} E\left\{y_{uv}(t)\, u(t-\tau_1)\, u(t-\tau_2)\right\} = h_{2_A}(\tau_1, \tau_2)$$

$$\frac{1}{p^2} E\left\{y_{uv}(t)\, v(t-\tau_1)\, v(t-\tau_2)\right\} = h_{2_A}(\tau_1, \tau_2) + h_{2_B}(\tau_1, \tau_2)$$

$$\frac{1}{p^2} E\left\{y_{uv}(t)\, u(t-\tau_1)\, v(t-\tau_2)\right\} = 2h_{2_A}(\tau_1, \tau_2) = \text{cross kernel} \qquad (5.6)$$

In this special case, the cross-kernel is essentially the second-order kernel for system A.

If the two boxes of Fig. 5-1b are receptor systems and the inputs are quasi-random stimuli of different wavelength , then the equations for Fig. 5-1b describe absorption of both inputs by receptor system A. A similar argument applies when the cross-input v to system A is scaled by some absorption constant K_1 . In this case, the cross-kernel becomes

$$\frac{1}{p^2} E\left\{y_{uv}(t)\, u(t-\tau_1)\, v(t-\tau_2)\right\} = 2K_1 h_{2_A}(\tau_1, \tau_2) \qquad (5.7)$$

Another relevant modification of Fig. 5-1b is to make receptor system B also receive a cross-input from stimulus u . If this cross-input is scaled by an absorption constant K_2 , then the cross-kernel becomes

$$\frac{1}{p^2} E\left\{y_{uv}(t)\, u(t-\tau_1)\, v(t-\tau_2)\right\} = 2K_1 h_{2_A}(\tau_1, \tau_2) + 2K_2 h_{2_B}(\tau_1, \tau_2) \qquad (5.8)$$

Finally, if additional cross-talk defined by $2h_{2_x}(\tau_1, \tau_2)$ occurs internally between receptor systems A and B , then the cross-kernel becomes

$$\frac{1}{p^2} E\{y_{uv}(t)\, u(t-\tau_1)\, v(t-\tau_2)\} = 2K_1 h_{2_A}(\tau_1, \tau_2) + 2K_2 h_{2_B}(\tau_1, \tau_2) + 2h_{2_x}(\tau_1, \tau_2) \tag{5.9}$$

In practice, the self-kernels will remain the same for the single- and double-input experiments, unless the adaptation state changes. Hence, for Fig. 5-1b it is important to consider the effect v might have on system A. If u were the only input, the self-kernels for system A might be entirely different from the two-input correlate because of a difference in the effective mean and depth of modulation of the stimulus. This tests the system with a different range of stimuli and can produce significant changes in adaptation. These effects can be reduced by holding v constant at the level of the corresponding quasi-random mean.

V -3. Method of Procedure

V -3-a. Equipment

The optical bench in Fig. 5-2 provides two independent channels of quasi-random stimuli. The two channels of light superimpose via a beam splitter and image into a coherent fiber optic bundle. The fiber optic leads to the condensed maxwellian optical system which connects to the eyecup electrode as described previously.

V -3-b. Stimulus characteristics

In these experiments the power spectrum of the stimulus is flat between . 2 and 45 Hz with a high-pass roll-off of 40 dB per decade and a low-pass roll-off of 160 dB per decade. This increased bandwidth is more appropriate for stimulating cone systems (Chapter IV). The probability distribution of stimulus amplitude is clipped at ± 3 standard deviations, but within this range the distribution is gaussian.

Narrow bandpass filters are used to provide light stimuli with energy distributed over a very small range of wavelengths. Fig. 5-3 shows the spectral transmission characteristics of the filters selected. The wavelengths maximize the differences in absorption between the different cone receptors as derived from Fig. 5-4.

We adjusted the mean intensity of each quasi-random color stimulus to give the same absorbed quantal flux based upon the I. C. I. photopic spectral sensitivity curves. This specified the following photopic corrected measurements for the selected wavelengths:

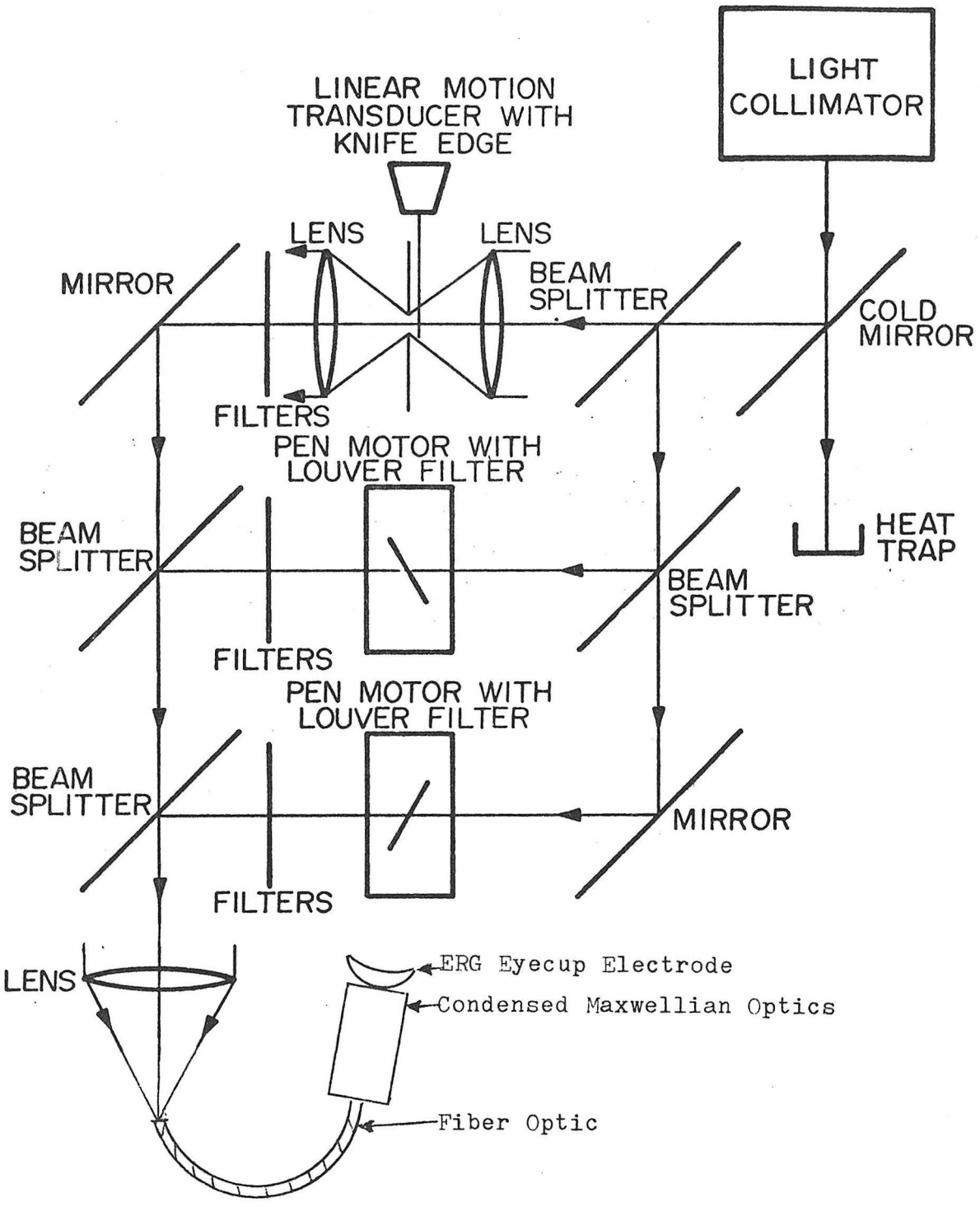

Fig. 5-2. Optical system.

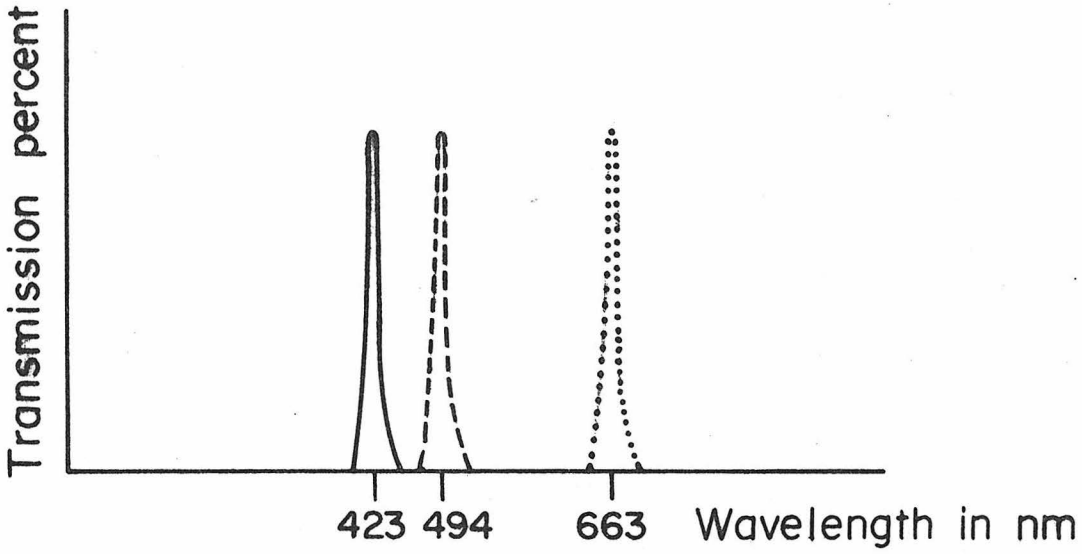

Fig. 5-3. Narrow bandpass filters.

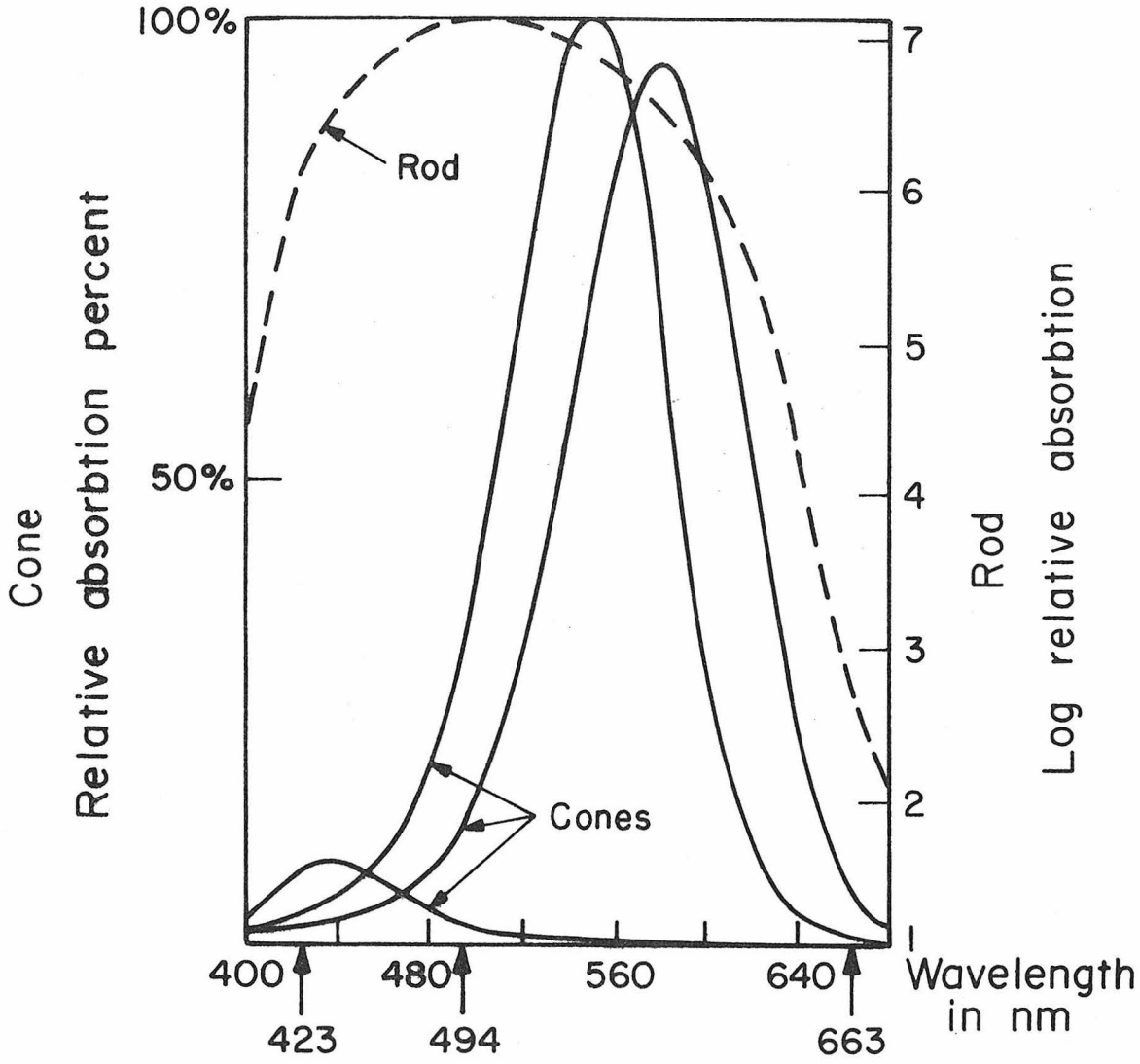

Fig. 5-4. Relative sensitivity of rods and cones, nota bene different scales for rods and cones.

wavelength nm	Mean illumination ft lamberts (with photopic sensitivity correction)
423 (Blue)	10.0
494 (Green)	8.6
663 (Red)	6.4

The conclusions made later in this paper will not require exact equivalence of quantal flux. However, it is important to recognize that the absorption correction is about the same for the 423 and 663 wavelengths.

V -3-c. Experimental protocol

The ERG was recorded from two adult male subjects. Each subject was first asked to adapt to ambient white light of 3 candles/m^2 for about 15 minutes; then the subject immersed his eyes into fluid contained by the eyecups and viewed the quasi-random stimuli in 45^o maxwellian view.

Each of the following combinations of wavelengths was presented with constant or independent modulation of intensity:

A Single inputs

1) 423 nm for 2 min

2) 494 nm for 2 min

3) 663 nm for 2 min

B Two inputs

1) 423 + 663 (two independent quasi-random inputs) for 2 min

2) 423 + mean 663 (one quasi-random and one constant input held at the mean of the corresponding quasi-random input) for 2 min
3) 663 + mean 423 (one quasi-random and one constant input held at the mean of the corresponding quasi-random input) for 2 min.

V -4. Results and Discussion

For each two minute segment of single color input, 100 sec of data was extracted and used to compute Wiener kernels. Fig. 5-5 shows the first-order kernels for both subjects. The kernels for the red stimuli are missing the scotopic b-wave as expected (Krill, 1972) Whereas the kernels for the other colors contain large scotopic b-waves, indicating large contributions from rod systems. Any low frequency c-wave components have been filtered out of all responses in an effort to attenuate low frequency noise levels.

The first-order kernels for experiments involving the 423 and 663 stimuli are shown in Fig. 5-6. The amplitude of the first-order kernel for the 423 system is somewhat reduced for both subjects when the 663 background is presented. However, scotopic components do not change significantly. There is also very little change between the quasi-random and constant background cases, reflecting only small adaptation differences for these two cases.

From Fig. 5-4, we expect the rods to be about 300 times more sensitive to the 423 stimulus than to the 663 stimulus, and we expect the blue cones to be insensitive to the 663 stimulus. Hence, any change in either photopic or scotopic components is surprising.

One possible explanation for the change in photopic components is that the 423 stimulus does not reflect the functioning of blue cones. For example, we expect green cones to respond to both the 423 and 663 stimuli.

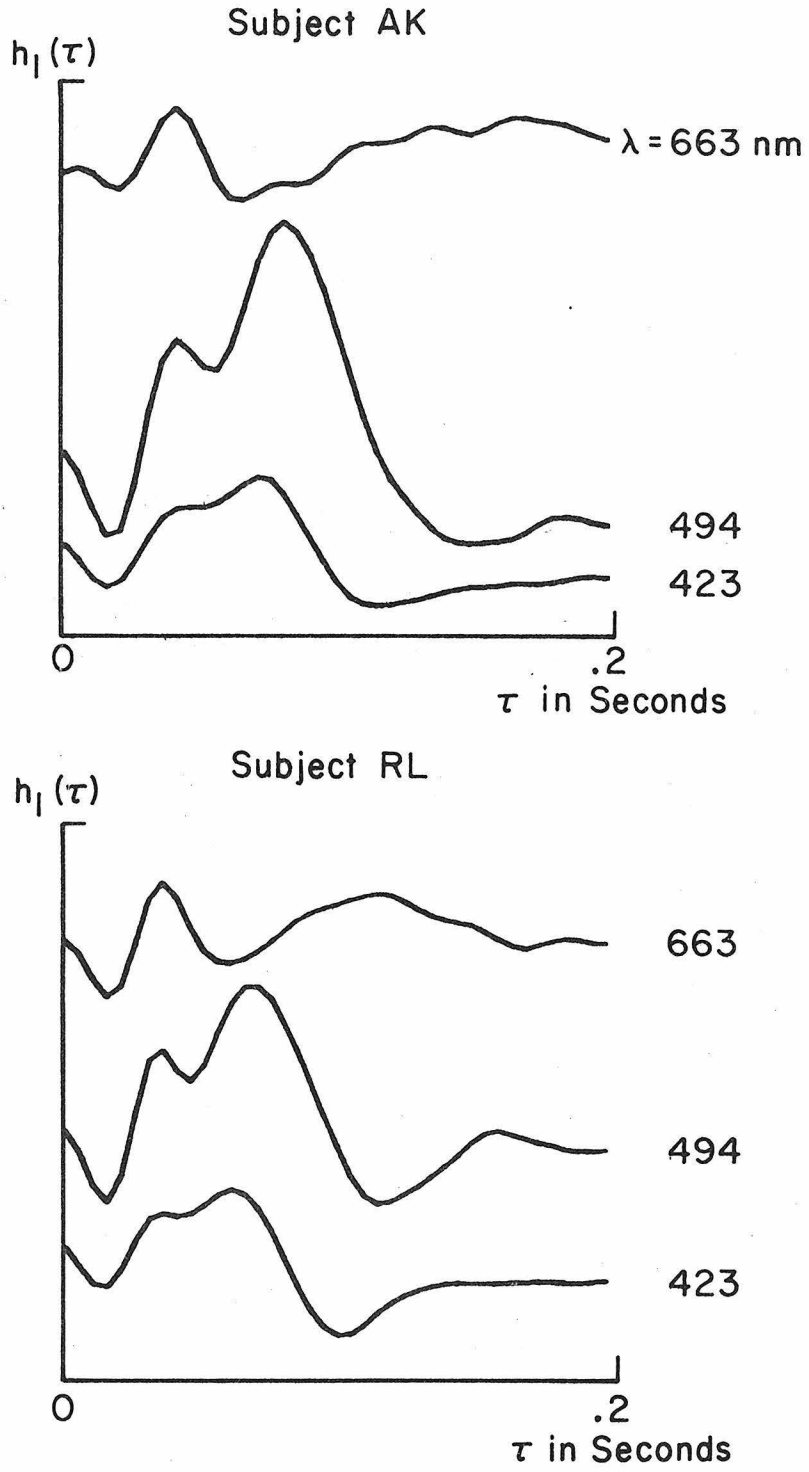

Fig. 5-5. $h_1(\tau)$ for different wavelength quasi-random stimuli, two subjects.

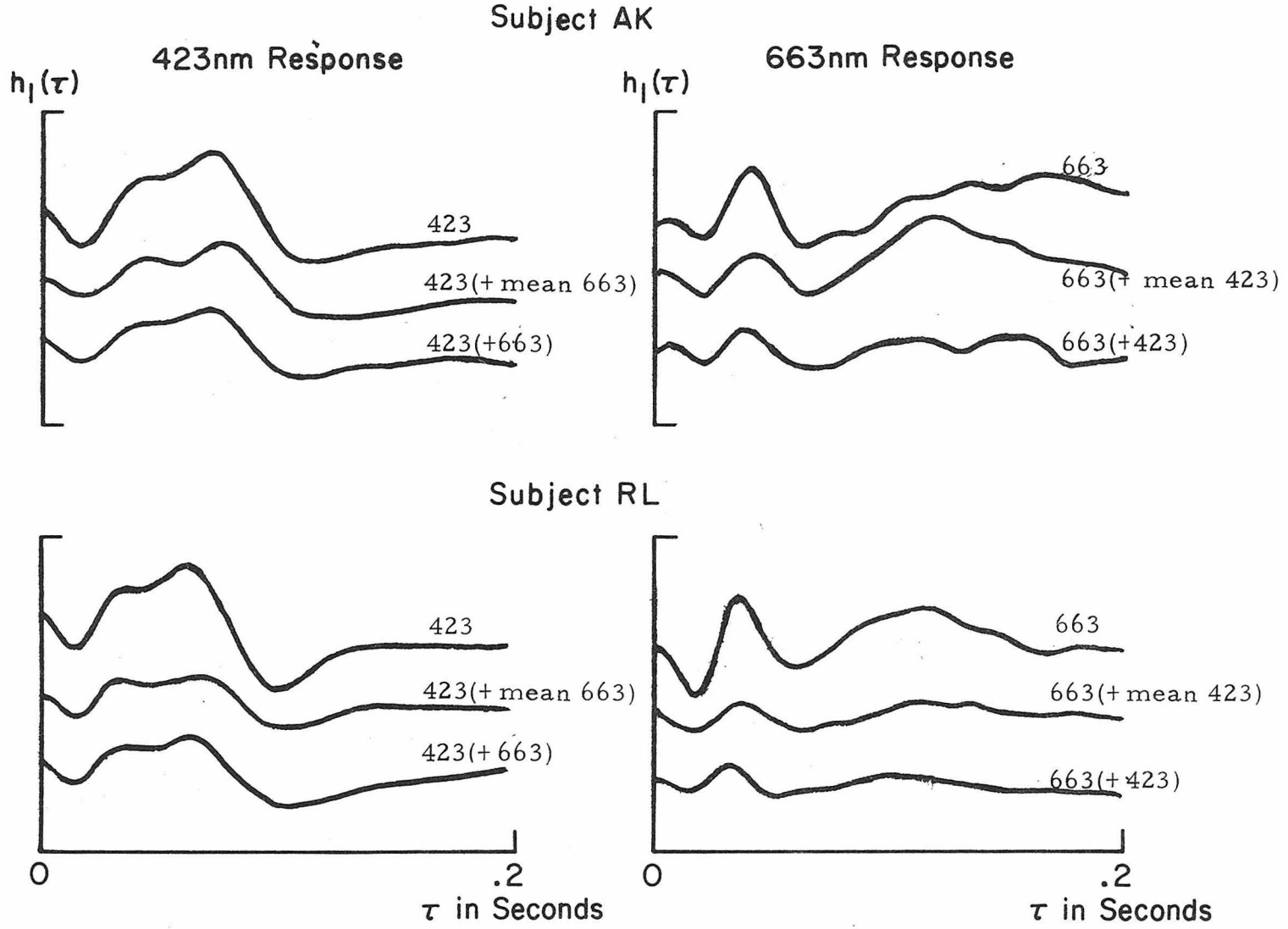

Fig. 5-6. $h_1(\tau)$ for single and double inputs involving 423 nm and 663 nm wavelengths.

Green cones are about twice as sensitive to the 423 stimulus as to the 663 stimulus; therefore, the 663 background should increase (to green cones) the effective mean of the 423 stimulus by 50% and reduce the depth of modulation by 33%. These effects should reduce the amplitude of the photopic components of the first-order kernel by about 25% (from Fig. 3-3 and Fig. 4-5b), which is close to what we observed.

The first-order kernel for the 663 system (Fig. 5-6) is also reduced in amplitude when the background stimulus is presented. However, again the changes can be accounted for by simple adaptation effects. The 423 background should increase (to red cones) the effective mean of the 663 stimulus by about 33% and decrease the depth of modulation by 25%. These effects should reduce the amplitude of the photopic component by about 40% which is also close to what we observed.

The cross-kernel for the two-input experiments (i.e., 423 plus 663 independently modulated) are presented in Fig. 5-7. From the above discussion, we know that the cross-kernel results in part from a weighted summation of the self second-order kernels for the 423 and 663 systems. Other nonlinear effects contribute to the cross-kernel as described by Eq. 5.9.

The first noteworthy observation of the cross-kernels of Fig. 5-7 is that both are rather symmetric about the main diagonal reflecting large contributions from the self-kernels. Nonlinear interactions

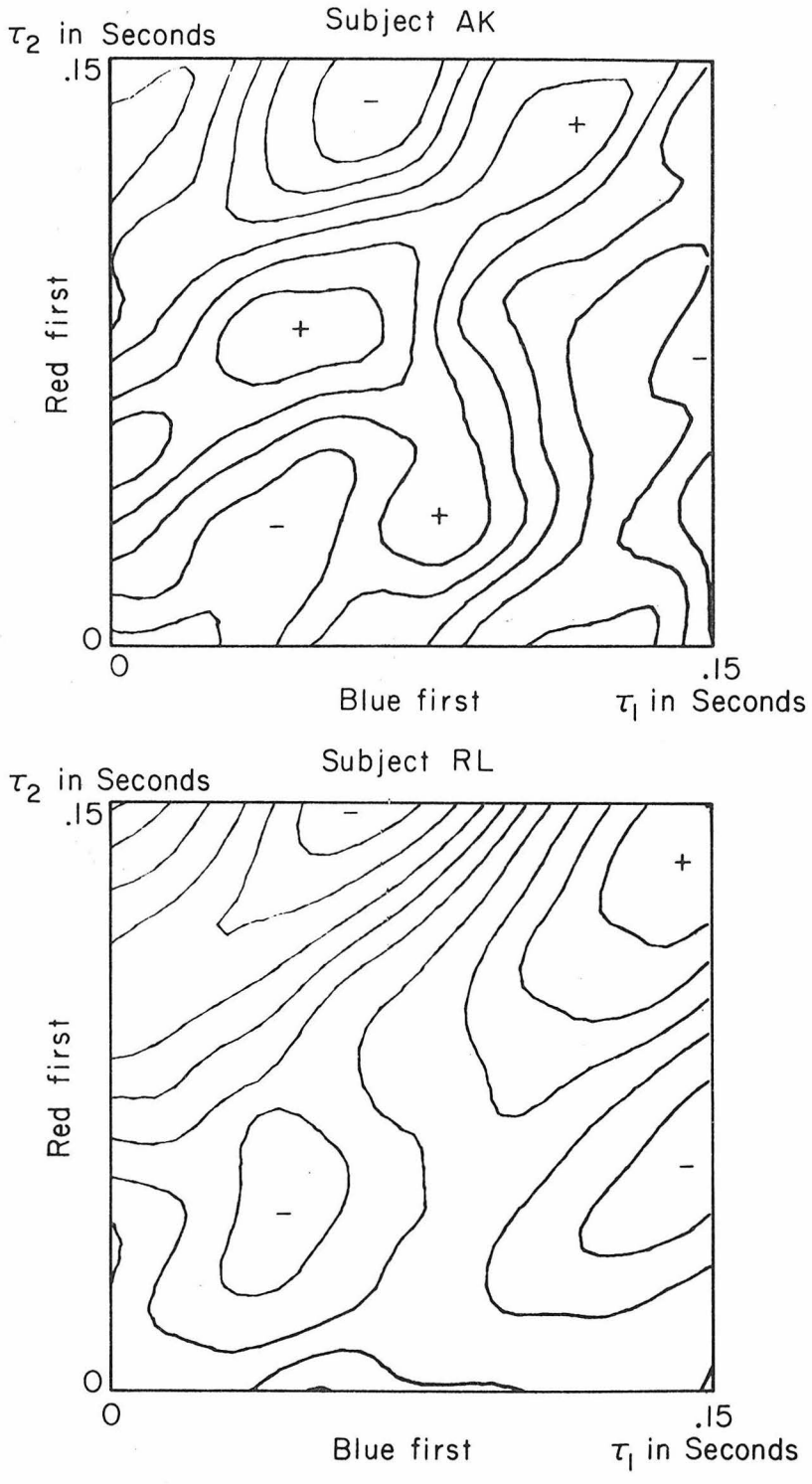

Fig. 5-7. Cross-kernels for 423 nm plus 663 nm stimulus, two subjects.

between the 423 and 663 systems are expected to produce asymmetric contributions to the cross-kernels. Hence, the more interesting asymmetric properties are hidden by the self-kernels.

Several schemes are being considered for future experiments which will attempt to eliminate the self-kernels from the cross-kernels of Fig. 5-7 and expose the asymmetric nonlinearities. No solid evidence can be presented at this time which supports the claim that receptor systems interact in any manner.

NOMENCLATURE

A	amplitude of pulse stimulus
c	constant
$G_n(h_n, x)$	n^{th} order term in Wiener functional expansion
I	input (Fuortes and Hodgkin adaptation model)
$h_n(\tau_1, \tau_2, \ldots, \tau_n)$	n^{th} order Wiener kernel
k	constant
m	magnitude of pulse stimulus
P	power density of quasi-random stimulus
s	distance along neuron (Fuortes and Hodgkin adaptation model)
t	time
T	period
V	output (Fuortes and Hodgkin adaptation model)
x	quasi-random stimulus
y	Electroretinogram response
α	leakance (Fuortes and Hodgkin adaptation model)
β	signal from bleached receptors (Fuortes and Hodgkin adaptation model)
δ	dirac delta function
τ	independent variable of Wiener kernels

APPENDIX

A-I. Quasi-Random Generator

There are various known designs for creating a bandlimited, white-noise voltage signal. We have denoted the associated intensity modulations as "quasi-random stimuli." In this section, we will describe our own design for a "quasi-random generator."

The complete schematic is shown in Fig. A-1. The noise source is an inexpensive zener diode (reverse biased). The quiescent current noise of the PN junction has a power spectrum which is flat down to 10 or 20 Hz.

We require a spectrum which is flat between DC and 100 Hz. To achieve this, the comparator (LM 311) and flip-flop (SN 7474) use the diode noise to generate a random binary signal which has a power spectrum as depicted in Fig. A-2. Note that the clock (NE 555) determines f_c shown in Fig. A-2. If f_c = 100 k Hz, then the section of the power spectrum between DC and 200 Hz will be nearly flat. The op amp (SN 72747b) perform a 4 pole low-pass filtering of the binary signal to attenuate the high frequency components. The resulting voltage signal is also nearly guassian, provided f_c is much larger than the corner of the low-pass filter. In this design, f_c is at least 1000 times greater than the highest low-pass corner.

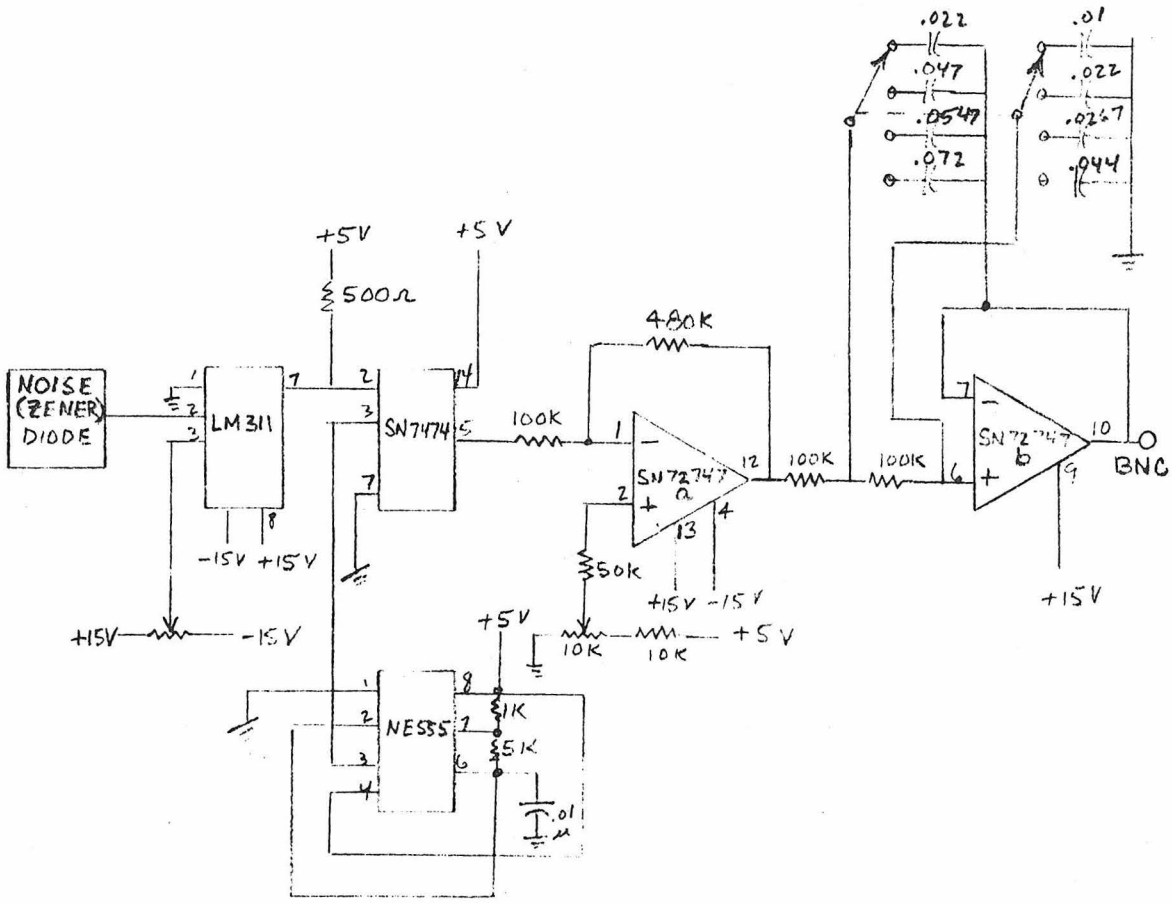

Fig. A-1. White-noise generator circuit using zener diode.

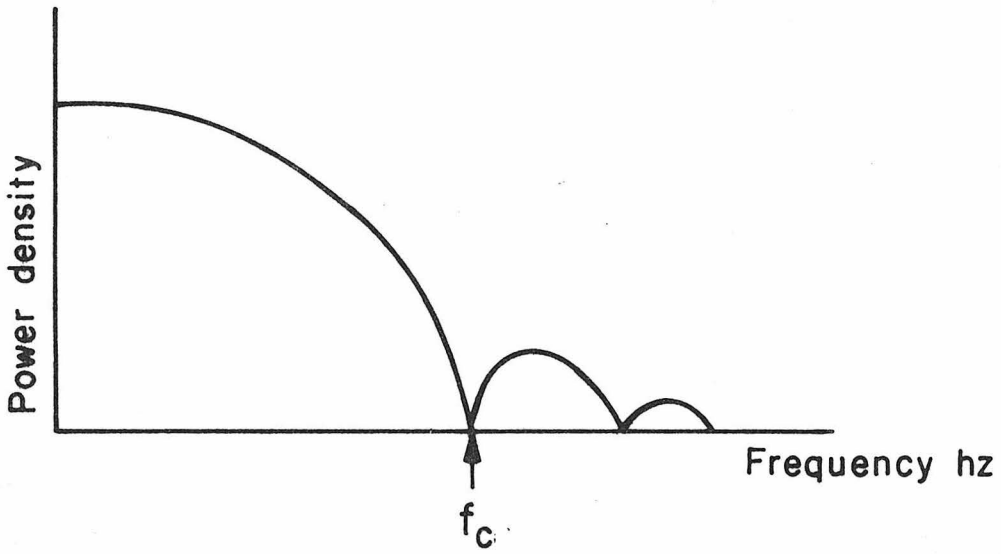

Fig. A-2. Power spectrum of random binary signal.

A-II. Current Control Circuit

We would like to drive the pen motors with a current signal which is proportional to the quasi-random voltage signal. Fig. A-3 is a circuit schematic which compensates for the impedance characteristics of the pen motor.

The current booster (LH 0002) provides up to 100 m A current output at unity voltage gain. Hence, the impedance of the pen motor z becomes the feedback load for the op amp (72741). The output voltage V_0 is simply

$$V_0 = \left(\frac{R_g + z}{R_g}\right) V_i \quad .$$

Hence, the current driving the pen motor is

$$I_0 = \frac{V_0}{R_g + z} = \frac{V_i}{R_g} \quad .$$

This simple trick makes the current I_0 independent of the impedance z and proportional to the input voltage V_i. R_g should be sufficiently small to protect the op amp.

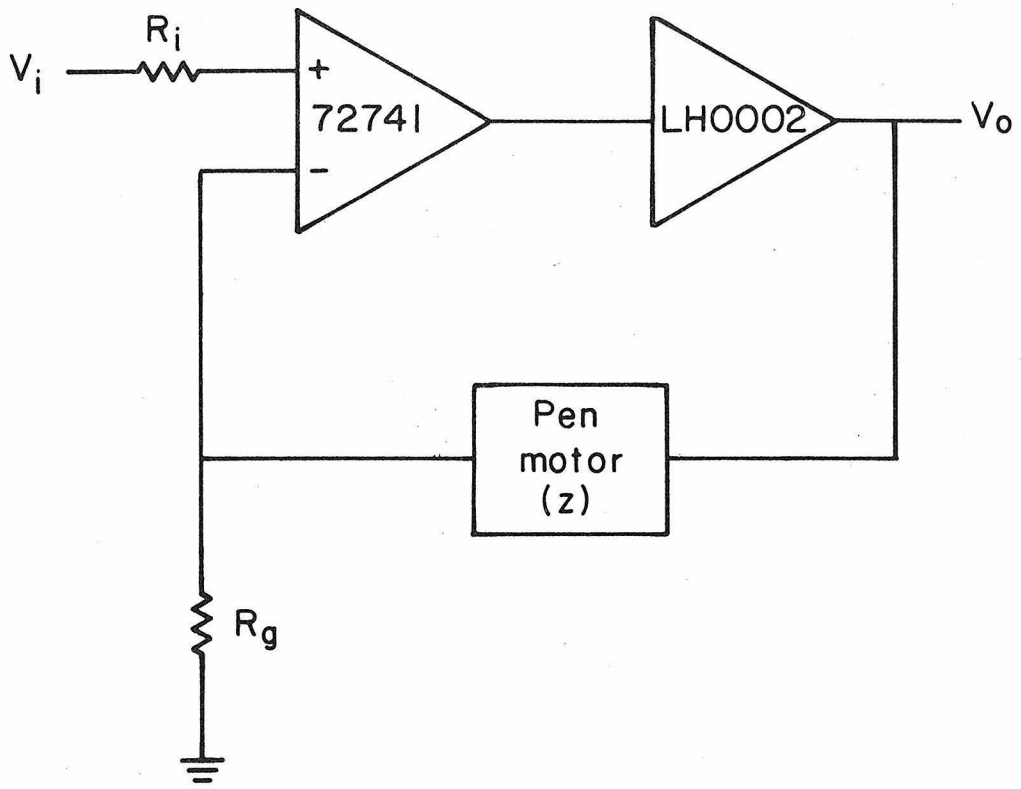

Fig. A-3. Impedence compensation circuit.

A-III. On-Line Computer System

A-III-1. Objectives

Two proposed real-time kernel computers will perform the same data processing as expensive computer systems currently employed. The stand-alone "Economy" computer will provide the minimum required subsystems for computing whereas the "Deluxe" model will provide microprocessor control of the Economy computer plus several peripherals. The following improvements are expected:

1. The computations will occur in real-time; thus conclusions about an experiment or clinical test may also occur in real-time. This is particularly important in applications involving clinical diagnoses.
2. All components required for the analyses of an experiment or clinical test will be contained in one small cabinet about 6" x 19" x 24".
3. The Economy computer will cost less than $1,000 in parts.
4. The Deluxe model will cost less than $5,000 in parts and provide the following peripherals:

   Dual cassette recorders

   5" video display

   16 character/line printer

   ASR 33 keyboard

   modem

A-III-2. Ternary Algorithm

Several approximation algorithms for computing first- and second-order Wiener kernels were considered and simulated. The optimum for real-time processing of the ERG seems to be cross-correlations between an 8 bit version of the response and a ternary version of the stimulus. The ternary signal is +1, 0, or -1; therefore, multiplications reduce to adds, subtracts and skips.

The first- and second-order kernels computed by the ternary quantization method closely resemble the desired Wiener kernels as demonstrated by Fig. A-4. The theoretical error associated with the ternary algorithm has been examined carefully by Yasui and Klein, 1976. The variance of the n^{th} order kernel estimate is a function of $\frac{\alpha^n}{T}$. α is a coefficient depending on the thresholds used for creating the ternary signal and T is the duration of the stimulus and response data sets. For the standard computational method, $\alpha = 1$. The optimum ternary quantization makes $\alpha = 1.3$; therefore, we must increase T by a factor of 1.3 to achieve the same variance for the first-order kernel estimate, and we must increase T by a factor of 2 to achieve the same variance for the second-order kernel estimate.

A-III-3. Economy kernel computer

The TTL circuit shown as a block diagram in Fig. A-5-a performs the high speed number crunching for both the economy and deluxe models of the on-line kernel computer. As indicated, the first operations are A/D conversions of the stimulus and response. The response is translated into 8 bits and the stimulus into 2 bits. The

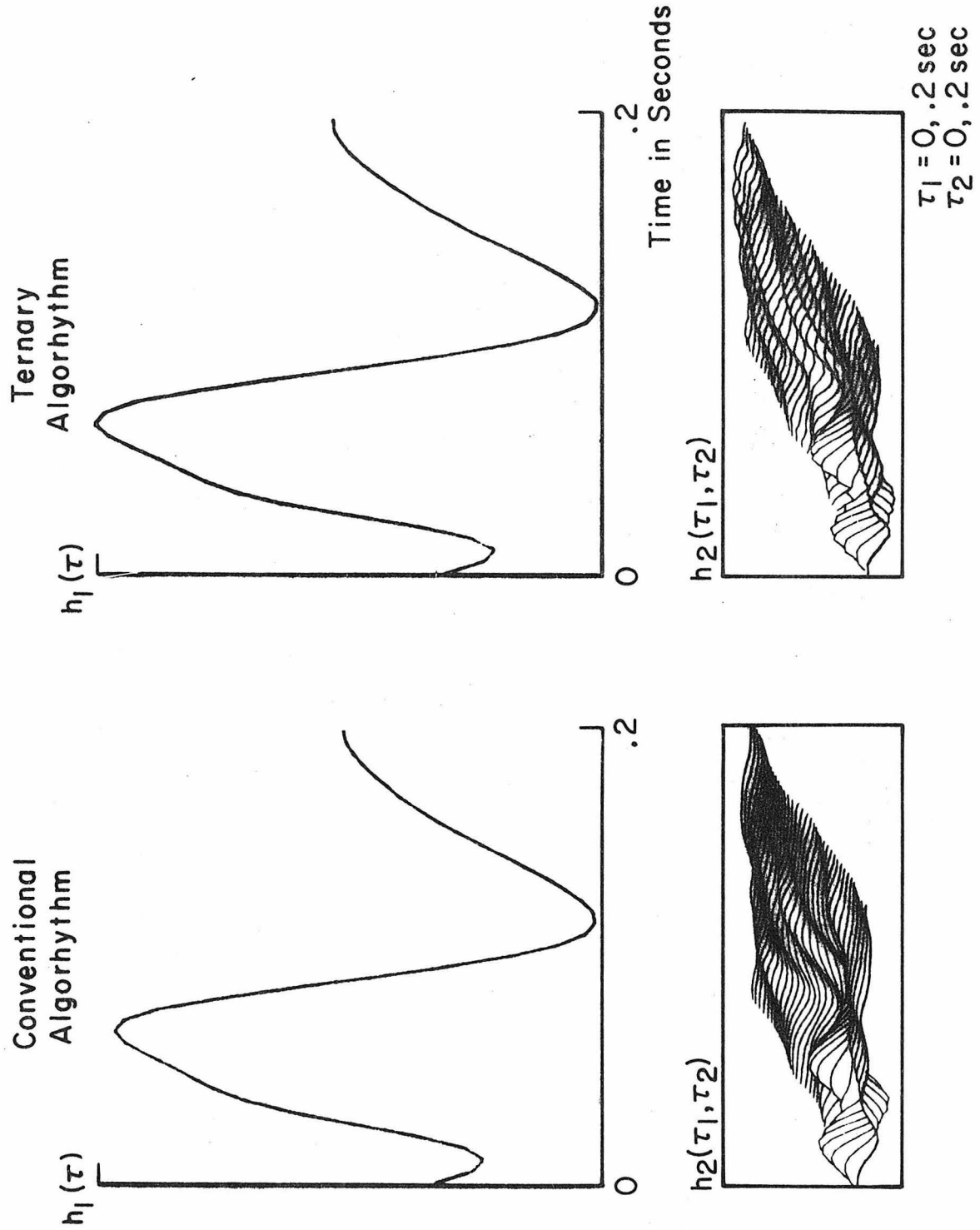

Fig. A-4. Kernels for real and ternary approximation algorithms.

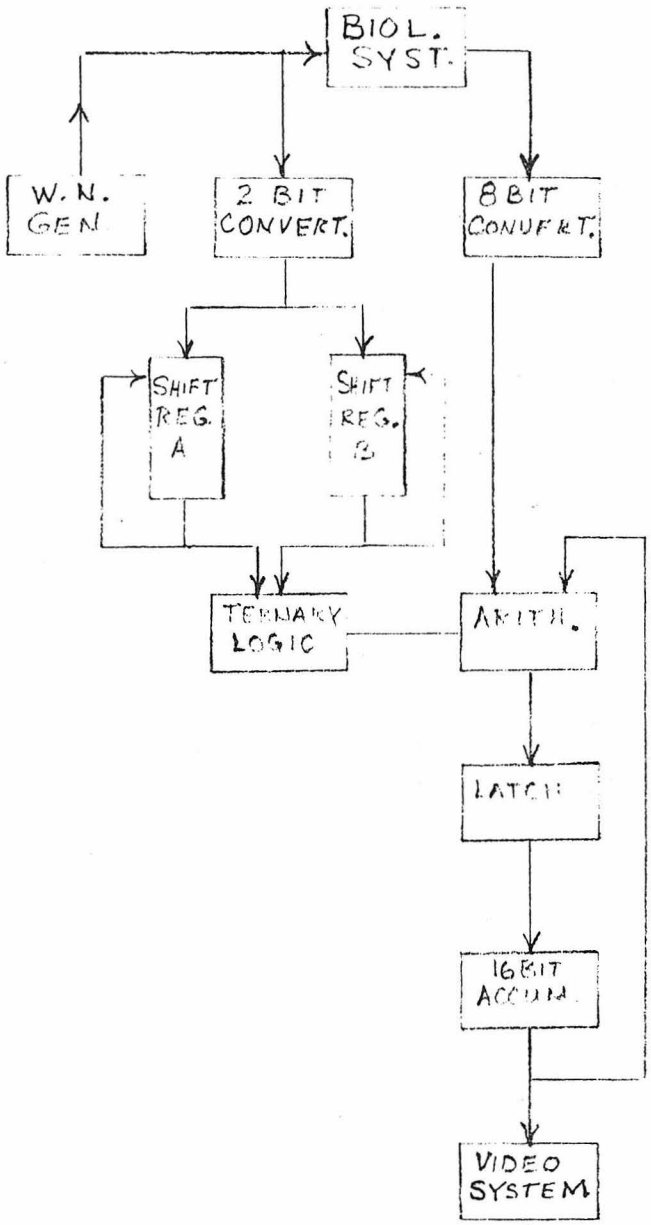

Fig. A-5. Block diagram of on-line kernel computer.

2 bit signal represents the stimulus as defined by the table in Fig. A-5-b. Shift register circuits A and B provide the appropriate sequence of inputs to the ternary logic control circuit to effect the desired first- and second-order cross-correlations. The y value is added to or subtracted from the accumulated 16 bit memory array, except when $X_H = 0$ and $X_L = 1$. This denotes a required skip (or multiplication by zero). The 16 bit accumulator dumps periodically into a 6 bit buffer memory which is part of the video interface.

The final display of the first-order kernel is a standard two-dimensional plot of 32 points. The second-order kernel is represented by a 32 x 32 matrix of squares with each buffer memory location controlling the intensity of one square. The configuration of the second-order kernel is shown in Fig. A-6-a. The form has changed slightly from the usual representation in order to make more efficient use of the CRT face and to make the timing simpler. The first-order kernel appears at the top of the display and the shades of gray representation of the second-order kernel appears at the bottom of the display as depicted in Fig. A-6-b.

The video display of the two kernels is held during a successive computation period. At the completion of this period, the display automatically changes to the new kernels produced by the computations.

The complete circuit for the Economy kernel computer is shown in Fig. A-7. Several counters are used to control the progression of operations by the arithmetic and logic sections. Events occur out of phase via the biphase master clock. The following novel features were incorporated into this inexpensive TTL computer:

a. Representation of h_2

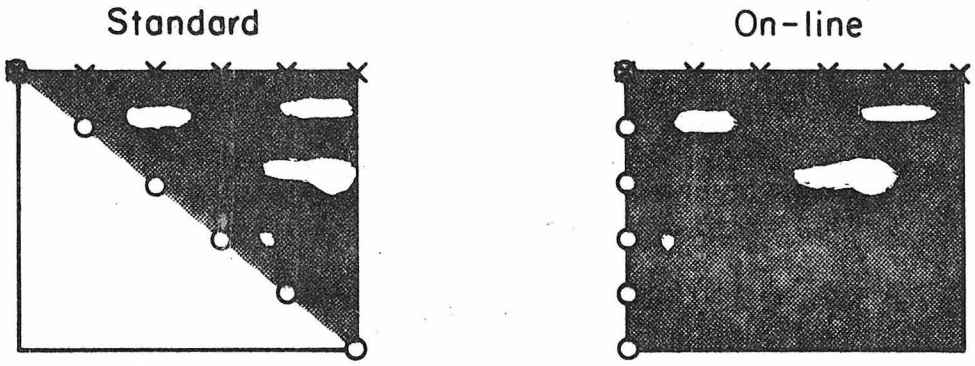

b. CRT Display of h_1 and h_2

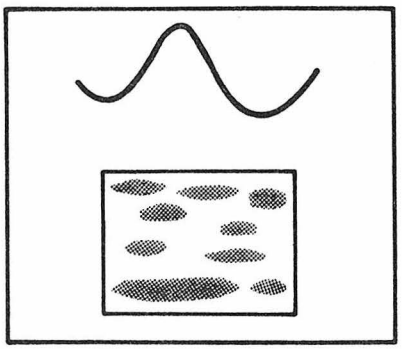

Fig. A-6. Display format for on-line kernel computer.

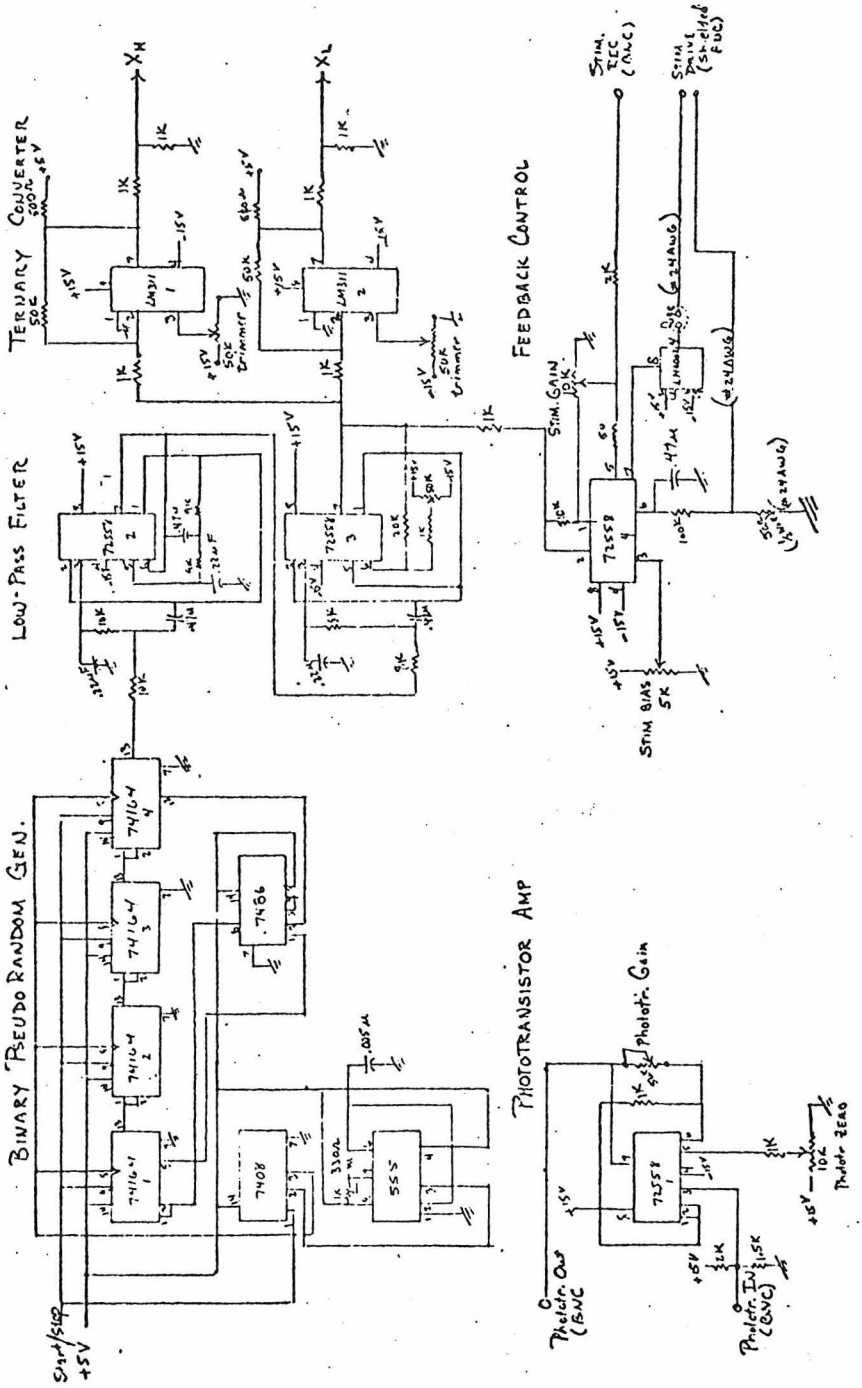

Fig. A-7. Complete circuit for economy kernel computer.

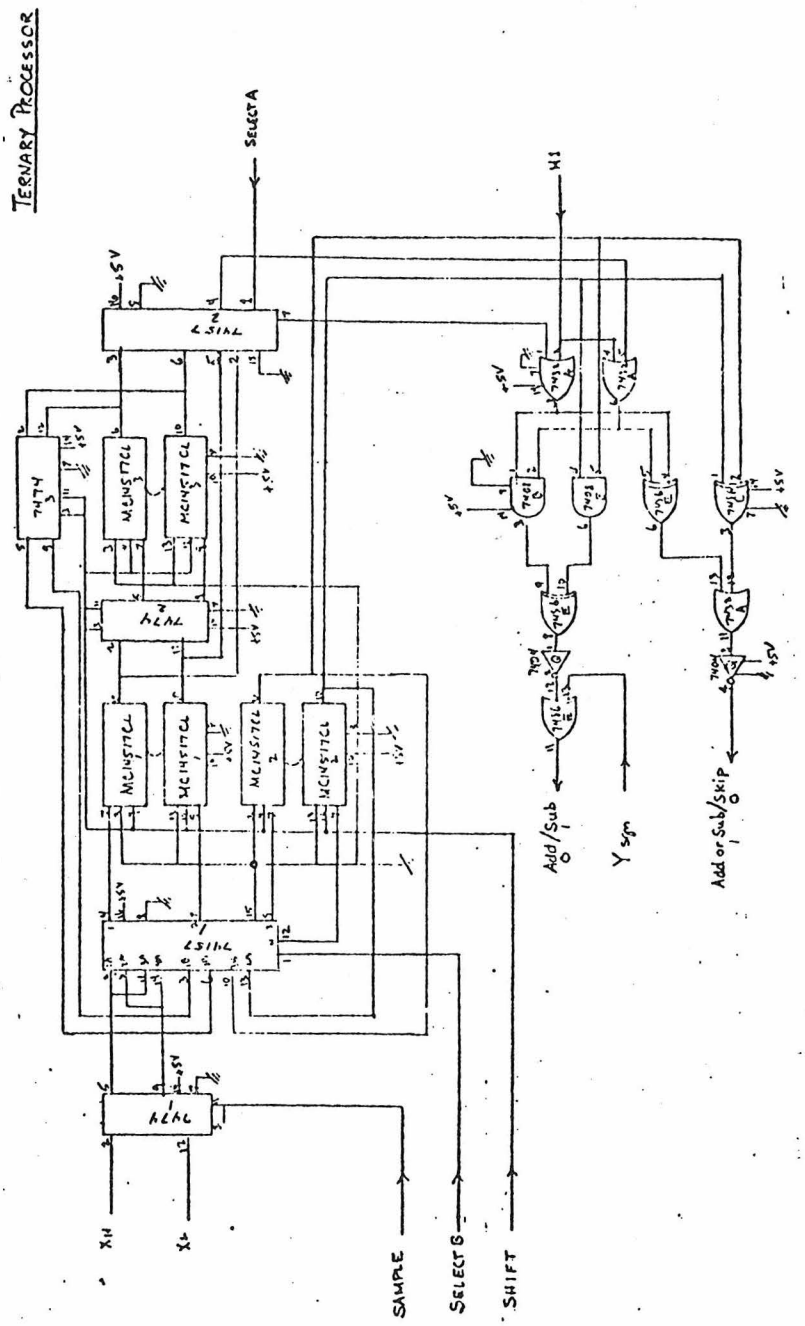

Fig. A-7 continued

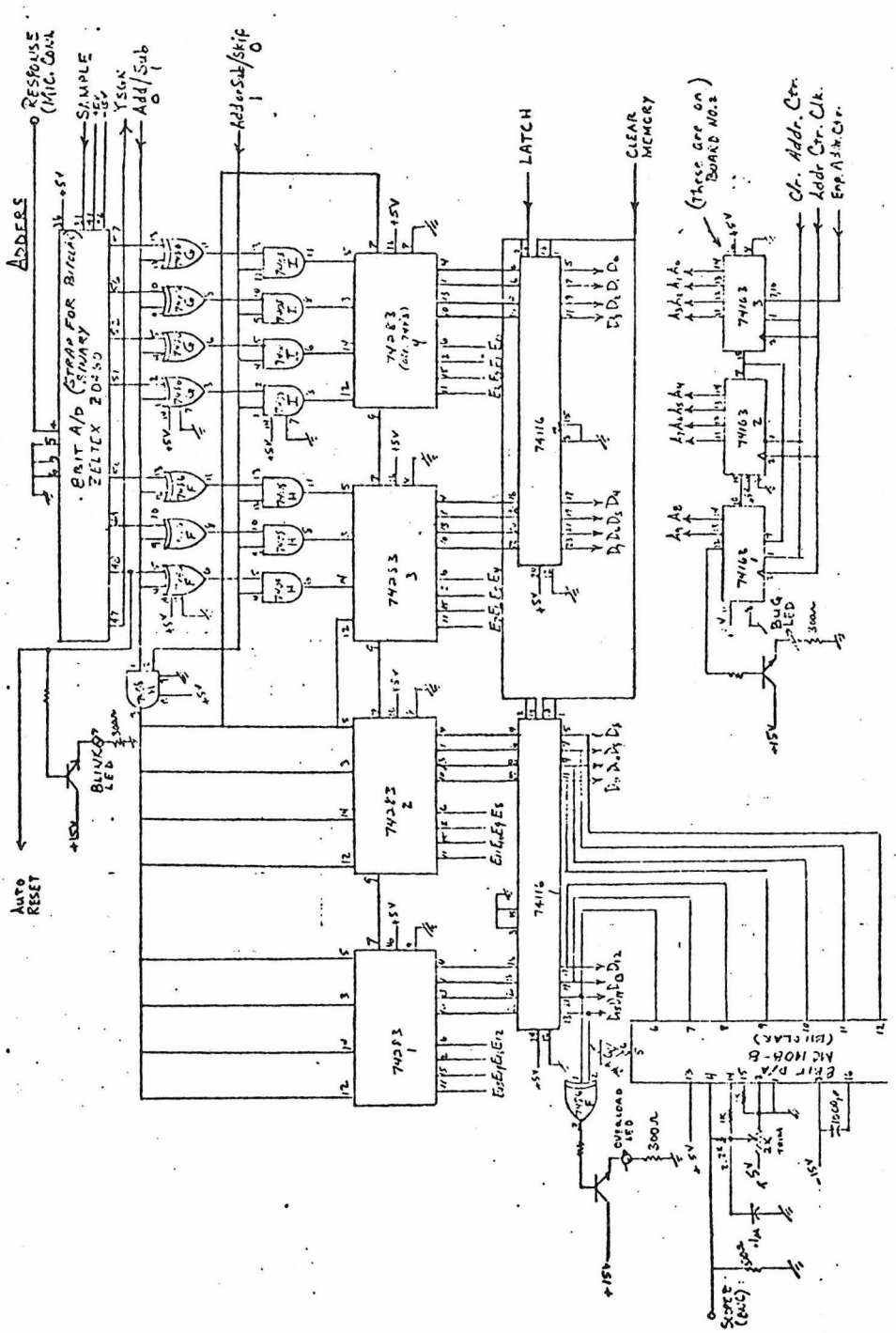

Fig. A-7 continued

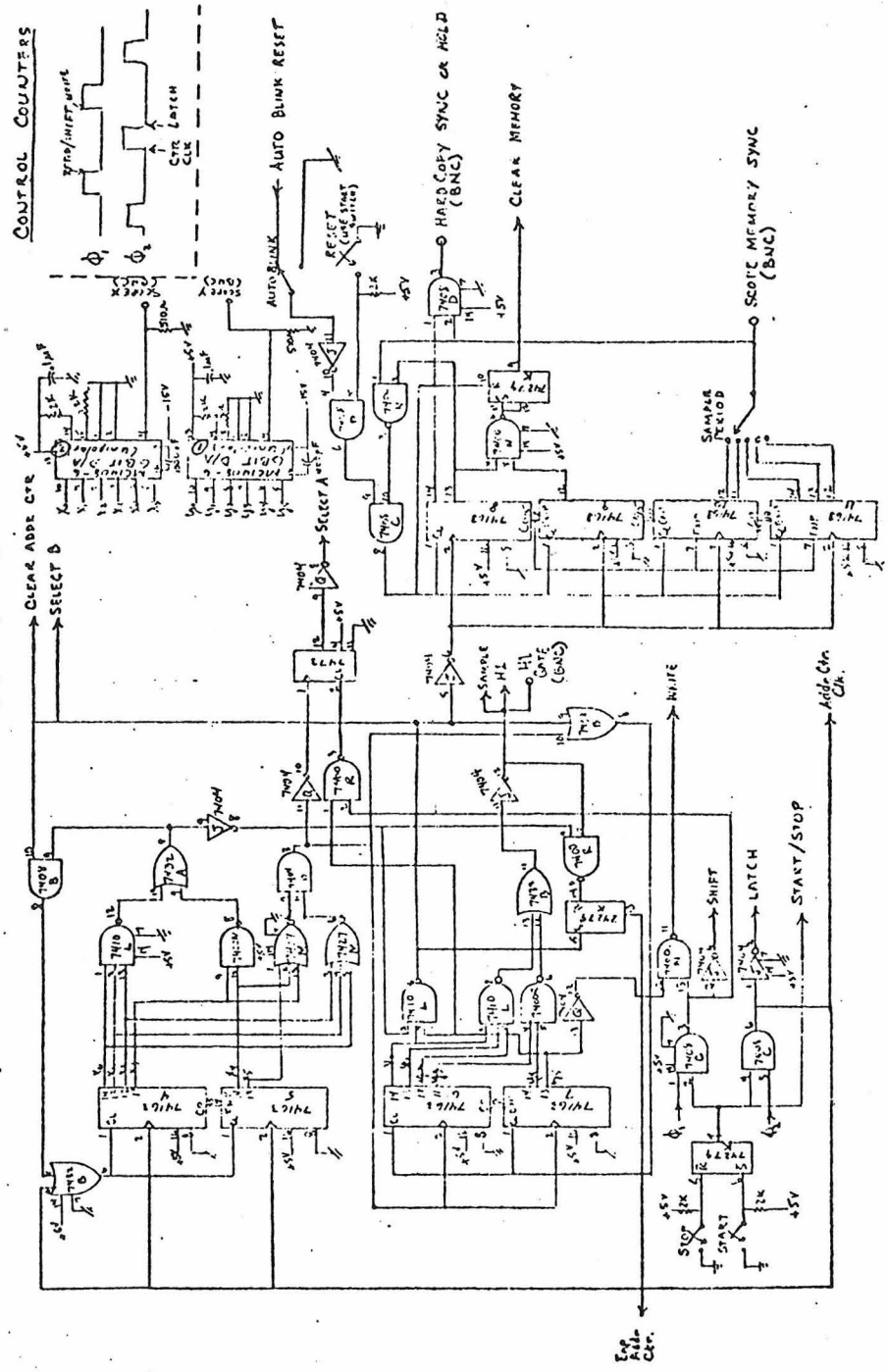

Fig. A-7 continued

1. The counters are monitored to check that all are functioning properly. If any part fails and causes counting errors then a "Bug" LED located on the face plate of the chassis box turns on to indicate a circuit malfunction.
2. Provisions were made to recognize the occurrence of a blink. A "Blink" LED turns on whenever a blink occurs and optionally causes the accumulators and counters to reset to zero and to begin a new computational period.
3. Another LED monitors the memory for the occurrence of an overload. This can also automatically reset the processing for a new computation period. However, repeated overloads indicate a bias error in the response data input.

A-III-4. Deluxe kernel computer

Fig. A-8 shows the design of a dual microprocessor system under construction. One microprocessor will exclusively control the previously described "Economy kernel computer." This microprocessor will also perform the necessary preliminary processing of the stimulus and response data sets, e.g., digital filtering. The second microprocessor will handle the peripheral devices shown. The two microprocessors will operate 180^{o} out of phase, permiting multiplexed access to the same memory.

The results of the processing will be displayed real-time on the video display. The first-order kernel will appear as a two-dimensional plot with scales set by the experimenter. The second-order kernel will be displayed using contour lines or a gray scale.

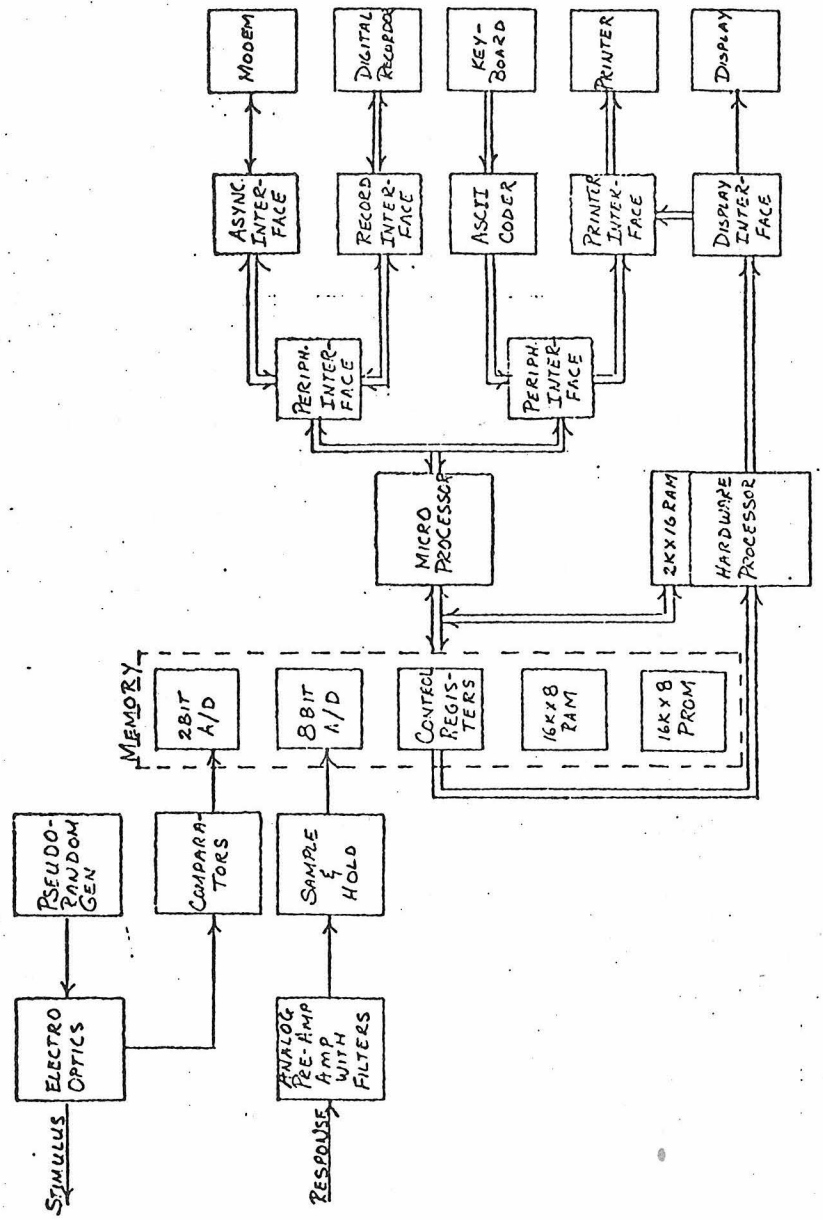

Fig. A-8. Deluxe kernel computer.

The electric discharge printer will be used for hardcopying the video display. Shades of gray will be accomplished by varying the density of dots produced by the printer. Contour lines and two-dimensional plots will be printed as sequences of dots. Finally, the values of any memory locations can be printed one word per line.

The modem will provide a means for the microprocessor to intercourse with the computing systems at Caltech and other commercial time-shared computing facilities. This makes new programs available to the microprocessor as they arise. A number of programs suitable for the kernel-computer will be available in the Caltech computer systems, these can be transmitted to a user over a data line. In addition, the Caltech system and many commercial time-shared systems have emulators and assemblers for the microprocessor. Hence, a user could write and debug his own program via this facility and then transfer the assembled program into his own equipment. New programs can be stored temporarily in the RAM or permanently in the digital recorder. Data can also flow in the other direction; i.e., experimental results could be passed on to another computing system for further analysis.

The digital recorder will be used either to store programs as described above or to store the stimulus and response data from an experiment.

The keyboard will be the only array of buttons the experimenter has to push to define and control his experiment. For example, the sequence of typed commands necessary to perform and record an

experiment producing first- and second-order kernels is as follows:

STIM = W. N.	(Use white-noise as stimulus)
DUR = 100	(Duration of expt = 100 sec.)
R = 256	(Sampling rate = 256 samples/sec.)
H1 = 0, .3	($0 \leq \tau \leq .3$)
H2 = 0, .3	($0 \leq \tau_1 \leq .3$, range of $\tau_2 = f(\tau, \tau_1)$)
WIN = .30	(Time window producing kernels = 30 sec.)
DIS = CONT	(Display h_1 as plot Display h_2 as contours)
START	(Start expt.)

During the experiment, various keyboard commands will be used to change the conditions, e. g. ,

C	(Copy video display with printer)
H	(Hold display, but continue expt.)
DUMP	(Stop everything, print values of kernels)
S = .1	(Multiply video display scales by 1/10)
DIS = GRAY	(Change video display to h_1 as plot and h_2 as shades of gray)
STOP	(Stop expt.)

Additionally, the keyboard will be used for inputing new programs into the RAM or the recorder.

REFERENCES

Aiba, T. S., M. Alpern and Maaseidvaag. 1967. The electro-retinogram evoked by the excitation of human foveal cones. J. Physiol. 189:43-62.

Alpern, M. and F. W. Campbell. 1962. The spectral sensitivity of the condensed light reflex. J. Physiol. 164:478-507.

Alpern, M. and S. Torii. 1968. The luminosity curve of the deuteranomalous fovea. J. Gen. Physiol. 52:738.

Alpern, M. and S. Torii. 1968. The luminosity curve of the protanomalous fovea. J. Gen. Physiol. 52:717.

Alpern, M. and J. J. Faris. 1954. Note on the electrical response of the human eye during dark adaptation. J. Opt. Soc. Amer. 44:74-79.

Arden, G. B. and H. Ikeda. 1966. Effects of hereditary degeneration of the retina on the early receptor potential and the corneo-fundal potential of the rat eye. Vision Res. 6:171-184.

Aoyagi, Takeo. 1970. Retinal damage by visible light as reflected in the ERG change. Acta Soc. Ophthalm., Jap., 74:927-935.

Armington, J. C. 1974. The Electroretinogram. Academic Press, New York.

Armington, J. C. 1970. Simultaneous electroretinograms and evoked potentials. Am. J. of Optometry. 47:450-459.

Armington, J. C. 1967. Pupil entry and the human electroretonogram. J. Opt. Soc. Amer. 57:838-839.

Armington, J. C. et al. 1961. Detection of the electroretinogram in retinitis pigmentosa. Exp. Eye Res. 1:74-80.

Armington, J. C. and W. R. Biersdorf. 1956. Chromatic adaptation and the human electroretinogram. XXth International Physiological Congress Proceedings, Brussels, Belgium, July 3-Aug. 4. p. 35.

Armington, J. C. and W. R. Biersdorf. 1956. Flicker and color adaptation in human electroretinogram. J. Opt. Soc. Amer. 40:393.

Armington, J. C., E. Johnson and L. Riggs. 1952. The scotopic a-wave in the electrical response of the human retina. J. Physiol. 118:289-298.

Barrett, J. F. 1963. The use of functionals in the analysis of non-linear physical systems. J. Electron Control. 15:567-615.

Bartley, S. H. 1941. Vision: a study of its basis. Van Nostrand-Reinhold, New Jersey.

Berson, E. L. Editorial. 1969. Retinitis pigmentosa without pigment. Arch. Ophthal. 81:453.

Berson, E. L. and E. B. Goldstein. 1972. Cone pigment regeneration, retinitis pigmentosa and light deprivation. Vision Res. Letter to the Editors. 12:749-752.

Berson, E. L., P. Gouras and R. Gunkel. 1968. Progressive cone degeneration, dominantly inherited. Arch. Ophthal. 80:77-83.

Berson, E. L. P. Gouras and R. Gunkel. 1968. Progressive cone-rod degeneration. Arch. Ophthal. 80:68-76.

Berson, E. L., P. Gouras and R. Gunkel. 1968. Rod responses in retinitis pigmentosa, dominantly inherited. Arch. Ophthal. 80:58-67.

Berson, E. L., P. Gouras, R. Gunkel and N. Myrianthopoulos. 1969. Dominant retinitis pigmentosa with reduced penetrance. Arch. Ophthal. 81:226-234.

Berson, E. L., P. Rouras, R. Gunkel and N. Myrianthopoulos. 1969. Rod and cone responses in sex-linked retinitis pigmentosa. Arch. Ophthal. 81:215-225.

Berson, E. L. and J. Howard. 1971. Temporal aspects of the electroretinogram in sector retinitis pigmentosa. Arch. Ophthal. 86:653-665.

Berson, E. L. and L. Kanters. 1972. Cone and rod responses in a family with recessively inherited retinitis pigmentosa. Arch. Ophthal. 84:288-297.

Biersdorf, W. R. 1968. Rod and cone contributions to the off-effect of the human ERG. Invest. Ophthal. 7:371.

Biersdorf, W. R. 1967. Purkinje shift in the human electroretinogram. Amer. J. Ophthal. 64:757.

Biersdorf, W. R. 1966. Increment thresholds and the human electroretinogram. Proc. 4th ISCERG Symp. Jap. J. Ophthal. Suppl., Tokyo. 10:191.

Biersdorf, W. R. 1958. Luminance-duration relationships in the light adapted electroretinogram. J. Opt. Soc. Amer. 48:412.

Biersdorf, W. R. and J. C. Armington. 1962. The effects of chromatic preexposure upon dark adaptation of the human electroretinogram. J. Comp. Physiol. Psychol. 55:161.

Biersdorf, W. R. and J. C. Armington. 1960. Level of light adaptation and the human electroretinogram. J. Opt. Soc. Amer. 50:78.

Biersdorf, W. R. and J. C. Armington. 1957. Response of the human eye to sudden changes in the wavelength of stimulation. J. Opt. Soc. Amer. 47:208.

Biersdorf, W. R. and D. Diller. 1969. Local electroretinogram in macular regeneration. Amer. J. Ophthal. 68:296.

Biersdorf, W. R. and A. M. Granda. 1962. Effects of stimulus duration upon spectral sensitivity of the human electroretinogram. J. Opt. Soc. Amer. 52:1402.

Biersdorf, W. R., A. M. Granda and H. F. Lawson. 1966. Incremental thresholds for colored and white lights in the human electroretinogram. J. Comp. Physiol. Psychol. 61:102.

Biersdorf, W. R., A. M. Granda and H. F. Lawson. 1965. Electrical measurement of incremental thresholds in the human eye. J. Opt. Soc. Amer. 55:454.

Blakemore, C. G. and W. A. H. Rushton. 1965a. The rod increment threshold during dark adaptation in normal and rod monochromat. J. Physiol. 181:629-640.

Blakemore, C. G. and W. A. H. Rushton. 1965b. Dark adaptation and increment thresholds in a rod monochromat. J. Physiol. 181:612.

Boring, E. G. 1942. Sensation and perception in the history of experimental psychology. Appleton, New York. pp. 55-57.

Bose, A. G. 1956. A theory of nonlinear systems. Technical Report 309. Research Laboratory of Electronics, M. I. T.

Boynton, R. M. and M. H. Triedman. 1953. A psychophysical and electrophysiological study of light adaptation. J. Exp. Psychol. 46:125-134.

Brindley, A. S. and G. Westheimer. 1968. How deeply nonlinear is the electroretinogram? J. Physiol. 196:78P-79P.

Brindley, G. S. 1955. The site of electrical excitation of the human eye. J. Physiol. 127:189.

Brindley, G. S. and G. Westheimer. 1965. The spatial properties of the human electroretinogram. J. Physiol. 179:518-537.

Brown, K. T. 1968. The electroretinogram: Its components and their origins. Vision Res. 8:633.

Brown, K. T. and T. N. Wiesel. 1961. Analysis of the intraretinal electroretinogram in the intact cat eye. J. Physiol. 158:229-256.

Buckser, S. 1965. Studies on the electroretinogram: II. Model of an a-wave regenerator mechanism. Bull. Math. Biophys. 27:223-233.

Buckser, S. and A. M. Potts. 1966. Studies on the a-wave: I. The a-wave during dark adaptation, in Burian, H. M. and J. H. Jacobson, eds., Clinical Electroretinography, Pergamon Press Ltd., Oxford, pp. 177-185.

Burian, H. M. and J. H. Jacobson, eds. 1966. Clincial Electro-retinography. Pergamon Press, Oxford.

Burian, H. M. and T. Lawwill. 1965. Electroretinographic studies in strabismic amblyopia. Amer. J. Ophthal. 61:422-430.

Burch, G. J. A. 1893. A manual of electrical science. Methuen, London.

Cameron, R. H. and W. T. Martin. 1947. The orthogonal development of nonlinear junctionals in series of Fourier-Hermite functionals. Annals of Math, 48, 2:385-392.

Campbell. F. W. and W. A. H. Rushton. 1955. Measurement of the scotopic pigment in the living human eye. J. Physiol. 130:313-147.

Carr, R. E. and P. Gouras. 1965. Oguchi's disease. Archiv. Ophthal. 73:646-656.

Carr, R. E., H. Ripps, I. M. Siegel and R. A. Weale. 1966. Rhodopsin and the electrical activity of the retina in congenital night blindness. Invest. Ophthal. 5:497-507.

Chaffee, E. L., W. T. Bovie and A. Hampson. 1923. The electrical response of the retina under stimulation by light. J. Opt. Soc. Amer. 7:1-44.

Cobb, W. and C. Morocutti, eds. 1967. The Evoked Potentials. EEG and Clin. Neurophysiol. Suppl. 26.

Cohen, L. H. and W. K. Noell. 1963. Relationships between visual function and metabolism. Biochemistry of the Retina. Clive N. Graymore, ed., Academic Press, p. 36.

Craik. K. J. W. and M. D. Vernon. 1941. Nature of dark adaptation. Brit. J. Phsychol. 32:62-81.

de Haas, H. K. 1903. Lichtprikkels en retinastroomen in hun quantitatief verband. Leiden: Eduard Ijdo.

Dewar, J. 1877. The physiological action of light. Nature. 15: 433-454.

Dewar, J. and J. G. McKendrik. 1873. On the physiological action of light. Proc. Royal Soc. Edinburgh. 8:100-104.

Dowling, J. E. 1970. Organization of Vertebrate Retinas. Invest. Ophthal. 9:655-680.

Dowling, J. E. 1967. The site of visual adaptation. Science. 155:273.

Dowling, J. E. 1960. Night blindness, dark adaptation, and the electroretinogram. Amer. J. Ophthal. 50:875-887.

Dowling, J. E. 1960. Chemistry of visual adaptation in the rat. Nature. 188:114-118.

du Bois-Reymond, E. 1849. Untersuchungen über thierische Elektricität, Vol. 2. Reimer, Berlin, pp. 256-257.

Edwards, W. and T. Lawwill. 1972. Genetic and environmental factors in ophthalmic practice. J. Kentucky Med. Ass. 70:457-462.

Edwards, W. and T. Lawwill. 1972. Hereditary and environmental factors in blindness. J. Kentucky Med. Ass. 70:457-462.

Ehrenfeld, E. N., H. Rowe and E. Auerbach. 1970. Laurence-Moon-Bardet-Biedl Syndrome in Israel. Amer. J. Ophthal. 70:524-532.

Einthoven, W. 1903. Ein neues Galvanometer. Annalen der Physick 4; Folge 130, 12:1059-1071.

Einthoven, W. and W. A. Jolly. 1908. The form and magnitude of the electrical response of the eye to stimulation by light at various intensities. Quarterly J. of Exp. Physiol. 1:373-416.

Elenius, V. and J. Heck. 1958. Relation of size of electroretinogram to rhodopsin concentration in normal human beings and one totally color blind. Nature. 180:810.

Enoch, J. and R. N. Sunga. 1969. Development of quantitative perimetric tests. Documenta Ophthal. 26:216-229.

Ernest, J. and A. M. Potts. 1969. Pathophysiology of distal portion of the optic nerve. III. The effect of the intraocular pressure on the optic nerve discharge. Am. J. Ophthal. 68:594-604.

Fechner, G. T. 1860. Elemente der Psychophysik. Breitkopf und Hartel, Leipzig.

Fender, D. and B. Julesz. 1967. Extension of Panum's Fusional Area in Binocularly Stabilized Vision. J. Opt. Soc. Amer. Vol. 57, 6:819-830.

Francois, J., ed. 1968. The Clinical Value of Electroretinography. Karger, Basel.

French, A. S. and E. G. Butz. 1973. Measuring the Wiener kernels of a nonlinear system using the fast Fourier transform algorithm. Int. J. Control. 17:(3)529-539.

Fricker, S. J. 1971. Analysis of the visual evoked response by synchronous detector techniques. I. Patients with cataracts. Invest. Ophthal. 10:340.

Fricker, S. J. 1971. Application of synchronous detector techniques for electroretinographic studies in patients with retinitis pigmentosa. Invest. Ophthal. 10:329.

Fricker, S. J. 1971. The clinical significance of ERG time delay determination by means of a phase-sensitive detection system. Proceedings of the VII ISCERG Symposium, Istanbul. Sept. 14-18, 1969. 262-282. Published 1971, Istanbul, Turkey.

Fricker, S. J. 1970. Use of the synchronous detector for ERG and VER measurements in children. Proceedings of the 1970 ISCERG symposium, Pisa, Italy. Sept. 7-12, 1970.

Fricker, S. J., ed. 1969. Electrical responses of the visual system. Internat. Ophthal. Clin. Vol. 9, No. 4, Winter, 1969. Little, Brown and Company, Boston.

Fricker, S. J., ed. 1969. ERG and VER with the synchronous detector. Electrical responses of the visual system. Internat. Ophthal. Clin. Vol. 9, No. 4, Winter, 1969. Little, Brown and Company, Boston.

Fricker, S. J. July 1966. Numerical measurements of retinal and occipital function. Arch. Ophthal. 76:37.

Fricker, S. J. 1962. Narrow-band filter technique for the detection and measurement of evoked responses. Electroenceph. Clin. Neurophysiol. 14:411.

Fricker, S. J. and J. J. Sanders. 1975. A new method of cone electroretinography: the rapid random flash response. Invest. Ophthal. 14:131-137.

Fricker, S. J. and J. J. Sanders. 1974. Clinical studies of the evoked response to rapid random flashes. Electroenceph. Clin. Neurophysiol. 36:525-532.

Fry, G. A. and S. H. Bartley. 1934-1935. Electrical responses of the retinal ganglion cell axons. J. Cellular and Comparative Physiol. 5:291-299.

Fuortes, M. G. F. and A. L. Hodgkin. 1964. Changes in the time scale and sensitivity in the ommatidia of Limulus. J. Physiol. 172:239-263.

Goodman, G. and R. D. Gunkel. 1958. Familial electroretinographic and adaptometric studies in retinitis pigmentosa. Amer. J. Ophthal. 46:142-178.

Goodwin. A. W. and D. H. Fender. 1973. The interaction between horizontal and vertical eye-rotations in tracking tasks. Vision Res. 13(9):1701-1712.

Gotch, F. 1904b. Further observations on the photoelectric responses of the frog's eyeball. J. Physiol. 30:i-ii (abstract).

Gotch, F. 1904a. The time-relations of the photo-electric changes produced in the eyeball of the frog by means of colored light. J. Physiol. 31:1-29.

Gotch, F. 1903. The time relations of the photo-electric changes in the eyeball of the frog. J. Physiol. 29:388-416.

Gouras, P. 1970. Electroretinography: Some basic principles. Invest. Ophthal. 9:557-569.

Gouras, P. 1966. Rod and cone independence in the electro-retinogram of the dark-adapted monkey's perifovea. J. Physiol. 187:455-466.

Gouras, P. and R. E. Carr. 1964. Electrophysiological studies in early retinitis pigmentosa. Arch. Ophthal. 72:104-110.

Gouras, P. and R. D. Gunkel. 1964. The frequency response of normal, rod achromat and nyctalope ERG's to sinusoidal mono-chromatic light stimulation. In H. E. Henkes and L. H. van der Tweel (eds.) Flicker. The Hague, Dr. W. Junk, 1964, p. 137.

Graham, D. and D. McRuer. 1961. Analysis of Nonlinear Control Systems. John Wiley, New York.

Granda, A. M. and W. R. Biersdorf. 1966. Spectral sensitivity of the human electroretinogram during temporal course of dark adaptation. Vision Res. 6:507.

Granda, A. M. and W. R. Biersdorf. 1963. Electrical responses of the human eye following intense chromatic pre-exposures. Vision Res. 3:431-445.

Granit, R. 1963. Sensory Mechanisms of the Retina. Hafner, New York (Reprinted).

Granit, R. 1935. Two types of retinas and their electrical responses to intermittent stimuli in light and dark adaptation. J. Physiol. 85: 421-438.

Granit, R. 1933. The components of the retinal action potential in mammals and their relation to the discharge in the optic nerve. J. Physiol. 77:207-239.

Granit, R. and T. Helme. 1939. Changes in retinal excitability due to polarization and some observations on the relation between the processes in retina and nerve. J. Neurophysiol. 2:556-565.

Hartline, H. K. 1925. The electrical response to illumination of the eye in intact animals, including the human subject; and in decerebrate preparations. Amer. J. Physiol. 73:600-611.

Henkes, H. 1950. Use of electroretinography in disturbances of the retinal and choroidal circulation. Proc. 16th International Congress of Ophthalmology. London, England.

Henkes, H. and L. H. Van der Tweel, eds. 1964. Flicker. The Hague, Dr. W. Junk.

Himstedt, F. and W. A. Nagel. 1902. Versuche über die Reizwirkung verschiedener Strahlenarten auf Menschen und Thieraugen. Festschrift der Universität in Freiburg. 259-274.

Himstedt, F. and W. A. Nagel. 1901. Die Verteilung der Reizwerte für die Froschnetzhaut im Dispersionspektrum des Gaslichtes, mittels der Aktionsströme untersucht. Annalen der Physik Series 4. XI, S. 153-162.

Hirose, T. 1969. Routine method for clinical electroretinogram, with special reference to the photopic b-wave in narrow sence. Acta Soc. Ophthal. Jap. 73:549-555.

Hirose, T. and Jerry H. Jacobson. 1969. ERG and VER studies of children with poor vision. Amer. Acad. Ophthal. Otolaryngol. 73:691-704.

Hirose, T. and Jerry H. Jacobson. 1968. Combined recording of the electroretinogram (ERG)and visual evoked occipital response (VER) in lesions of the visual pathways. Advances in electrophysiology and pathology of the visual system. B. Schmoger, ed. pp. 125-138. Veb Georg Thieme, Leipzig.

Hirose, T., Jerry H. Jacobson and K. Kawasaki. 1969. The human electroretinogram and occipital potential in response to focal illumination of the retina. Invest. Ophthal. 8:545-556.

Hirose, T., Jerry H. Jacobson and Arnold B. Popkin. 1968. Independence of the oscillatory potential, photopic b and scotopic b-wave in human electroretinogram. Clinical Value of Electroretinography, J. Francois, ed., Karger, Basel/New York, pp. 8-20.

Hirose, T., Jerry H. Jacobson and Arnold B. Popkin. 1967. The electroretinogram in Harada's disease. Amer. J. Ophthal. 64: 1152-1154.

Hirose, T., Jerry H. Jacobson and Arnold B. Popkin. 1967. Oscillatory potential of electroretinogram: Relationships to the photopic b-wave in humans. Arch. Ophthal. 78:58-67.

Hirose, T., Jerry H. Jacobson and P. E. Stokes. 1969. Changes in human ERG induced by intravenous alcohol. Proc. 3rd Congress of Europ. Soc. of Ophthal. Amsterdam. Ophthalmologica Additamentum. 158:669-677.

Hirose, T., Jerry H. Jacobson and T. A. Suzuki. 1968. Simultaneous ERG and VER in lesions of the optic pathway. Invest. Ophthal. 6: 279-292.

Hirose, T., E. Wolf and S. Malin. 1972. Human visual evoked responses to focal illumination of the retina with special reference to extra-foveal responses. Invest. Ophthal. 11:72.

Holmgren, F. 1879-1880. Über die Retinaströme. Untersuch. Physiolisches Institüt der Universität Heidelberg. 3:278-326.

Holmgren, F. 1865-1866. En method att objektivera effecten of ljusintryck pä retina. Upsala Läkareförenings Förhandlingar. 1:177-191.

Ishihara, M. 1906. Versuch einer Deutung der photoelektrischen Schwankungen am Froschauge. Pfüger's Archiv für die Gesamte Physiologie des Menschen und der Tiere. 114:569-618.

Jacobson, Jerry H., T. Hirosè and T. A. Suzuki. 1968. Simultaneous ERG and VER in lesions of the optic pathway. Invest. Ophthal. 6:279.

Johnson, E. P. 1958. The character of the b-wave in the human electroretinogram. Arch. Ophthal. 60:565.

Johnson, E. P. and L. A. Riggs. 1951. Electroretinal and psychophysical dark adaptation curves. J. Exp. Psychol. 41:139-147.

Johnson, E. P., L. A. Riggs and A. M. L. Schick. 1966. Photopic retinal potentials evoked by phase alternation of a barred pattern. In Clin. Electroretino., Vision Res. Suppl. p. 75.

Karpe, G., ed. 1962. First symposium of ISCERG. Acta Soc. Ophthal. Suppl. No. 70. Copenhagen, Denmark.

Karpe, G. 1945. The basis of clinical electroretinography. Acta Soc. Ophthal. Jap. Suppl., 24.

Katzenelson, J. and L. A. Gould. 1962. The design of nonlinear filters and control systems. I. Inform. and Control. 5:108-143.

Kelsey, J.H. 1969. Electrophysiological tests of visual function. Internat. Ophthal. Clin. No. 4, Winter, 1969. 9:883.

Kohlrausch. A. 1931. Electrische Erscheinungen am Auge. Handbuch der normalen und pathologischen Physiologie. A. Bethe, et al., eds. Springer-Verlag, Berlin. pp. 1393-1496.

Krill, A. 1972. Heriditary Retinal and Choroidal Diseases. Harper and Row, New York.

Krill. A.E. 1970. The electroretinogram and electro-oculogram: clinical applications. Invest. Ophthal. 9:600.

Krill. A., E. Folk and I. Rosenthal. 1961. Electroretinography in the Laurence-Moon-Biedl syndrome. Amer. J. Dis. Child. 102:205-209.

Krill. A., A.M. Potts, C.E. Johanson and J.M. Enoch. A discrepancy between dark-adaptation and the electroretinogram in chloroquine retinopathy.

Kühne, W. 1878a. Untersuchungen Physiologies. Institüt der Universität Heidelberg. 1:1-14.

Kühne, W. 1878b. Untersuchungen Physiologies. Institüt der Universität Heidelberg. 1:15-103.

Kühne, W. and J. Steiner. 1881. Über elektrische Vorgänge im Sehorgane. Untersuchungen Physiologies, Institüt der Universität Heidelberg. 4:64-168.

Kühne, W. and J. Steiner. 1880. Über das elektromotorische Verhalten der Netzhaut. Untersuchungen Physiologies, Institüt der Universität Heidelberg. 3:327-377.

Lawwill, T. 1971. Electrodiagnostic techniques in ophthalmology. J. Kentucky Med. Assn. 69:97-99.

Lawwill, T. and H.M. Burian. 1966. A modification of the Burian-Allen contact lens electrode for human electroretinography. Amer. J. Ophthal. 61:1506-1509.

Lawwill. T. and F. Sharp. 1969. Study of ocular effects of chronic exposure to laser radiation. Report II, Army Cont. DADA 17-68-C-8105. April 1969-March 1969.

Lawwill. T. and F. Sharp. 1968. Study of ocular effects of chronic exposure to laser radiation. Report I, Army Cont. DATA 17-68-C-8105. April 1968-December 1968.

Lawwill, T. and L. Stokes. 1972. Clinical ERG with bar pattern stimuli. Amer. J. Ophthal.

Lawwill. T., W. Wacker and R. MacDonald. 1972. The electroretinogram: Its role in evaluating posterior uveitis. Thesis submitted to the American Ophthalmological Society in 1972.

Lee, Y. W. and M. Schetzen. 1961. Measurement of the kernels of a nonlinear system by crosscorrelation. Quarterly progress report No. 60. Research Lab of Electronics, M. I. T.

Levett, J. 1970. Nonlinear-linear transition in the frog intraretinal electroretinogram. Vision Res. 10:1347-1354.

Levett, J. 1970. Nonlinearities in the ERG. Amer. J. Optom. 47:965-975.

Marmarelis, P. Z. 1971. Nonlinear transfer functionals for certain retinal neuronal systems. Ph. D. Thesis, California Institute of Technology.

Marmarelis, P. Z. 1975. Proceedings of the First Symposium on Testing and Identification of Nonlinear Systems. California Institute of Technology.

Marmarelis, P. Z. and K. -I. Naka. 1972. Spatial distribution of potential in a flat cell: application to the catfish horizontal cell layers. Biophys. J. 12:1515-1532.

Marmarelis, P. Z. and K. -I. Naka. 1973. Nonlinear analysis and synthesis of receptive field responses in the catfish retina. J. Neurophysiol. 36:619-653.

Marmarelis, P. Z. and K. -I. Naka. 1973a. Nonlinear analysis and synthesis of receptive-field responses in the catfish retina. I. Horizontal cell–ganglion cell chain. J. Neurophysiol. 36:605-618.

Marmarelis, P. Z. and K. -I. Naka. 1973b. Nonlinear analysis and synthesis of receptive–field responses in the catfish retina. II. One-input white-noise analysis. J. Neurophysiol. 36:619-633.

Mayo, J. E., R. F. Pawula and S. O. Rice. 1973. On a nonlinear problem involving RC. noise. IEEE Transaction on Info. Theory. 19:128-135.

Naka, K. -I. 1972. The horizontal cell. Vision Res.

McCann, G. D. 1974. Nonlinear identification theory models for successive stages of visual nervous systems of flies. J. Neurophysiol. 37:869-895.

Noell, W.K. 1954. The origin of the electroretinogram. Amer. J. Ophthal. 38:78-90.

Pawula, R. and A. Tsai. 1969. Theoretical and experimental results for the distribution of a certain nonlinear functional of the Orstein-Uhlenbeck process. IEEE Transactions on Info. Theory. 15:532-535.

Pirenne, M.H. 1958. Some aspects of the sensitivity of the eye. Ann. New York Acad. Sci. 74:377-384.

Piper, H. 1911. Über die Netzhautströme. Archiv für Anatomie und Physiologie, Physiologische Abteilung (Leipzig). pp. 85-132.

Piper, H. 1904. Das Elektromotorische Verhalten der Retina bei Eledone moschata. Archiv für Anatomie und Physiologie, Physiologische Abteilung (Leipzig). pp. 453-474.

Potts, A.M. and T. Nagaya. 1965. Studies on the visual evoked response: I. The use of the 0.06° red target for evaluation of foveal function. Invest. Ophthal. 4:303-309.

Riggs, L.A. 1965. Electrophysiology of Vision. In Vision and Visual Perception, C. Graham, ed., Wiley, New York, pp. 81-131.

Riggs, L.A. 1958. The human electroretinogram. Arch. Ophthal. 60:739-754.

Riggs, L.A. and S. Sokol. 1969. Electrical and psychophysical response of the human visual system to modulated light. Proceedings of the National Academy of Sciences. 64:1431.

Rushton, W.A.H. Nov. 8, 1962. Visual Adaptation. The Ferrier Lecture. Cambridge University.

Rushton, W.A.H. April 1961. Rhodopsin measurement and dark adaptation in a subject deficient in cone vision. J. Physiol. 156: 193-205.

Rushton, W.A.H. 1961a. Dark adaptation and the regeneration of rhodopsin. J. Physiol. 156:166-178.

Rushton, W.A.H., F.W. Campbell, W.A. Hagins and G.S. Brindley. 1955. The bleaching and regeneration of rhodopsin in the living eye of the albino rabbit and of man. Optica Acta. 1:183-190.

Rushton, W. A. H., A. B. Fulton and H. D. Baker. 1969. Dark adaptation and the rate of pigment regeneration. Vision Res. 9:1473-1479.

Rushton, W. A. H. and G. H. Henry. 1968. Bleaching and regeneration of cone pigment in man. Vision Res. 8:617-631.

Rushton, W. A. H. and G. Westheimer. Nov. 1962. The effect upon the rod threshold of bleaching neighboring rods. J. Physiol. 164: 318-329.

Sachs, E. 1929. Aktionströme des menschlichen Auges, ihre Beziehung zu Reiz und Empfindung. Klinische Wochenschrift. 8:136-137.

Stark, L. 1968. Neurological Control Systems: Studies in Bio-engineering. Reenum Press, New York. Ch. 4.

Toyoda, J., H. Nosaki and T. Tomita. 1969. Light-induced resistance changes in single photoreceptors of Necturus and Gekko. Vision Res. 9:453-463.

Troelstra, A. 1975. Electrical response of human eye to sinusoidal light stimulation. IEEE Biomed. 22:369-378.

Troelstra, A. 1971. Harmonic distortion in the frog's ERG and its possible relation to differences in latencies. Vision Res. 11:393-403.

Troelstra, A. and N. M. J. Schweitzer. 1968. Nonlinear analysis of the electroretinographic b-wave in man. J. Neurophysiol. 31: 588-606.

Troelstra, A. and N. M. J. Schweitzer. 1966. The electroretino-graphic response to weak stimuli of large subtense. Doc. Ophthalmologica. 20:365-378.

Troelstra, A. and N. M. J. Schweitzer. 1966. A model for the scotopic electroretinographic system. Chap. IV in Studies in Perception, National Defense Research Organization. The Netherlands, 1966.

Troelstra, A. and N. M. J. Schweitzer. 1965. A negative component in the b-wave of the human ERG. Doc. Ophthalmologica. 149:230-378.

Troelstra, A. and N. M. J. Schweitzer. 1964. The recovery of the b-wave during dark adaptation. Vision Res. 4:345-353.

Troelstra, A. and N. M. J. Schweitzer. 1964. On the relationship between the single flash ERG and the ERG elicited by more complex stimuli. Doc. Ophthalmologica. 18:114-127.

Troelstra, A. and N. M. J. Schweitzer. 1963. An analysis of the b-wave in the human ERG. Vision Res. 3:213-226.

Troelstra, A. and N. M. J. Schweitzer. 1963. An end effect in the human ERG. Doc. Ophthalmologica. 145:119-122.

Troelstra, A. and N. M. J. Schweitzer. 1963. On the physiological standardization of the light source in electroretinography. Doc. Ophthalmologica. 146:114-123.

van Doren, C. 1938. Benjamin Franklin. Viking Press, New York.

Volterra. 1959. Theory of Functionals and of Integral and Integro-differential Equations. Dover publications, New York.

Waller, A. D. 1900. On the excitability of nervous matter with special reference to the retina. Brain. 23:1 38.

Westerlund, A. 1912. Einige Beobachtungen über die photo-elektrische Potential-Verteilung an der Oberfläche eines isolierten Froschauges. Scandinavian Archives of Physiology. 27:260-276.

Wiener, N. 1958. Nonlinear Problems in Random Theory. Wiley, New York.

Yasui, S. 1975. Volterra kernels, Wiener kernels and nonlinear systems. Orally presented at Conf. on Testing and Identification of Nonlinear Systems. California Institute of Technology, Pasadena, California. Also under preparation for publication.

Yasui, S. and D. H. Fender. 1975. Methodology for measurement of Spatio-Temporal Volterra and Wiener kernels for visual systems. Proc. First Symp. on Testing and Identification on Nonlinear Systems, California Institute of Technology, Pasadena, California, pp. 366-383.